

**UMD - CONDOR**  
*Mountain Rescue Helicopter*



Alfred Gessow Rotorcraft Center  
Department of Aerospace Engineering  
University of Maryland  
College Park, MD 20742  
June 1, 2004

# University of Maryland



Alfred Gessow Rotorcraft Center  
Department of Aerospace Engineering  
University of Maryland  
College Park, MD 20742

## UMD - Condor Design Proposal

In response to the 2004 Annual AHS International  
Student Design Competition - Graduate Category  
June 1, 2004

---

Joshua Ellison

---

Dr. Inderjit Chopra - Faculty Advisor

---

Joseph Conroy

---

Robin Preator

---

Jaye Falls

---

Abhishek Abhishek

---

Shaju John



## **Acknowledgements**

The Condor design team would like to acknowledge the following people and thank them for their valuable assistance and guidance.

Dr. Vengalattore T. Nagaraj - Research Scientist, Dept. of Aerospace Engineering, University of Maryland, College Park.

Dr. Marat Tishchenko - Former Chief Designer, Mil Design Bureau.

Dr. Inderjit Chopra - Professor, Dept. of Aerospace Engineering, University of Maryland, College Park.

Dr. J. Gordon Leishman - Professor, Dept. of Aerospace Engineering, University of Maryland, College Park.

Dr. Jayant Sirohi - Research Associate, Dept. of Aerospace Engineering, University of Maryland, College Park.

Dr. David Lewicki - Research Scientist, NASA Glenn, Cleveland, Ohio.

Paul Samuel, Shreyas Ananthan, Jinsong Bao, Anubhav Datta, Beatrice Roget, Gaurav Gopalan, Beerinder Singh, Jayasimha Atulasimha, Maria Ribera, Vineet Gupta, Wei Hu - Graduate Students, Department of Aerospace Engineering, University of Maryland, College Park.

Mark Rager - Director of Maintenance, Glenwood Aviation LLC.

Jeff McDaniels, Lifeport, Inc.



**Table of Contents**

**ACKNOWLEDGEMENTS..... I**

**LIST OF FIGURES ..... VI**

**LIST OF TABLES ..... VIII**

**LIST OF SYMBOLS / ABBREVIATIONS ..... IX**

**RFP COMPLIANCE ..... X**

**EXECUTIVE SUMMARY ..... XI**

**PERFORMANCE SUMMARY AND DESIGN FEATURES ..... 1**

**SECTION 1 - INTRODUCTION.....4**

**SECTION 2 - IDENTIFICATION OF DESIGN DRIVERS.....4**

    2.1 - MOUNTAIN SAR PERFORMANCE CAPABILITIES .....5

        2.1.1 - SAR Mission Requirements.....5

        2.1.2 - Mission Profile .....5

    2.2 - OPERATING ENVIRONMENT .....6

    2.3 - RFP REQUIREMENTS .....7

    2.4 - DESIGN DRIVERS .....7

**SECTION 3 - CONFIGURATION SELECTION.....9**

    3.1 - QUALITATIVE EVALUATION .....9

        3.1.1 - Evaluation Method .....9

        3.1.2 - Evaluation Results .....10

    3.2 - HISTORICAL SURVEY.....12

    3.3 - FINAL CONFIGURATION SELECTION .....12

**SECTION 4 - PRELIMINARY SIZING.....13**

    4.1 - DESIGN REQUIREMENTS .....13

    4.2 - METHOD OF ANALYSIS.....14

    4.3 - TRADE STUDIES.....15

    4.4 - INITIAL SIZING .....15

    4.5 - ENGINE SELECTION .....19

    4.6 - SELECTION OF FINAL CONFIGURATION .....21

**SECTION 5 - AIRCRAFT CERTIFICATION .....25**

    5.1 - APPLICABILITY .....26

    5.2 - CATEGORY A Vs. CATEGORY B .....26

    5.3 - SUMMARY OF DESIGN REQUIREMENTS FROM CFR .....27

**SECTION 6 - MAIN ROTOR & HUB DESIGN.....28**

    6.1 - BASELINE ROTOR DESIGN .....28

        6.1.1 Blade Twist .....28

        6.1.2 Airfoil Sections.....29

        6.1.3 Tip Speed .....29

        6.1.4 Tip Geometry .....29

    6.2 - SWASHPLATELESS ROTOR CONTROL.....30

        6.2.1 - Trailing Edge Flaps.....30

        6.2.2 - Lift Flaps vs. Moment Flaps.....31

        6.2.3 - Details of Moment Flap Design.....32

        6.2.4 - Moment Flap: Parametric Design Studies .....34

    6.3 - COMPACT FLAP ACTUATOR.....36



6.3.1 - Actuator Design.....	36
6.3.2 - Actuator Mounting and Operation .....	38
6.3.3 - Safety and Monitoring .....	39
6.4 - SLIP RING .....	39
6.5 - BLADE STRUCTURAL DESIGN.....	39
6.5.1 - Blade Design Details.....	39
6.5.2 - Lightning Protection and Electromagnetic Shielding.....	42
6.6 - HUB DESIGN.....	42
6.7 - AUTOROTATION CHARACTERISTICS .....	43
6.8 - ACTIVE VIBRATION CONTROL.....	44
6.9 - ROTOR DYNAMICS .....	45
6.9.1 - Dynamic Analysis .....	45
6.9.2 - Aeroelastic Analysis .....	46
6.9.3 - Ground & Air Resonance.....	47
<b>SECTION 7 - FAN-IN-FIN ANTI-TORQUE SYSTEM.....</b>	<b>48</b>
7.1 - ANTI-TORQUE SYSTEM TRADE STUDY .....	48
7.2 - FAN-IN-FIN DETAILED DESIGN.....	49
7.2.1 - Duct/Shroud Design .....	50
7.2.2 - Fan Design .....	51
7.2.3 - Vertical Fin Design .....	53
<b>SECTION 8 - AIRFRAME/LANDING GEAR DESIGN .....</b>	<b>54</b>
8.1 - AIRFRAME DESIGN .....	54
8.1.1 - Structural Details .....	54
8.1.2 - Crash Resistance .....	56
8.1.3 - Materials, Manufacturing, Construction.....	56
8.1.4 - Doors.....	57
8.2 - LANDING GEAR DESIGN .....	57
8.2.1 - Configuration .....	58
8.2.2 - Tire Sizing.....	59
8.2.3 - Oleo Sizing .....	59
<b>SECTION 9 - DETAILS OF COCKPIT/CABIN SYSTEMS.....</b>	<b>59</b>
9.1 - CREW STATION FEATURES .....	59
9.2 - COCKPIT LAYOUT.....	60
9.2.1 - Cockpit and Cabin Access.....	60
9.2.2 - Pilot/Copilot Stations .....	60
9.3 - COCKPIT SYSTEMS .....	62
9.3.1 - Sensor Suite .....	62
9.3.2 - Multi-function Displays .....	62
9.3.3 - Communication Systems .....	63
9.3.4 - Mission Systems Equipment.....	63
9.3.5 - Flight Management System .....	64
9.3.6 - Alternate Avionics Package.....	65
9.4 - CABIN SYSTEMS .....	65
9.5 - CABIN EQUIPMENT LAYOUT.....	65
<b>SECTION 10 - MISSION EQUIPMENT.....</b>	<b>67</b>
10.1 - RESCUE GEAR .....	67
10.1.1 - Retrieval Gear .....	67
10.1.2 - Hoist .....	68
10.1.3 - Additional Rescue Equipment.....	68
10.2 - MEDICAL EQUIPMENT .....	68
<b>SECTION 11 - FLIGHT CONTROL SYSTEM.....</b>	<b>70</b>



11.1 - DESIGN OF FCS .....	70
11.1.1 - Details of Flight Control System .....	70
11.1.2 - Neural Network Based Fault Detection.....	72
11.2 - STABILITY AND CONTROL ANALYSIS .....	73
11.2.1 - Lateral & Longitudinal Modes .....	73
11.2.2 - Tail Sizing.....	74
11.3 - HANDLING QUALITIES .....	74
<b>SECTION 12 - MECHANICAL SUBSYSTEMS (ENGINE/TRANSMISSION) .....</b>	<b>76</b>
12.1 - ENGINES .....	76
12.1.1 - Engine Structural Integration.....	76
12.1.2 - Engine Performance.....	77
12.1.3 - Engine Subsystems.....	77
12.2 - TRANSMISSION DESIGN .....	77
12.2.1 - Design Baselines .....	77
12.2.2 - Configuration Study.....	78
12.2.3 - Optimization Considerations .....	80
12.2.4 - Structural Integration .....	82
12.2.5 - Stress Calculations .....	82
12.2.6 - Weight Estimation .....	83
12.2.7 - Generator and APU.....	83
12.2.8 - Tail Rotor Drive and Gearbox.....	84
12.2.9 - Power Losses .....	84
12.2.10 - Oil System.....	84
12.3 - HEALTH AND USAGE MONITORING .....	85
12.3.1 - Rotor.....	86
12.3.2 - Engines.....	86
12.3.3 - Main Gearbox.....	87
12.3.4 - Tail Gearbox.....	87
12.3.5 - Structure .....	87
<b>SECTION 13 - WEIGHT ANALYSIS.....</b>	<b>88</b>
13.1 - HISTORICAL TRENDS .....	88
13.2 - PRELIMINARY WEIGHT ESTIMATES .....	89
13.3 - COMPONENT WEIGHTS .....	89
13.3.1 - Fuselage and Cowling .....	89
13.3.2 - Fan-in-fin and Empennage.....	89
13.3.3 - Engines .....	89
13.3.4 - Transmission.....	90
13.3.5 - Rotor System.....	90
13.3.6 - Avionics .....	90
13.3.7 - Landing Gear.....	90
13.3.8 - Fuel and Fuel System .....	90
13.3.9 - Electric System .....	91
13.3.10 - Crashworthiness .....	91
13.3.11 - Passengers and Crew .....	91
13.3.12 - Rescue and Medical Equipment.....	91
13.4 - WEIGHT EFFICIENCY .....	91
13.5 - WEIGHT AND BALANCE.....	91
<b>SECTION 14 - PERFORMANCE ANALYSIS .....</b>	<b>92</b>
14.1 - DRAG ESTIMATION .....	93
14.2 - HOVER PERFORMANCE.....	93
14.3 - FORWARD FLIGHT PERFORMANCE .....	95
14.4 - MISSION CAPABILITY .....	97



**SECTION 15 - CONCLUSIONS .....100**  
**MIL-STD-1374 WEIGHT BREAKDOWN**  
**REFERENCES**

## **List of Figures**

- Figure 2.1 - SAR Mission Profile
- Figure 4.1 - Block Diagram for Design Code
- Figure 4.2 - Empty Mass vs. Disk Loading for Varying Number of Blades (3 Engines)
- Figure 4.3 - Main Rotor Diameter Comparison
- Figure 4.4 - Takeoff Weight Comparison
- Figure 4.5 - Payload-MGW Ratio Comparison
- Figure 4.6 - Acquisition Cost Comparison
- Figure 4.7 - Engine Layout for Three TM Arrius 2F Engine
- Figure 4.8 - Specific Fuel Consumption for Existing Helicopter Engines [TISH04]
- Figure 4.9 - Two-Engine Results for Takeoff Power Required for One Engine
- Figure 4.10 - Two-Engine Results for Main Rotor Diameter vs. Disk Loading
- Figure 4.11 - Two-Engine Results for Takeoff Weight vs. Disk Loading
- Figure 5.1 - Category Distinctions
- Figure 6.1 - Maximum Flap Deflection for Level Flight
- Figure 6.2 - Blade Pitch Angles Required to Trim, Zero Twist
- Figure 6.3 - Collective Flap Deflections
- Figure 6.4 - Maximum Cyclic Flap Amplitude
- Figure 6.5 - Effect of Varying Flap Location
- Figure 6.6 - Effect of Varying Flap Size
- Figure 6.7 - Flap Hinge Moment
- Figure 6.8 - Flap Deflections for Trim
- Figure 6.9 - Piezo-hydraulic Flap Actuator
- Figure 6.10 - Layup of Composite Tailored Blade
- Figure 6.11 - Spanwise Ply Layup for the D-spar
- Figure 6.12 - Scheme for Active Vibration Control
- Figure 6.13 - Blade Stiffness and Mass Distribution
- Figure 6.14 - Rotor Fan Plot
- Figure 6.15 - Pitch Flap Flutter/Divergence Stability Boundary
- Figure 6.16 - Ground Resonance Analysis
- Figure 6.17 - Flap/Lag/Torsion Analysis
- Figure 6.18 - Air Resonance Analysis
- Figure 7.1 - Duct Cutaway Layout (Plan View)



- Figure 7.2 - Blade Loading Coefficient at Altitude
- Figure 7.3 - Thrust to Total Thrust Ratio
- Figure 7.4 - Fan Power vs. Speed
- Figure 8.1 - Required Power for Fixed and Retractable Landing Gear
- Figure 9.1 - FLIR
- Figure 10.1 - Skedco Rescue Litter
- Figure 10.2 - Two-person Rescue Seat
- Figure 10.3 - Rescue Basket
- Figure 10.4 - Goodrich External Hoist
- Figure 10.5 - Cardiac Science AED
- Figure 10.6 - Zoll CCT Monitor, Pacemaker, & Defibrillator
- Figure 11.1 - FCS Architecture for Condor
- Figure 11.2 - Longitudinal and Lateral Flight Stability Poles
- Figure 12.1 - LHTEC CTS800-4N
- Figure 12.2 - Power Variation with Altitude
- Figure 12.3 - Standard Gearbox Design
- Figure 12.4 - Typical Sensor Integration Scheme
- Figure 13.1 - Longitudinal c.g. Travel
- Figure 14.1 - HOGE Power Required @ MGW and Power Available vs. Altitude
- Figure 14.2 - HOGE Altitude vs. Gross Weight for Various Engine Ratings
- Figure 14.3 - Maximum Vertical Rate of Climb vs. Altitude at MGW
- Figure 14.4 - Power Required in Forward Flight for Various Altitudes
- Figure 14.5 - Maximum Cruise Speed vs. Altitude at MGW
- Figure 14.6 - Fuel Flow vs. Air Speed @ 3,658 m (12,000 ft)
- Figure 14.7 - Payload-Range at Sea-Level and at Altitude (20 min. Reserve)
- Figure 14.8 - Payload-Range at Altitude Incorporating Hover Time (20 min Reserve)
- Figure 14.9 - Payload-Endurance at Sea-Level and at Altitude (20 min Reserve)



## **List of Tables**

Table 2.1 - SAR Mission Profile

Table 2.2 - Description of Design Drivers

Table 3.1 - Weighting Factors

Table 3.2 - Ratings

Table 3.3 - Configuration Selection Matrix

Table 3.4 - RFP Performance Requirements

Table 3.5 - Historical Survey

Table 4.1 - Preliminary Sizing Results

Table 4.2 - Candidate Engines for Two and Three-Engine Configurations

Table 4.3 - Selected Engines

Table 4.4 - Results for Three-engine Configuration

Table 4.5 - Blade Aspect Ratio Comparison for 2-Engine 4-Bladed Rotor Configuration

Table 4.6 - Final Number of Engines Comparison

Table 6.1 - Main Rotor Design Parameters

Table 6.2 - Swashplateless Rotor Design Parameters

Table 6.3 - Comparison of Potential Smart Materials

Table 6.4 - Properties of Materials Used in Blade Structure

Table 6.5 - Spring Design Details

Table 6.6 - Autorotation Index Comparison

Table 6.7 - Main Rotor Blade Natural Frequencies

Table 7.1 - Survey of Existing Fan-in-Fins

Table 8.1 - Landing Gear Configuration Comparison

Table 10.1 - Rescue and Medical Equipment Weights

Table 11.1 - Stability Derivatives

Table 11.2 - Control Derivatives in Hover and Forward Flight

Table 12.1 - Power Ratings for CTS-800-4N

Table 12.2 - Design Baselines [Heat93]

Table 12.3 - Final Transmission Details

Table 12.4 - Calculated Stresses and Weight Estimation

Table 13.1 - Preliminary Weight Estimates

Table 14.1 - High Altitude Performance Summary

Table 14.2 - Component Drag Breakdown

## List of Symbols / Abbreviations

Actuator Control Computers (ACCs)	Individual Blade Control (IBC)
Advance Ratio ( $\mu$ )	Inertial Navigation System (INS)
Advanced Life Support (ALS)	Instrument Flight Rules (IFR)
All Engines Operative (AEO)	Inter-Communication Select (ICS)
American Helicopter Society (AHS)	Joint Aviation Requirements (JAR)
Angle-of-Attack (AOA)	Line Replacement Units (LRU)
Attitude Command Attitude Hold (ACAH)	Magnetorheological (MR)
Attitude Retention Systems (ATTs)	Main Rotor Diameter (DMR)
Automatic External Defibrillator (AED)	Maximum Gross Weight (MGW)
Automatic Flight Control System (AFCS)	Multi-Function Displays (MFDs)
Autopilot Systems (APs)	Night Vision Goggle (NVG)
Auxiliary Power Unit (APU)	No Tail Rotor (NOTAR)
Blade Aspect Ratio (R/c)	Number of Blades (Nb, N_b)
Blade Pitch ( $\theta$ )	One Engine Inoperative (OEI)
Center of Gravity (c.g.)	Original Equipment Manufacturer (OEM)
Code of Federal Regulations (CFR)	Primary Flight Control System (PFCS)
Control Display Units (CDUs)	Primary Flight Displays (PFDs)
Differential GPS (DGPS)	Rate Command Attitude Hold (RCAH)
Dihedral Effect ( $L_v$ )	Rate Damping (RD)
Enhanced Ground Proximity Warning System (EGPWS)	Request for Proposals (RFP)
Flap Deflection ( $\delta$ )	Search and Rescue (SAR)
Flap-Bending/Torsion (FBT)	Solidity ( $\sigma$ )
Flight Control Computers (FCCs)	Specific Fuel Consumption (SFC)
Flight Control System (FCS)	Stability Augmentation Systems (SASs)
Flight Director Systems (FDs)	Thrust Coefficient ( $C_T$ )
Flight Management System (FMS)	Torsional Frequency ( $v_\theta$ )
Fly-By-Wire (FBW)	Traffic Alert & Collision Avoidance System (TCAS)
Forward Looking Infra-Red (FLIR)	Translational Rate Command (TRC)
Full Authority Digital Electronic Control (FADEC)	University of Maryland Advanced Rotor Code (UMARC)
Global Positioning System (GPS)	Vectored Thrust Ducted Propellar (VTDP)
Health Usage and Monitoring (HUM)	Vertical Rate of Climb (VROC)
Hinge Moments (HM)	Warning/Caution/Advisory (WCA)
Hover-Out-of-Ground-Effect (HOGE)	Yaw Due to Roll Rate ( $N_p$ )



## RFP Compliance

<b>RFP Requirement</b>	<b>Action Taken to Comply</b>	<b>Reference</b>
Meet CFR Title 14, Part 27 or 29	Designed under CFR Title 14, Part 29 - Airworthiness Standards: Transport Category Rotorcraft	Throughout Report / Section 5
Certify for Single Pilot day/night IFR operations	Design utilizes Stabilization and Automatic Flight Control System (AFCS) to meet CFR for Single Pilot IFR operations	Section 11.1
Capable of OEI HOGE at MGW up to 12,000 feet Hd, standard ISA	Uses two engine system – each engine capable of providing power for 12,000 feet OEI HOGE	Section 14.2
Capable of HOGE at MGW up to 15,000 feet Hd, standard ISA	Two high power engines provide a hover ceiling in excess of 15,000 feet	Section 14.2
Cruise speed of at least 145 Knots	High powered helicopter designed for low drag can exceed cruise speed of 145 Knots	Section 14.3
Anti-torque control system capable of maintaining heading in hover with wind from any azimuth up to at least 40 Knots at 15,000 feet	Fan-in-fin tail rotor designed to provide adequate power in 40 Knot crosswind in hover up to 15,000 feet	Section 7.2
Perform mission with takeoff from 6,000 feet, 1 hour outbound leg with 4 crew at 140 Knots, 20 minutes on station hoist operation with recovery of 2 patients at 12,000 feet, and 1 hour return leg at 140 Knots	Designed with adequate cruise speed, hovering capability, range, and endurance to complete mission	Section 14.4
Provided with accommodations for 2 pilots, at least 2 paramedics, and 2 6-foot patients to be in a supine position on litters or cots	Cabin and cockpit layout designed to utilized internal volume of the helicopter	Section 9.5
CG envelope to allow for all flyable combinations of crew, passengers and fuel	Provisions made for CG envelope to allow all flyable combinations of crew and passengers	Section 13.5
Capable of operation on snow	Wheeled landing gear fitted with skis for snow landings	Section 8.2
Provisions for in flight recovery and stowage of loaded basket litter after the first patient has been already recovered and secured to its supine accommodation	Hoisting controls provided for in flight recovery and stowage of loaded basket litter	Section 10.1
Provided with outlined equipment such as weather radar, GPS, searchlight, FLIR, etc.	All necessary equipment included for navigation, communication, and search and rescue	Section 9.3
Equipped with outlined electrical system	Electrical systems provided for engine starting and operation of hoist and other equipment	Section 12.2.7
Designed using currently certified engines or models currently under development	Designed using 2 CTS800-4N model engines (civil version of Comanche engines)	Section 12.1
Provisions for stowage and use of medical equipment listed	Medical equipment situated for ease of use and access	Section 10.2



## **Executive Summary**

The *Condor* is a dedicated mountain search and rescue (SAR) helicopter designed in response to the 2004 American Helicopter Society's (AHS) Request for Proposals (RFP) for "Design for Certification: Mountain Rescue Helicopter". The RFP, sponsored by Agusta Westland, outlined the need for a helicopter conceived from the start as a platform specifically designed for mountain rescue operations. Helicopters currently performing these operations are adaptations of models characterized by good high-altitude performance, and lack several specific attributes desired in a search and rescue aircraft. The Condor features a high-powered twin engine system, with high altitude one engine inoperative (OEI) capabilities, an efficient rotor for hovering at extreme altitudes, and state-of-the-art search and rescue equipment. The Condor's superior performance capabilities and operational safety make it the ideal search and rescue helicopter for mountain extractions.

### **Mission Requirements**

The primary mission outlined in the RFP is the rescue of 2 patients stranded in a mountainous environment. The rescue mission consists of a takeoff from 1,829 m (6,000 ft), a 1 hour outbound cruise flight at 140 knots, a 20 minute hoist operation with the recovery of 2 patients at 3,658 m (12,000 ft), and finally, a 1 hour return cruise flight. Furthermore, several performance capabilities are required including a cruise speed of at least 145 knots at 3,658 m (12,000 ft), a hover-out-of-ground-effect (HOGE) at maximum gross weight (MGW) at 4,572 m (15,000 ft), and the ability to maintain heading at that condition with a 40 knot crosswind from any azimuth. The most stringent of the performance requirements is the ability for HOGE at MGW with OEI at 3,658 m (12,000 ft). The RFP also specifies the equipment to be carried and the need for single pilot day/night Instrument Flight Rules (IFR) operations.

### **Configuration Selection**

A thorough analysis of the RFP and the requirements stipulated therein preceded the selection of the most suitable aircraft characteristics. Initially, a set of design parameters were identified based on the specific needs of the outlined rescue mission. Several helicopter configurations were then comprehensively studied and evaluated on their ability to meet the given design requirements. The analysis showed that a conventional single rotor helicopter with a fan-in-fin anti-torque system was an optimal choice. The all-around performance capabilities of a conventional helicopter, in both cruise speed and hovering efficiency, low acquisition and operating cost, and the operational safety of a fan-in-fin tail rotor were among the primary features favoring this selection.



## Design Methodology

The Condor design was performed in conjunction with the ENAE634 - Helicopter Design course taught at the University of Maryland in Spring 2004. This one semester course is aimed at introducing students to the various aspects of helicopter design and providing them with a fundamental understanding of the major design issues. During the course, the students developed analytical tools to perform the design study, and no commercial codes were used. The detailed rotor dynamics analysis was performed using the University of Maryland Advanced Rotor Code (UMARC), and all graphics were developed using I-DEAS CAD software.

## Design Features

Designed from the start as an SAR helicopter for mountainous terrain, the Condor is a 3.25 ton, twin engine helicopter with a fan-in-fin anti-torque system. Along with the latest in search and rescue technologies, the Condor offers a high power-to-weight ratio with excellent high altitude performance. With particular attention paid to operational safety and reliability, the Condor is the ideal mountain helicopter for rescue mission success. Salient design features are listed below:

***Two Engine Configuration: OEI Capability*** - To meet the stringent OEI HOGE requirement at 3,658 m (12,000 ft), the Condor uses 2 high-powered CTS800-4N model gas turbine engines. Each engine has sufficient OEI continuous power to allow the helicopter to hover at 3,658 m (12,000 ft). Furthermore, the high level of power available from both engines enables the Condor to HOGE at extreme altitudes up to of 6,700 m (22,000 ft) and reach cruise speeds of 170 knots. In several situations, such as lower altitude rescues, it is possible to accommodate additional passengers or crew members.

***Fan-in-Fin Anti-Torque System*** - A fan-in-fin anti-torque system enhances safety during flight and rescue operations, as well as on the ground, by housing the tail rotor in a duct. The system was designed to provide yaw authority under extreme mountainous conditions such as high altitude and high crosswinds. Furthermore, a vertical fin is utilized to offload the tail rotor during forward flight, reducing the shaft power required for the tail rotor.

***Compact Configuration*** - The Condor features a compact configuration for operation in confined spaces. The fuselage shape is optimized for minimum footprint and maximum use of internal volume. Furthermore, the ducted fan-in-fin ensures safe flight near obstacles.

***Autonomous Flight Control System*** - A full authority, triple redundant, Fly-By-Wire (FBW) Flight Control System (FCS) is implemented on the Condor. The autonomous system provides augmented stability control as well as mission specific auto navigation that substantially decreases pilot workload and increases safety.



***Spacious Cabin Layout*** - To allow sufficient room for medical equipment, paramedics, and 2 patients in supine position, the cabin layout was designed to utilize the space efficiently and judiciously. To take advantage of vertical space, the patient litters are stacked on top of one another. This allows ample room for the paramedics to apply medical care to both patients.

***Advanced Search and Rescue Equipment*** - The Condor is equipped with the latest in SAR technology, including forward looking infra-red (FLIR), global positioning system (GPS), and an integrated tracking device to locate beacons from stranded mountain climbers.

***Retractable Wheel/Ski Landing Gear*** - The Condor uses a retractable wheeled landing gear with attachable skis for snow landings. The wheeled gear allows better ground maneuverability and mission readiness and does not interfere with the hoist during rescue operations. A retractable gear provides less parasitic drag than a fixed gear and therefore increases efficiency in high speed forward flight.

***Onboard Medical Equipment*** - The Condor is equipped with onboard medical equipment so that paramedics can provide in-flight medical attention to passengers in need of care. Included are two Advanced Life Support (ALS) kits, two combination defibrillator/cardiac monitors rated for helicopter use, and a drop-off survival kit for victims who may have to be left behind.

***Hoisting Operations*** - The Condor uses an externally mounted Goodrich 42325 hoist for recovery of passengers when landing is not possible. The cabin of the Condor is designed with a large sliding door for easy loading of hoisted litters. An internally mounted camera displays a view of the hoisting operation on the multi-function display in the cockpit. This assists the pilot in stabilizing the aircraft above the rescue site. Furthermore, the 12 m diameter rotor creates low downwash, minimizing interference with rescue operations.

***Swashplateless Rotor Control*** - The Condor utilizes two trailing edge flaps on each blade for primary rotor control, thus eliminating the need for a conventional swashplate. The absence of mechanical linkages and bearings results in an aerodynamically clean and mechanically simple rotor. The control system consists of two trailing edge moment flaps embedded in a torsionally soft blade and actuated using compact piezo-hydraulic hybrid actuators. In addition to primary control, the flaps are capable of providing individual blade control (IBC) for vibration reduction throughout the flight envelope.

***Composite Tailored Rotor Blades*** - Four composite rotor blades with a dual spanwise segmented flap-bending/torsion coupling (FBT-P/N) significantly reduce the 4/rev vibratory hub loads on the Condor. Along with the vibration reduction provided by the active flap IBC, the composite tailored rotor blades eliminate most of the vibrations from the helicopter fuselage, providing a *jet smooth* ride.



***Bearingless Hub*** - The Condor uses a bearingless hub for higher control power which provides excellent handling qualities. Furthermore, the bearingless hub creates less parasitic drag in high speed forward flight.

***De-icing System*** - Provision for de-icing the rotor blades and other vulnerable areas have been provided to enable the Condor to operate in the low temperature environment associated with high altitudes.

***Crashworthiness*** - Special attention has been paid to the crashworthiness of the CONDOR, particularly in the design of the airframe, the selection of equipment, and the arrangement of the fuel system. In the airframe, the structural members are designed for maximum energy dissipation in the event of a crash. In addition, all furnishings such as seats and litters are rated for the inertial loads specified for certification (14CFR29.561), and medical equipment is securely packed and stowed.

***Health Usage and Monitoring System (HUMS)*** - HUMS capability is designed into the Condor to help track the usage of flight critical components, and provide credits to standard maintenance schedules. The HUMS will lead to reduced maintenance cost as well as increased reliability, readiness, and safety.

***Cost*** - Through use of high reliability subsystems and thoroughly proven technology, the Condor will have reduced maintenance and operational costs. This is especially attractive to prospective users such as volunteer rescue organizations who have limited budgets.

***Certification*** - The Condor is designed for certification under CFR Title 14, Part 29, Airworthiness Standards: Transport Category Rotorcraft. Designed with currently available engines and subsystems, the Condor will be easy to certify and at the same time offers high reliability and safety in all modes of flight operation.

## **Conclusions**

The Condor design offers an affordable and reliable platform designed to meet the unique requirements of a mountain search and rescue operation. The use of existing state-of-the-art equipment and subsystems satisfies certification requirements and results in a short development program. The Condor's use of innovative design technologies provides unsurpassed safety and reliability while reducing maintenance and operating costs. Specifically tailored for high altitude operation, the Condor meets, and in many cases exceeds the performance requirements in the RFP. Furthermore, its high power-to-weight ratio allows for multi-mission capability. The Condor design is the ideal solution for the task of high altitude rescue operations.



## Performance Summary and Design Features

### Performance Data

	Sea-Level	3,658 m (12,000 ft)
Design Cruise Speed (knots)	140	145
Speed for Best Range (knots)	140	145
Speed for Best Endurance (knots)	60	70
Max Cruise Speed (knots)	170	170
Max Range - Full w/ Reserve (km)	678	685
Max Endurance - Full w/ Reserve (h)	2.56	2.48
Max VROC (m/s)	13.3	13.1
Max Climb Rate (m/s)	34	33.3
HOGE Ceiling, Cont Power (m)	6,705	
OEI HOGE Ceiling, Cont Power (m)	3,660	
Service Ceiling (m)	7,620	

### Vehicle Dimensions

Fuselage Length (m)	10.96
Overall Length (m)	13.91
Height - Hub (m)	3.44
Wheel Height (m)	0.5
Fuselage Width (m)	1.6
Horizontal Stabilizer Span (m)	0.4
Fuel Capacity (L)	970

### Weights

Design Gross Weight (kg)	3024
Empty Weight (kg)	1533
Useful Load (kg)	1491
- Max Useable Fuel (kg)	650
- Crew (kg)	191
- SAR Equipment (kg)	113
- Max Payload (kg)	537

### Engine Ratings

Engine TO Power (kW)	2028
Engine Max Cont (kW)	1910
Engine OEI Cont (kW)	1014
Engine OEI 2 min (kW)	1108
Transmission Max Cont (kW)	1360
Transmission OEI Cont(kW)	680
Transmission OEI 2 min (kW)	800

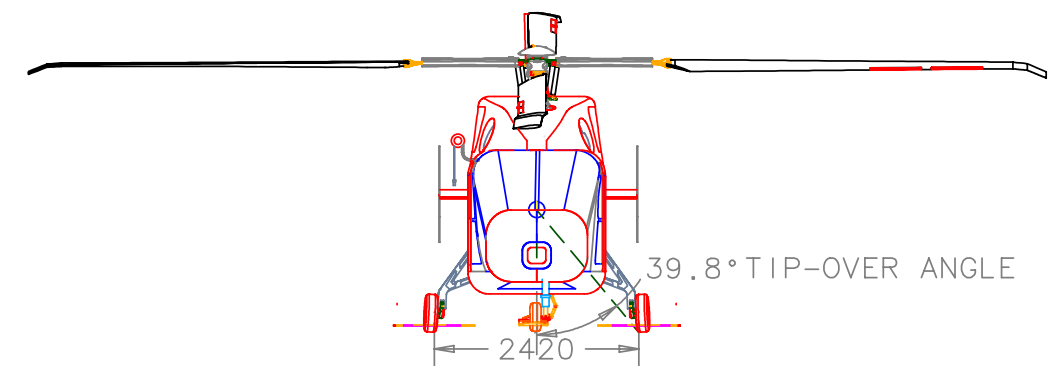
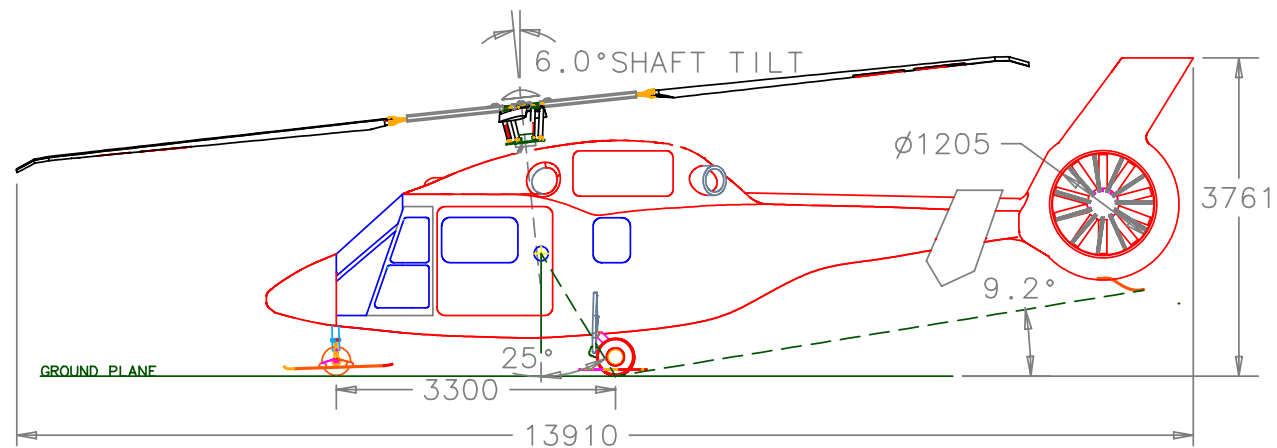
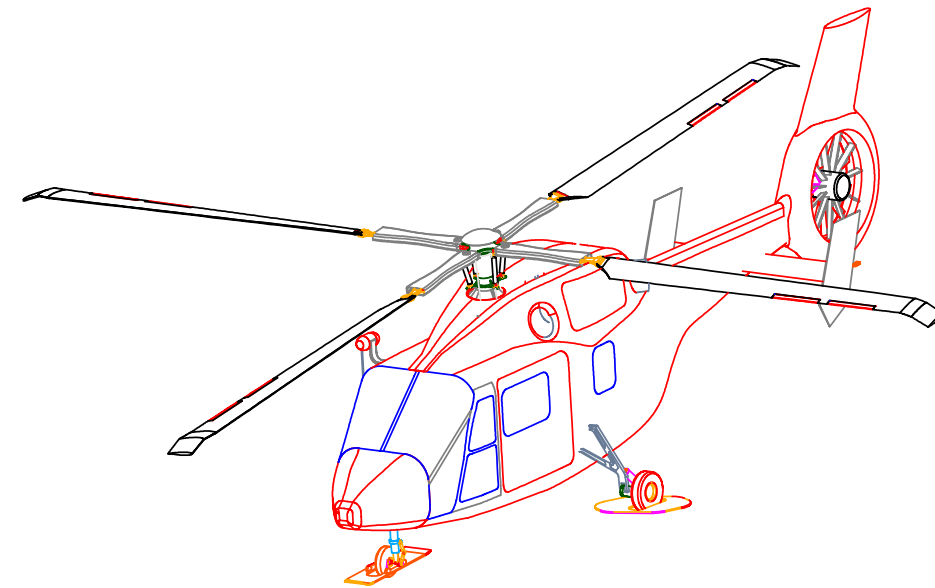
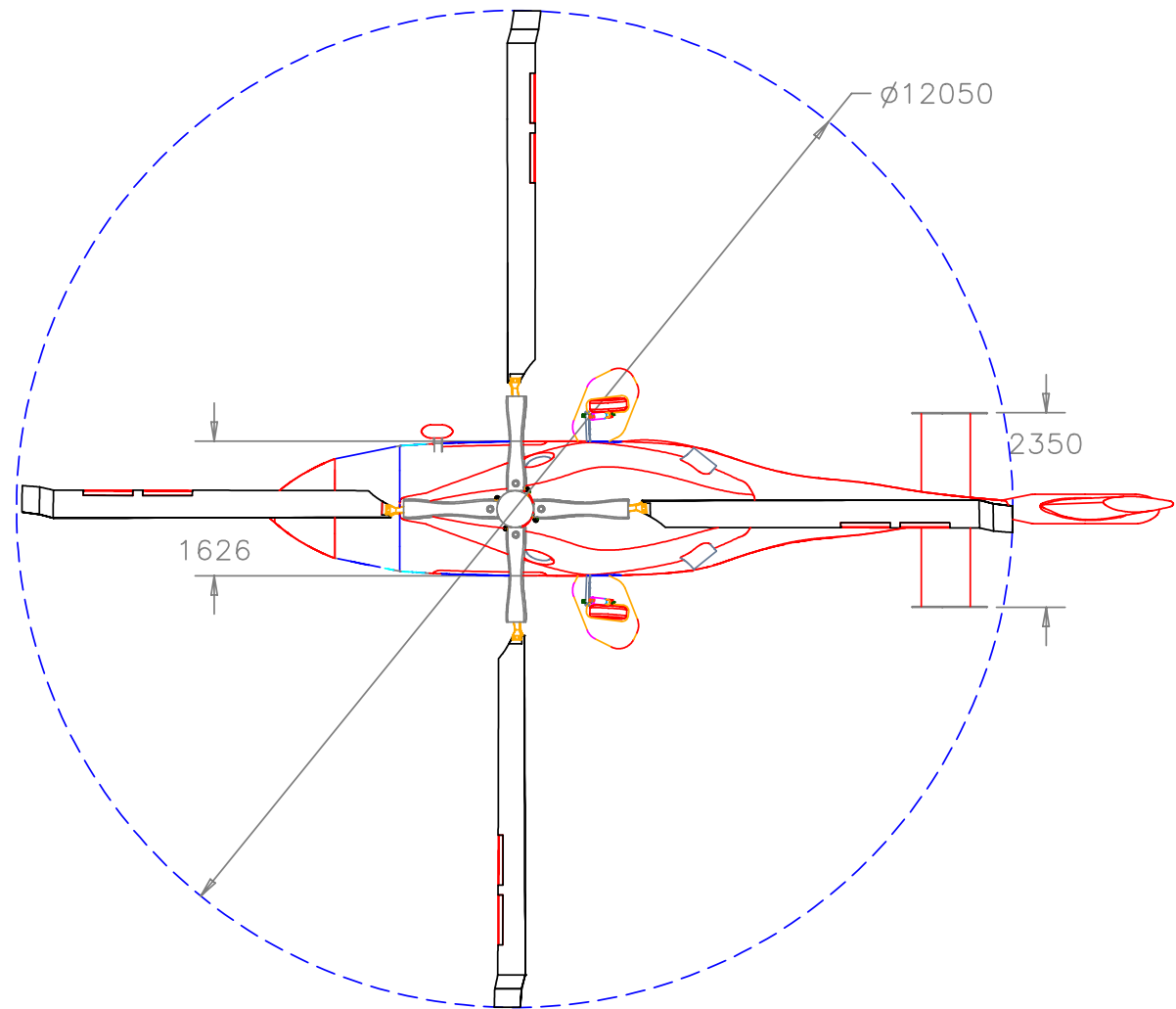
### Main Rotor Specifications

Diameter (m)	12.05
Number of Blades	4
Chord	
- Root (m)	0.344
- Tip (m)	0.31
Solidity	0.0727
Disk Loading (kg/m <sup>2</sup> )	26.5
Blade Twist (deg)	-12
Tip Speed (m/s)	210
Shaft RPM	333
Shaft Tilt (deg)	6
Tip Sweep (deg)	20
Tip Anhedral (deg)	20
Root Cutout	25%
Airfoil Sections	RC(4)-10, RC(6)-8

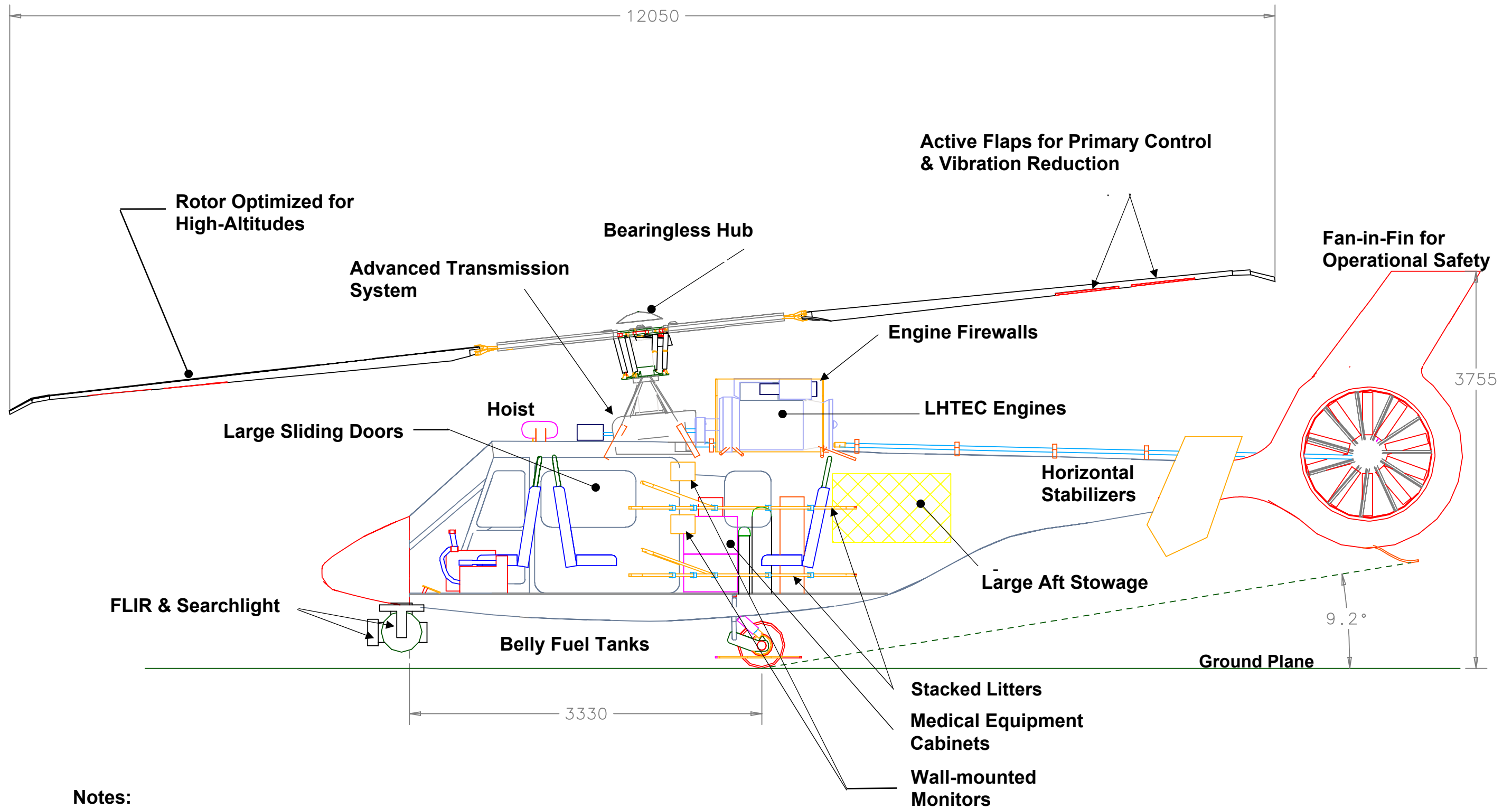
### Fan-in-Fin Specifications

Diameter (m)	1.2
Number of Blades	10
Chord (m)	0.114
Solidity	0.606
Blade Twist (deg)	-10
Tip Speed (m/s)	180
Shaft RPM	2853
Root Cutout	30%
Airfoil Sections	NACA 63A312

# Four View Drawing



All dimensions in millimeters



**Notes:**  
 All Dimensions in Millimeters  
 For Clarity, Nose Gear & Cowling Not Shown

**Inboard Profile**



## **Section 1 - Introduction**

This proposal describes the design of the Condor, a mountain search and rescue helicopter designed specifically for high altitude rescue operations including the use of a hoist. The design was developed in response to the Request for Proposals for the AHS/NASA Student Design Competition sponsored by Agusta Westland. The RFP identified the need for a helicopter conceived from the start as a platform specifically designed for mountain rescue operations. Indeed, the RFP recognizes that existing helicopters performing SAR missions in mountainous areas are adaptations of models designed to meet other requirements. Consequently, several aircraft features desired by crews performing these missions are either unavailable or are accomplished inefficiently. It is the objective of this proposal to present a design not only performing well at high altitude, but also including several features aimed at making the aircraft more reliable and mission capable.

Steps were taken throughout the design process to meet, and even exceed, all of the design requirements stipulated by the RFP, while at the same time developing a cost effective design solution that was safe and reliable, and included state-of-the-art technologies. While the Condor's subsystems include many innovative technologies, the design team was conscious of the RFP's intent for a proposal capable of being certified under CFR/JAR. Special care was taken not to incorporate any unproven and infeasible technology, ensuring a realistic aircraft and leading to greater mission success - the ultimate goal.

## **Section 2 - Identification of Design Drivers**

This section outlines the steps taken to identify the design drivers of the envisaged mission. These design drivers would later be used to select the general aircraft configuration, as well as provide a fundamental justification for all decisions made throughout the design process. The primary sources for the design drivers were identified as being: the need to meet the SAR performance capabilities, the requirements set forth in the RFP including certification requirements, and the demands imposed by the unfriendly operating environment of the helicopter inherent to mountain rescue operations. These are reviewed in the following sections, along with their impact on the design task.



## **2.1 - Mountain SAR Performance Capabilities**

As stated previously, no existing helicopter has been conceived for the sole purpose of mountain rescue operations. It was, therefore, difficult to judge the characteristics that would be inherent to such an aircraft. As a result, a detailed mission study was performed to identify the primary elements of mountain SAR missions, which have the most impact on mission success.

### **2.1.1 - SAR Mission Requirements**

A general SAR mission consists of three distinct operating segments:

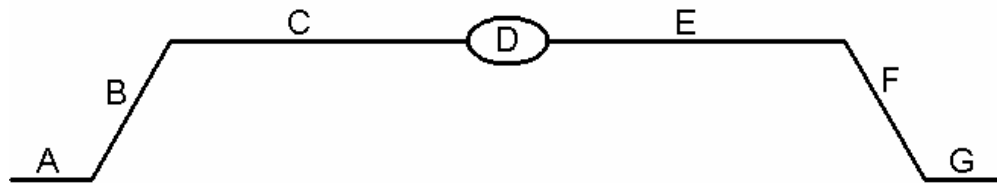
- (i) *Cruise* - The primary need during this mode is a higher flight speed. Victim survival rate decreases dramatically with time enroute, so it is necessary to respond to distress calls and arrive at the rescue location as quickly as possible. Likewise, flight speed during the return flight to a hospital or medical center is critical. Adequate on-board medical equipment must also be available and effectively used to provide care to the victims while in route to the hospital.
- (ii) *Search* - After arriving at the general rescue location, a search for the victim begins. This mode involves low speed flight while the SAR team searches for victims. The primary need in this mode is the efficient use of advanced search equipment to locate the victim in a low visibility environment. Good low-speed flight handling characteristics and low fuel burn for good endurance are important factors in this mode.
- (iii) *Rescue/Hoist Operations* - Soon after location of the victims, the objective of the SAR team is to load the victims onboard as quickly and as safely as possible. Low downwash from the main rotor will assist the SAR team by not kicking up snow, loose dirt, etc., that would limit visibility or frighten victims. Placement of the door and hoist are also key factors in the execution of this mission. After the victims have been hoisted on-board, a roomy cabin is required for the placement of the victims and medical team, as well as for storage of the various required medical equipment.

### **2.1.2 - Mission Profile**

The RFP stipulates a SAR mission consisting of takeoff from 1,829 m (6,000 ft), a one hour outbound leg with 4 crew at 140 knots, a 20 minute on station hoist operation with recovery of 2 patients at 3,658 m (12,000 ft), and a one hour return leg at 140 knots. The RFP does not identify the altitude at which the cruise leg of the mission takes place. Because mountain ranges have various terrains, it was necessary to examine all possible scenarios. As a result, several mission profiles were developed as possibilities for typical mountain rescue operations. The most



demanding mission profile was used to identify design drivers which is summarized in Table/Figure 2.1. Because the cruise legs of the mission profile occur at 3,658 m (12,000 ft), the rotor will be operating at high thrust coefficients, making it more susceptible to blade stall. To meet the requirement of 140 knot cruise speed, the aircraft will need to be aerodynamically clean so that it is efficient in cruise. Another design driver presented by the mission profile is the hovering capability required at 3,658 m (12,000 ft) during the rescue operation. This capability will require high power, and so a good hovering performance is essential to mission success.



**Table/Figure 2.1 - SAR Mission Profile**

Segment	Description	Altitude	Time	Distance	Speed	Power req'd	Flight Condition
A	Warm up	1,829 m	10 min.	0	0	Idle	~
B	Take off/Climb	1,829 ft - 3,658 m	5 min.	11.5 km	75 knots (ROC=365 m/min)	Climb	Max TO weight
C	Cruise	3,658 m	57.3 min.	247.8 km	≥140 knots	Cruise	~
D	Loiter/Rescue	3,658 m	20 min.	0	0	Hover	Maintain heading in 40 knot wind (4,572 m)
E	Cruise	3,658 m	57.3 min.	247.8 km	≥140 knots	Cruise	2 extra passengers
F	Descend/Land	3,658 m - 1,829 m	5 min.	11.5 km	75 knots	Descend	2 extra passengers
G	Shut down	1,829 m		~	~	Idle	~

**2.2 - Operating Environment**

In addition to demanding SAR requirements, the mountainous terrain may also involve operation in extreme weather conditions. The operating environment for most mountain rescue missions can be risky and even hazardous and, therefore, the design should include adequate measures to ensure mission safety. Among the hazards of operating at high altitudes in a mountainous environment are aircraft icing, high velocity winds and gusts, and low visibility from snow or fog. In addition, the mountain terrain itself may force the aircraft to operate in confined spaces. The



design should, therefore, be compact and the helicopter must have good low speed handling and maneuvering flight capabilities.

### **2.3 - RFP Requirements**

Several design drivers were identified from the requirements stipulated directly in the RFP. The most demanding of the RFP requirements is the HOGE at MGW up to 3,658 m (12,000 ft), under OEI conditions. This requirement should be met with the engines at their 30 minute power rating. The need to meet this high power condition with OEI significantly raises the amount of power needed from the aircraft's engines. Some of the other important requirements stipulated in the RFP are:

- (i) All engines operative (AEO), HOGE at MGW up to 4,572 m (15,000 ft).
- (ii) Cruise speed of at least 145 knots.
- (iii) Anti-torque control system capable of maintaining heading in hover at 4,572 m (15,000 ft) with wind of at least 40 knots from any azimuth.
- (iv) Capability of operation on snow (snow landings).
- (v) Designed to meet CFR Title 14, Part 27 or Part 29, or JAR Part 27 or Part 29. Also, certifiable for Single Pilot day / night IFR operations.

### **2.4 - Design Drivers**

A list of desirable design characteristics developed for the specific design task from a combination of the mission requirements, RFP requirements, and flight operating environment is given in Table 2.2. These characteristics will be used in the following section to rate several candidate helicopter configurations.



**Table 2.2 - Description of Design Drivers**

Driver	Description	Source
Hovering Efficiency	Because of high altitude requirements stipulated in the RFP, it is important for the aircraft to hover with as little power as possible. <u>Requires:</u> large rotor diameter, large blade twist.	RFP
Cruise Efficiency	Cruise at high lift/drag to minimize fuel consumed and increase range and distance. <u>Requires:</u> small rotor diameter, low blade twist.	SAR
Max Speed	A helicopter with a high maximum speed will decrease the overall rescue time, increasing the chances of survival for the rescued victims. <u>Requires:</u> low rotor diameter, low parasite drag.	SAR / RFP
Low Speed Endurance	If the aircraft has a high endurance during low speed flight, it will allow more time for the search and rescue parts of the mission. This is especially helpful if the exact location of the victims is unknown. <u>Requires:</u> efficiency in low speed flight.	SAR
Power Req'd for Anti-Torque	The ability of the anti-torque system to provide control with a small amount of power will ensure adequate handling during high power modes of flight, such as high altitude hover out of ground effect. <u>Requires:</u> low main rotor torque, high authority anti-torque system.	RFP
Downwash	Low downwash velocities will assist the crew in performing rescue operations and allow the helicopter to land at unprepared sites. <u>Requires:</u> large rotor diameter.	SAR / Environment
Compact Configuration	A compact aircraft allows operation in confined locations that may be encountered in a mountainous environment. <u>Requires:</u> short tail boom, small rotor diameter.	SAR / Environment
Rescue Operational Safety	Because of the extreme environment inherent to rescue missions, it is necessary to design the helicopter as safely as possible to increase the rate of mission success. <u>Requires:</u> good handling characteristics, low pilot workload, and autopilot capabilities.	SAR / Environment
Cost	Lower operational and acquisition costs of the aircraft will make the designed helicopter affordable and attractive to rescue organizations. <u>Requires:</u> low maintenance need, low fuel consumption, low certification cost.	SAR
Mechanical Complexity	Overly complex designs will decrease reliability and increase required maintenance leading to higher cost. <u>Requires:</u> simple technology, low moving parts count.	SAR
MGW/Payload	A lower ratio will lead to a lighter, cheaper helicopter. Also, particular consideration is given to low MGW to payload ratios from the RFP. <u>Requires:</u> efficient rotor, low empty weight.	SAR / RFP
Technology Maturity	Use of unproven technology in the design decreases reliability and makes aircraft certification involved and difficult. <u>Requires:</u> simple design, use of proven technology.	RFP
Autorotation	Autorotative capability increases mission safety and allows for aircraft certification. <u>Requires:</u> high rotor inertia.	SAR / RFP
Fast Loading and Unloading	Without obstacles such as wings, tail booms, etc. in the way, critical patients can quickly be transported from the rescue site to the hospital. <u>Requires:</u> unobstructed loading and unloading paths.	SAR
Multi-mission Capability	Having the ability to adapt the aircraft for various missions expands its market and makes it more affordable. <u>Requires:</u> all-around good performance capability.	~



## Section 3 - Configuration Selection

In this section, the final helicopter configuration selection, as well as the methods employed to arrive at the selection are presented. A qualitative configuration evaluation, based on the design drivers developed in the previous section, as well as a thorough study of existing aircraft, were used to determine the best choice for this design.

### 3.1 - Qualitative Evaluation

#### 3.1.1 - Evaluation Method

A configuration selection matrix was created by assigning numerical scores to each configuration in categories based on the previously developed design drivers. Each design driver was given a predetermined weighting factor based on its impact on the design task. The weighting factors are shown in Table 3.1. The inherent characteristics of the configurations were studied and evaluated with numerical scores based on their ability to meet the specified design drivers. The scores were based on a qualitative analysis using design experience, information from the literature, and team discussions. Scores were determined based on ratings from excellent to poor, and are shown in Table 3.2. To allow for greater flexibility, fractions of points were assigned in the scoring method. The scores for each category were then multiplied by the weighting factor in each category and summed up for each configuration. The maximum possible score was 128 points. This was used to short list configurations for further consideration. The completed configuration selection matrix is shown in Table 3.3.

**Table 3.1 - Weighting Factors**

Weighting Factor	Description
3	Critical
2	Major
1	Minor

**Table 3.2 - Ratings**

Rating	Description
4	Excellent
3	Good
2	Fair
1	Poor



**Table 3.3 - Configuration Selection Matrix**

Design Drivers	Weight Factor	Conventional - Tail Rotor	Conventional - Fan-in-Fin	Conventional - NOTAR	Tilt-rotor	Co-axial	Compound	VTDP	Synchropter
Hovering Efficiency	3	3.6	3.6	3.6	3	4	3.4	3	4
Cruise Efficiency	3	3	3.2	3.2	4	2	3	3	2.5
Low Speed Endurance	2	4	4	4	2	4	4	4	4
Max Speed	2	2.9	3	3.1	4	2.8	3.2	3.2	2.9
Power Req'd for Anti-Torque	1	2.5	2.3	2.1	4	4	2.5	2.2	4
Downwash	3	4	4	4	2	3.8	4	4	3.8
Compact Configuration	2	3	3	3	2.5	4	3	3	4
Rescue Operational Safety	3	3	4	4	3	4	3	3	3
Cost	3	4	3.8	3	2	3.5	3	3	3.5
Mechanical Complexity	2	4	4	3.5	2	3.5	3	2.5	3.5
Payload/MGW	2	4	4	3.8	2	4	3	2.9	4
Technology Maturity	1	4	4	3	3	3.5	3	3	4
Autorotation	3	4	4	4	2	3.8	3	3	3.8
Fast Loading and Unloading	1	3	4	3.8	2.5	4	2.5	2.5	3.5
Multi-mission Capability	1	3.5	3.5	3.5	2	3.5	3	3	2.5
<b>Final Score</b>	<b>128</b>	<b>113.6</b>	<b>117.6</b>	<b>112.6</b>	<b>84.5</b>	<b>114.9</b>	<b>101.6</b>	<b>98.9</b>	<b>112.6</b>

**3.1.2 - Evaluation Results**

The following configurations were considered as possibilities for this design. The advantages and disadvantages of the candidate configurations are summarized along with the scores resulting from the qualitative evaluation. The candidate configurations are listed in order from best to worst score.

**Conventional - Fan-in-Fin (Score: 117.6):** The conventional single rotor helicopter with a fan-in-fin anti-torque device was the highest scoring configuration. The fan-in-fin scored well because of its all-around good attributes, as well as the added bonus of safety from the shrouded tail rotor. Because safety during both rescue operation and ground loading and unloading of patients is a high priority for this design task, the fan-in-fin is an attractive option.



**Co-axial (Score: 114.9):** The co-axial rotor design consists of two counter-rotating main rotors mounted on a single axis. This configuration generally has better hovering efficiency than a single rotor, and because it does not require an anti-torque device, the resulting configuration is very compact. The lack of a tail rotor and lengthy tail boom also make the configuration compact, allowing safe flight operations in confined areas. However, because adequate clearance is required between the two rotors to prevent blade collisions, the resulting hub is complex and has a high drag, which in turn results in poor efficiency at the required cruise speed of 145 knots.

**Conventional - Tail Rotor (Score: 113.6):** This configuration uses an unshrouded tail rotor that is usually about twice the area of the shrouded rotor of the fan-in-fin. Although the larger unshrouded rotor requires less power to produce the same anti-torque as the shrouded rotor, its exposed configuration makes it more susceptible to safety hazards. Since safety is a primary concern for this design, the advantages of the lower power requirements were deemed to be less important than the safety issues.

**Conventional - NOTAR (No tail rotor) (Score: 112.6):** The NOTAR system relies on the Coanda effect in hover to produce anti-torque. The lack of a tail rotor makes the NOTAR ideal for safety in ground and rescue operations, but the system generally requires more power than the fan-in-fin, and may have problems operating in high cross winds. Furthermore, the cost, complexity, and less mature technology make the NOTAR less desirable than the conventional or fan-in-fin configurations.

**Synchropter (Score: 112.6):** The synchropter configuration uses two intermeshing main rotors, resulting in an efficient hovering capability. However, the drag penalty incurred by having two rotor hubs, as well as stability problems at high speeds, limits the synchropter's maximum forward flight speed. In addition, clearance of the intermeshing rotors over the doors of the helicopter is a safety issue and could limit the speed at which loading and unloading could occur.

**Compound (Score: 101.6):** A compound configuration relies on some type of augmented thrust and/or lift system, in addition to the main rotor. In forward flight, the main rotor is off-loaded, allowing the compound configuration to exceed the maximum speeds of a conventional helicopter. However, the presence of the additional thrust/lift system such as a wing, propeller, etc., can increase the empty weight fraction of the aircraft as well as impede passenger loading and hoisting paths.

**Vectored Thrust Ducted Propeller (VTDP) (Score: 99.5):** The VTDP is a type of compound configuration, but was considered separately because of its unique propulsion system. The VTDP uses a shrouded tail rotor/propeller to provide anti-torque as well as an additional propulsion source. Because the tail rotor/propeller is shrouded, the VTDP offers greater operational safety



than most other compound helicopters. Drawbacks of the VTDP are the mechanical complexity and cost of the tail rotor/propeller, and the high power requirements of the anti-torque system in hover. Overall, the unproven technology used in the VTDP makes it a risky choice for this design.

**Tilt Rotor (Score: 84.5):** The tilt rotor uses its highly loaded main rotors tilted forward as propellers during cruise flight, relying on wings to produce lift. Because the tilt rotor is not limited to the same forward flight constraints of the conventional helicopter, it can achieve much higher cruise speeds and is generally more efficient in cruise. During hover, however, the highly loaded main rotors generate high downwash velocities that can hinder rescue operations. Furthermore, the technology for this configuration is mechanically complex and more expensive. Finally, the lack of safe autorotative capability makes this concept less attractive for rescue operations.

**3.2 - Historical Survey**

Before choosing a final configuration type for this design, it was necessary to examine existing helicopters with performance capabilities meeting the design requirements. An extensive survey was carried out, and it was found that although several helicopters nearly matched the performance requirements of the RFP (Table 3.4), none satisfied all of them. A selection of these aircraft, obtained from *Jane's All the World's Aircraft*, is shown in Table 3.5, along with their key performance specifications. Most of the existing helicopters with a combination of high cruise speed and high altitude capabilities were of the conventional helicopter configuration. The KA-50 is an existing military co-axial rotor helicopter that has performance capabilities close to those envisaged in the RFP. This aircraft, however, is a high-powered military combat helicopter and is not ideal for this type of rescue operation.

**Table 3.4 - RFP Performance Requirements**

Requirement	Weight	Available Power	Altitude	Speed
HOGE, OEI	MGW	30 min.	3,658 m	~
HOGE, AEO	MGW	Max. Continuous	4,572 m	~
Cruise Speed	MGW	Max. Continuous	≤3,658 m	145 knots

**3.3 - Final Configuration Selection**

After performing a qualitative analysis on several configurations and reviewing existing helicopters with high altitude and high cruise speed performance capabilities, only two options appear attractive for this design solution. The first candidate configuration is the conventional



rotor type with a fan-in-fin tail rotor. The conventional single rotor helicopter has excellent all around performance capabilities and is the most proven among all the configurations. In addition, the shrouded tail rotor provides increased safety during flight operation in confined spaces, as well as during the loading and unloading of patients. This is especially relevant during rescue missions, when it can be assumed that people, such as paramedics, rescuers, etc., will be moving quickly without caution around the helicopter.

**Table 3.5 - Historical Survey**

Description	Configuration	# of Engines	D <sub>MR</sub> (m)	MGW (kg)	Payload (kg)	HOGGE Ceiling (ft)	Speed (knots)
Agusta A109 K2	Conventional	2	11	3,000	1,200	4,023	143
Agusta A119 Koala	Conventional	1	11	3,150	1,290	3,261	144
Astar AS 350 B3	Conventional	1	10.5	2,250	1,069	3,210	133
Bell/Augusta AB 139	Conventional	2	13.5	6,000	2,500	3,658	157
Bell 407	Conventional	1	10.5	2,268	1,065	5,365	136
Bell 430	Conventional	2	13	4,218	1,800	4,450	143
EC 135	Fan-in-fin	2	10	2,835	1,375	3,581	140
V-22	Tiltrotor	2	11.5 x 2	21,545	6,804	4,328	275
KA-50	Coaxial	2	14.5	13,127	1,811	4,000	149

## Section 4 - Preliminary Sizing

The goal of the preliminary sizing stage was to develop designs that meet the requirements of the RFP and to perform trade studies to select the best design. The trade studies performed in this stage were the variation in the number of rotor blades, rotor solidity and number of engines. The overall size of each design was determined in terms of MGW and rotor diameter. In addition, the component weights and acquisition costs were estimated using a methodology developed by Marat Tishchenko of the Mil Design Bureau [Tish04]. The candidate designs were then compared over various design parameters to select the best configuration.

### 4.1 - Design Requirements

The payload requirements for the helicopter are given in the RFP are two crew members, two paramedics, two patients and the necessary equipment to provide medical care to the patients. The required mission is described in the RFP as takeoff at 6,000 ft, an outbound leg of 1 hour cruising at 140 knots, a 20 minute hoisting operation hovering at 3,658 m (12,000 ft) and an



inbound leg of 1 hour cruising at 140 knots. The key performance requirements for the helicopter are a cruise speed of 145 knots at up to 3,658 m (12,000 ft), a HOGE capability at MGW up to 4,572 m (15,000 ft), and the capability for OEI HOGE at MGW up to 3,658 m (12,000 ft). The latter requirement proved to be the most stringent in the analysis in terms of engine power requirements, giving the number of engines trade study great importance.

**4.2 - Method of Analysis**

The analysis, modified specifically for the high altitude requirements of this design, uses an iterative process that begins with input specifications such as the required payload and range of the aircraft. A series of performance and sizing calculations based on these requirements and other user inputs such as propulsive efficiency, lift-to-drag ratio, transmission efficiency, tip speeds, and figure of merit are performed. Once these calculations are complete, a series of

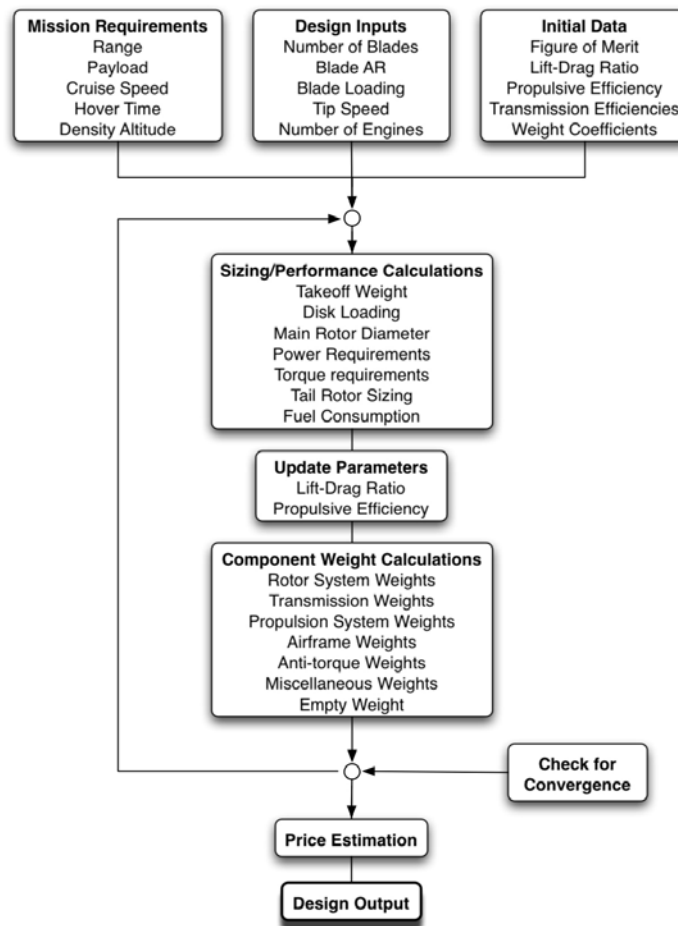


Figure 4.1 - Block Diagram for Design Code



component weight calculations are performed based on correlation equations obtained from historical data. Next, these component weights are used to sum up the empty weight and recalculate the weight efficiency. This value is then substituted into the previous calculations and the program runs iteratively until convergence is achieved. After the analysis converges, acquisition and operating costs are evaluated based on empirical equations and factors developed by Tishchenko [Tish04]. The flow of the design methodology is depicted in Figure 4.1. This entire process is run concurrently for various combinations of number of blades, blade aspect ratio, and number of engines. This allows the direct comparison of various configurations and ultimately the selection of the best design. The tail rotor sizing and weight equations were modified to model the fan in fin design of the Condor.

### **4.3 - Trade Studies**

The trade studies performed in the preliminary sizing process included the variation in the number of rotor blades, the rotor solidity, and the number of engines. The most critical trade study was the selection of the number of engines. To satisfy the RFP and certification requirements, a multi-engine configuration must be used. Therefore, it was decided to assess the relative benefits of two-engine and three-engine configurations.

This study was conducted in two parts. The first analysis performed design predictions using engine data based on averages of existing helicopter engines. Thus, the power-to-weight ratio, variation in available power with altitude, specific fuel consumption (SFC) and variation in SFC with engine power were constant across all configurations. While there is considerable variation in these parameters for different engines, the use of average values simplified the analysis enabling the assessment of the design characteristics of multiple configurations. This part of the study was useful in examining the effects of changing various design parameters and selecting the best configuration in terms of number of blades and rotor solidity for the two-engine and three-engine cases. The calculated power requirements for the candidate configurations were then used to aid in the selection of actual engines for each case. Then a final analysis was performed using the actual data for the selected engines to size each configuration for comparison.

### **4.4 - Initial Sizing**

In performing the first analysis, it was found that the high altitude operation created the need for high engine weights, leading to relatively high empty weight fractions (0.55+) and low payload to



MGW ratios for most configurations. Because of this, minimizing the power requirements became a critical driver to bring down the overall weight and cost of the helicopter. This was done initially by operating at low disk loadings. Figure 4.2 shows that for a given number of blades ( $N_b$ ), the lowest disk loading is obtained by choosing the largest blade aspect ratio ( $R/c$ ). Because the analysis holds blade loading constant, the highest blade aspect ratio also corresponds to both the lowest rotor solidity and largest rotor diameter for a given number of blades. It is also clear from Figure 4.2 that choosing the highest blade aspect ratio (lowest disk loading and solidity) results in the lowest empty weight for the same number of blades. It was also found that the highest blade aspect ratio corresponds to the lowest gross weight, lowest empty weight fraction, highest payload to max gross weight ratio, lowest fuel weight, and lowest acquisition

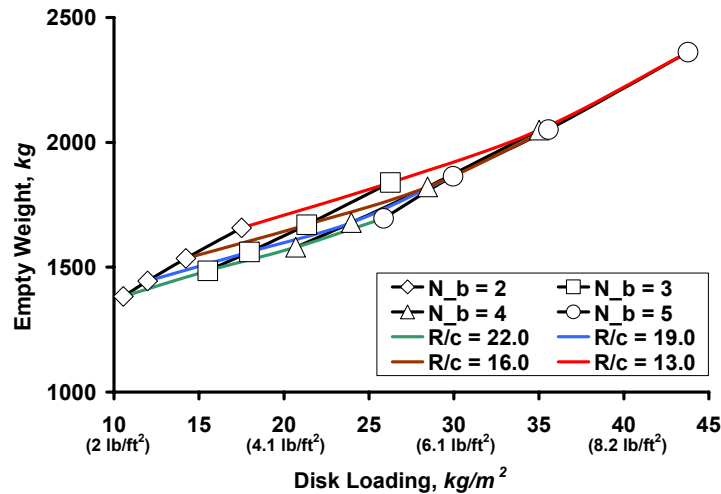


Figure 4.2 - Empty Weight vs. Disk Loading for Varying Number of Blades (3 Engines)

price. However, it also resulted in the highest main rotor diameter, which is a significant disadvantage in coming up with a compact aircraft design - a key design driver. For this stage of the sizing, however, the emphasis was placed on overall weight and price. Thus, the highest blade aspect ratio ( $R/c = 22$ ) was selected for the number of engines trade study except for the three engine, two-bladed rotor case, in which a higher solidity was needed to achieve the design cruise speed of 140 knots. The two and three-engine cases were compared at different number of blades ( $N_b=2-5$ ), comparing various design parameters. Figures 4.3 and 4.4 show the comparisons of the main rotor diameter and takeoff weight versus number of blades for the two-engine and three-engine cases. It can be seen in Figure 4.3 that for all values of  $N_b$ , the three-engine case leads to a smaller rotor diameter. Furthermore, it can be seen that the rotor diameter decreases with increasing number of blades. This is because of the blade aspect ratio and blade

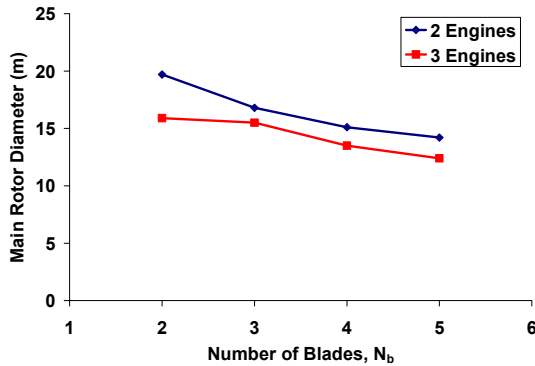


Figure 4.3 - Main Rotor Diameter Comparison

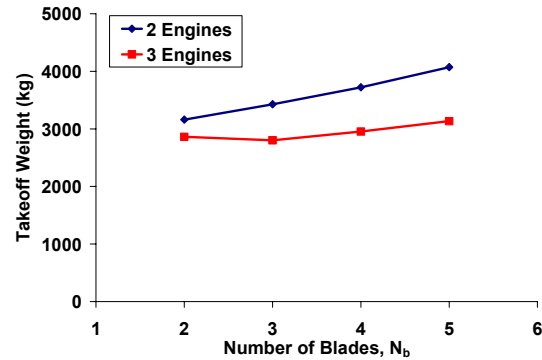


Figure 4.4 - Takeoff Weight Comparison

loading being held constant, leading to increasing solidity and disk loading for the design. In Figure 4.4, it is shown that for all values of  $N_b$ , the three-engine case has a lower takeoff weight relative to the two-engine case. This is because of the two-engine configurations being forced to meet the high OEI power requirement at 50% engine power, where the three-engine configurations are able to meet it at 66% engine power. This means that 50% more total engine power would be required for a two-engine configuration designed to meet the OEI requirement as compared to a three-engine configuration of the same takeoff weight. Because the engine parameters were assumed to be identical for all cases, the additional installed power leads to more empty weight, which drives up the power requirements and takeoff weight. It can also be seen in Figure 4.4 that for the three-engine case, a three-bladed rotor yields the most lightweight design. Figures 4.5 and 4.6 show the comparisons of payload to max gross weight ratio and acquisition cost versus number of blades for the two-engine and three-engine case.

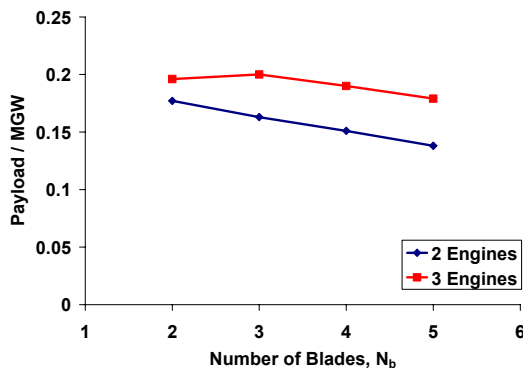


Figure 4.5 - Payload-MGW Ratio Comparison

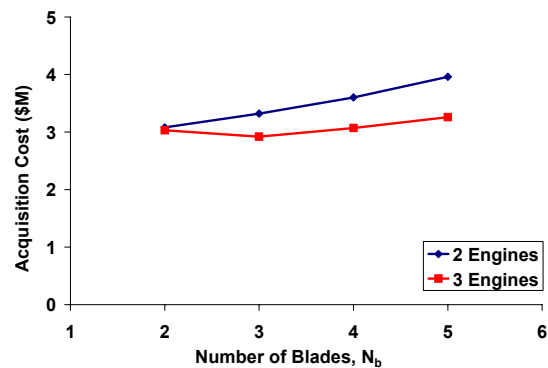


Figure 4.6 - Acquisition Cost Comparison

It can be seen in Figure 4.5 that the three-engine configurations have better payload to max gross weight ratios for all number of blades. However, it should be noted that these weight efficiencies



are low compared to what is seen in most existing helicopters. This is because the helicopter was designed for missions at 3,658 m (12,000 ft). The payload to max gross weight ratio will be higher at sea-level, just as the payload to max gross weight ratios for existing helicopters will

**Table 4.1 - Preliminary Sizing Results**

<b>Number of Engines</b>	<b>2</b>	<b>3</b>
Number of Blades, $N_b$	3	3
Blade AR (R/c)	22	22
Solidity	0.0434	0.0434
Disk Loading (kg/m <sup>2</sup> )	15.5 (3.2 lb/ft <sup>2</sup> )	14.8 (3.0 lb/ft <sup>2</sup> )
M/R Diameter (m)	16.8	15.5
Takeoff Weight (kg)	3428	2801
Empty Weight (kg)	1960	1485
Payload/MGW Ratio	0.163	0.2
Fuel Required (kg)	691	541
Acquisition Cost (\$M)	3.32	2.92
TO Power per Engine (kW)	830	340

suffer considerably at high altitude. Once again, it can be seen that for the three-engine case, a three-bladed rotor gives the best result in terms of weight efficiency. Figure 4.6 shows that the three-engine configurations lead to a lower acquisition cost for a given number of blades. This is a surprising result, considering the extra costs expected in purchasing an additional engine. However, the smaller overall helicopter plays a large factor, and ultimately in this case leads to a lower acquisition price. Thus it was concluded if engine capabilities are held constant, three engines will lead to a design that is lighter, more compact and less expensive to acquire and operate. This is because of the excess power required to meet hover requirements at 3,658 m (12,000 ft) using one engine rather than two, which leads to extra engine weight, higher empty weight and ultimately even higher power requirements. However, because the actual engines have large disparities in performance capabilities, it was necessary to use the power requirements obtained from this analysis to select existing engines and resize the helicopter based on actual engine data.

The design point selected for the three-engine case was the three-bladed rotor at maximum blade aspect ratio, which is shown in Figures 4.3-4.6 to be the most lightweight and least expensive design. For the two-engine case, the two-bladed rotor was found to be the best design in terms of weight and cost, but the size of the rotor and vibration problems associated with two-bladed



rotors led to the selection of the three-bladed case. These design points, listed in Table 4.1, were used to select engines for each configuration

**4.5 - Engine Selection**

There were several factors considered in the engine selection process. The first was the actual engine power required based on the previous analysis. The power requirements per engine were found for both the two and three-engine cases based on the OEI requirements. The power requirements given by the analysis were adjusted to give the required available power at sea-level. The engines were compared based on 30 minute OEI ratings. It was found that for the three-engine design point, approximately 340 kW (455 hp) was required for each engine for a total of 1,020 kW (1,370 hp). For the two-engine design point, approximately 830 kW (1,113 hp) was required for a total of 1,660 kW (2,226 hp). Other requirements for selecting engines were high power-to-weight ratios, specific fuel consumption, and emergency ratings for the strict OEI condition. Candidate engines for each design point are listed in Table 4.2.

**Table 4.2 - Candidate Engines for Two and Three-Engine Configurations**

	Manufacturer	Model	TO Power (kW)	Weight (kg)	P/W (hp/lb)
	Rolls Royce	Gem 42	746	183	2.2
<b>2 Engs.</b>	Pratt & Whitney	PT6B-37A	747	175	2.3
	Turbomeca	TM 333 2B2	840	156	2.9
	LHTEC	CTS-800-4N	1014	185	4.7
	Rolls Royce	Model 250-C28	372	99	2.3
	Rolls Royce	Model 250-C30	546	114	2.8
<b>3 Engs.</b>	Pratt & Whitney	PW 206B	463	112	1.70
	Turbomeca	Arrius 1A	376	103	2.2
	Turbomeca	Arrius 2F	376	103	2.00

A primary consideration for the three-engine case was compactness of design. It was determined that with the given candidate engines and the width of the fuselage that engine layouts with all three engines side-by-side would not be feasible. Therefore, engine layouts having two engines fore and one engine aft of the main rotor were considered, such as in the layout shown in Figure 4.7. This configuration was considered best for center of gravity location but led to significant issues in the design of the main gearbox and the requirement for the engine output shafts to have multidirectional capability. This weighed in heavily on the engine selection for the three-engine

case. The Rolls Royce Model 250-C28 was ultimately selected for the three-engine case because of this multi-directional capability of the output shaft and for having the most compact design.

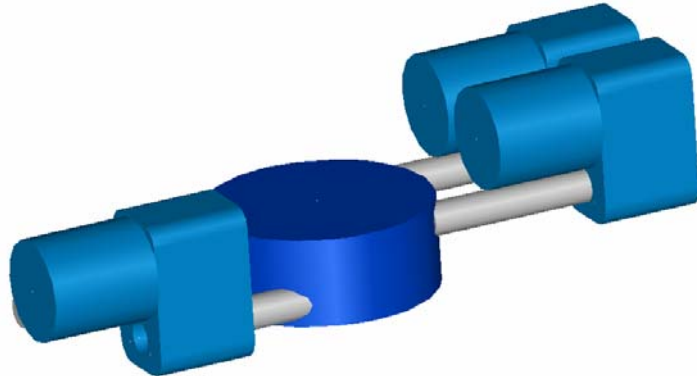


**Figure 4.7 - Engine Layout for Three TM Arrius 2F Engine**

For the two-engine configuration, compactness and multi-directional capability were not such major drivers. It was found that engine layouts for a two-engine configuration presented fewer difficulties in the design of the main gear box and offered the capability to place both engines side-by-side. This allowed the focus to be placed on best power-to-weight ratio and specific fuel consumption. For these criteria, it was found that the LHTEC CTS-800 was far superior to the rest of the candidate engines. The CTS-800 is the civil derivative of the T-800 engine developed for the RAH-66 Comanche. A comparison of specific fuel consumption with output power is given in Figure 4.8.

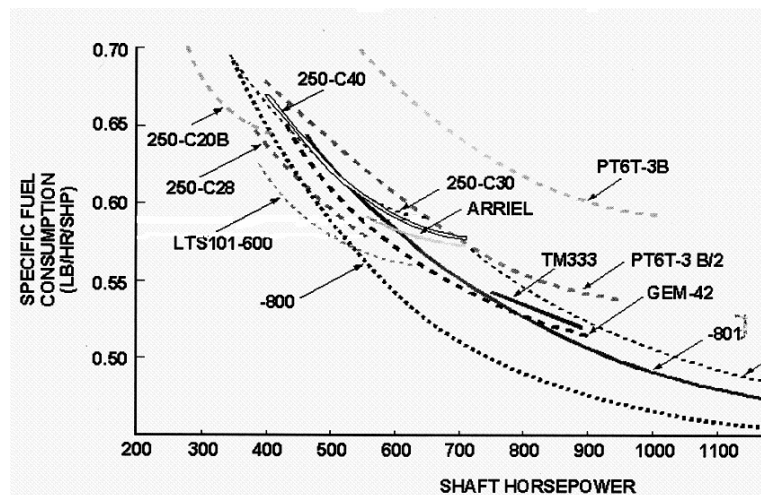


**Figure 4.8 - Specific Fuel Consumption for Existing Helicopter Engines [Tish04]**



As shown in Figure 4.8, the CTS-800 has much lower specific fuel consumption than other existing engines for a wide range of power outputs. This is in large part because of the CTS-800 being a more modern, state-of-the-art engine. It can also be seen in Table 4.2 that the CTS-800 has a much higher power-to-weight ratio than the other candidate engines for the two-engine configuration, making it the lightest of the candidate engines. The only downside to the CTS-800 is its large excess power relative to the design point identified by the previous analysis (830 kW). However, the previous analysis assumed a much lower power-to-weight ratio (1.25 kW/kg) than is realized by the CTS-800.

**Table 4.3 - Selected Engines**

	<b>CTS-800-4N</b>	<b>Model 250-C28</b>
<b>Configuration</b>	Two-Engine	Three-Engine
<b>TO Rating (1 Eng)</b>	1014 kW (1480 shp)	372 kW (500 shp)
<b>TO Rating (Total)</b>	2028 kW (2960 shp)	1116 kW (1500 shp)
<b>Max Cont. (Total)</b>	1910 kW (2561 shp)	1068 kW (1432 shp)
<b>Dry Weight (Total)</b>	370 kg (814 lb)	297 kg (657 lb)
<b>Power/Weight Ratio</b>	2.74 (kW/kg)	1.25 (kW/kg)
<b>SFC (100% Power)</b>	0.28 kg/kW/h	0.35 kg/kW/h

Therefore, installing the CTS-800 engine will allow a smaller rotor diameter to be used (higher disk loading) with no weight penalty relative to the results of the previous analysis (see Table 4.1). A comparison of the engines selected for the two and three-engine configurations is given in Table 4.3. It can be seen that the superior power-to-weight ratio of the CTS-800 leads to a configuration with nearly twice the available power without requiring twice the engine weight. The performance data for these engines were combined with the previous methodology to resize the designs and select the final configuration.

#### **4.6 - Selection of Final Configuration**

The analysis was modified to include the actual engine data for values of power-to-weight ratio, variation in available power with altitude, and specific fuel consumption as a function of relative engine power. For the three-engine case, the Model 250 data were used to obtain a final design, as detailed in Table 4.4. It can be seen that using actual engine data yielded a less desirable design than previously obtained from the results in Table 4.1. This was because the power losses with altitude and specific fuel consumption assumed in the initial sizing were much lower than the actual values for the Model 250. The primary disadvantage of this design point is the large diameter of the main rotor, which was sized to minimize power requirements. However, even at



this low disk loading ( $\sim 3 \text{ lb/ft}^2$ ), the weight efficiency in terms of payload to max gross weight is relatively low.

**Table 4.4 - Results for Three-engine Configuration**

<b>No. of Blades</b>	3
<b>Blade AR (R/c)</b>	22
<b>M/R Diameter</b>	15.8 m (51.9 ft)
<b>Takeoff Weight</b>	3047 kg (6718 lb)
<b>Empty Weight</b>	1641 kg (3618 lb)
<b>PL/MGW</b>	0.184
<b>Fuel Weight</b>	630 kg (1389 lb)
<b>Acquisition Cost</b>	\$3.12 Million

The performance data for the CTS-800 engine was included in the analysis for the two-engine configuration. Unlike the three-engine case, the result was not a point design but for a range of acceptable design configurations. This was because of the high available power, which allowed higher disk loadings and therefore lower main rotor diameters to be achieved. Figure 4.9 shows the results for one engine takeoff power required against disk loading for various configurations of number of blades and blade aspect ratios, keeping engine weight fixed. It can be seen that the available takeoff power of the CTS-800 engine (1014 kW) is high enough to allow disk loadings as high as  $30 \text{ kg/m}^2$  ( $\sim 6 \text{ lb/ft}^2$ ). Such disk loadings are comparable to existing helicopters similar in size to the Condor. The effects of increasing the disk loading on the main rotor diameter is given in Figure 4.10.

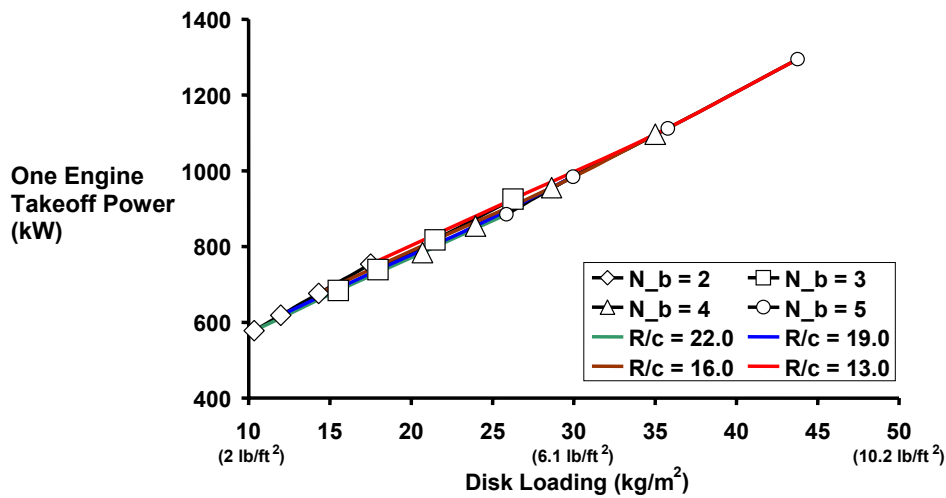


**Figure 4.9 - Two-Engine Results for Takeoff Power Required for One Engine**

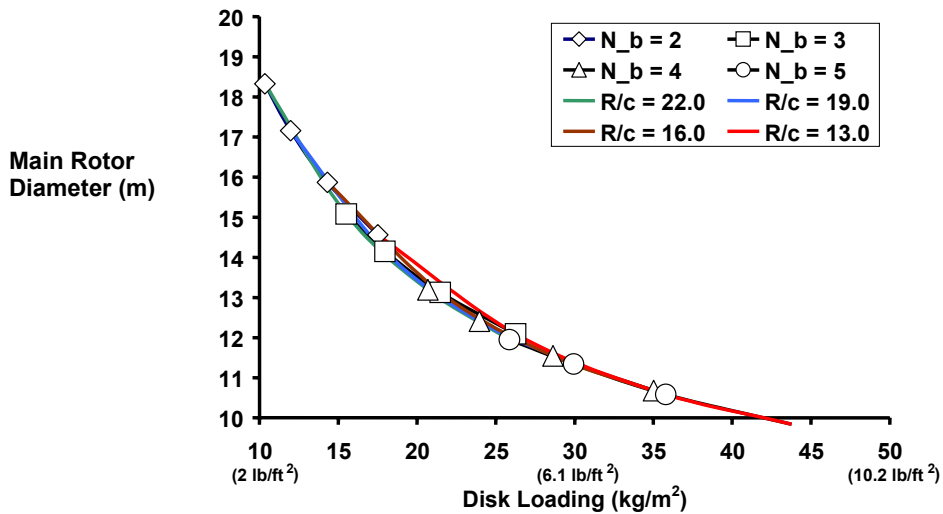


Figure 4.10 - Two-Engine Results for Main Rotor Diameter vs. Disk Loading

It is clear that increasing disk loading decreases the main rotor diameter at a significant rate. The original design point (3-blades, R/c = 22) yielded a diameter of over 15 m, while operating at the maximum allowable disk loading gives a diameter of under 12 m, a much more compact design. Higher disk loadings allows the helicopter to operate closer to the maximum rated power of this engine, which improves the thermodynamic efficiency and, therefore, the specific fuel consumption in all modes of flight. The disadvantages of higher disk loading are increased takeoff weight, fuel weight and acquisition cost. The effects of increasing disk loading on the two-engine results for takeoff weight is shown in Figure 4.11. It can be seen that while increasing disk loading for a given number of blades (lowering blade aspect ratio, increasing solidity) drives up the overall weight of the helicopter, the increase is not extreme because of the total engine weight remaining fixed. This was found to be true of other parameters tested including fuel weight, empty weight, and acquisition cost. It can also be seen in Figure 4.11 that a three-bladed rotor leads to higher takeoff weight relative to four and five-bladed rotors at the same range of disk loadings (25-30 kg/m<sup>2</sup>). In addition, there appears to be little or no difference between the four and five-bladed configurations in terms of takeoff weight for the same disk loading. This was found to hold true for all other parameters investigated, suggesting that there was no significant advantage in choosing a five-bladed rotor over a four-bladed rotor. A four-bladed rotor was, therefore, selected for simplicity of design and lower cost. The tradeoff in disk loading and blade aspect ratio is given in Table 4.5.

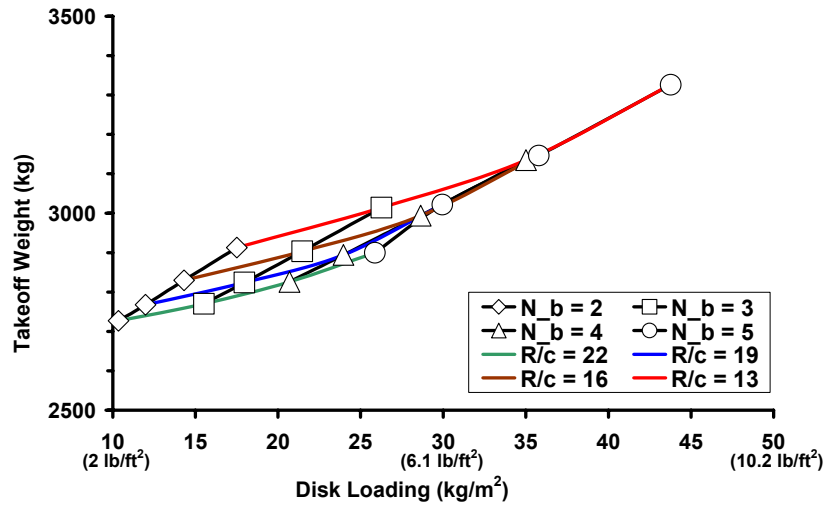


Figure 4.11 – Two-Engine Results for Takeoff Weight vs. Disk Loading

Table 4.5 - Blade Aspect Ratio Comparison for Two-Engine, Four-Bladed Rotor Configuration

Number of Blades, $N_b$	4	4	4
Blade AR (R/c)	16	17.5	19
Solidity, $\sigma$	0.0796	0.0728	0.0670
M/R Diameter	11.63 m (38.2 ft)	12.05 m (39.5 ft)	12.46 m (40.9 ft)
Takeoff Weight	3018 kg (6654 lb)	2964 kg (6535 lb)	2918 kg (6434 lb)
Empty Weight	1637 kg (3610 lb)	1606 kg (3541 lb)	1580 kg (3483 lb)
Disk Loading	29 kg/m <sup>2</sup> (5.9 lb/ft <sup>2</sup> )	26.5 kg/m <sup>2</sup> (5.4 lb/ft <sup>2</sup> )	24.5 kg/m <sup>2</sup> (5.0 lb/ft <sup>2</sup> )
PL/MGW	0.186	0.189	0.192
Fuel Weight	602 kg (1327 lb)	580 kg (1279 lb)	562 kg (1239 lb)
Acquisition Cost	\$3.03 Million	\$2.96 Million	\$2.90 Million
OEI Power Req'd	960 kW (1287 shp)	906 kW (1214 shp)	861 kW (1155 shp)

It can be seen from Table 4.5 that the gross takeoff weight, empty weight, fuel weight and acquisition cost decrease with increasing blade aspect ratio (decreasing disk loading and solidity). The penalties of choosing a higher disk loading (larger rotor diameter, lower solidity) are not severe. The advantages of choosing a lower blade aspect ratio (higher disk loading and solidity) are a smaller diameter rotor and lower excess installed power, which leads to more efficient engine operation. Some of this excess installed power could be used to power auxiliary systems such as a deicing system, which was not factored into the initial calculations. Some excess available power could also be devoted to exceeding some of the requirements in the RFP, such as an increased hover ceiling or cruise speed, or the addition of an extra passenger or paramedic to the RFP mission requirements. A configuration with large excess installed power, however, could significantly degrade the specific fuel consumption of the helicopter in cruise. The final



decision was a compromise between the two extreme cases, taking the median blade aspect ratio of  $R/c = 17.5$  ( $\sigma = 0.0728$ ). This design reaps some of the benefits of a lower disk loading, such as lower weight and cost, while not allowing the rotor diameter to increase significantly.

The design parameters for the two-engine and three-engine configurations are compared in Table 4.6. It can be seen that the two-engine configuration is the ideal choice and is a lighter and more efficient design. The primary advantage of the two-engine configuration is the compactness of the design. The three-engine case requires a rotor that is nearly 4 m (~12 ft) larger in diameter than the two-engine case. In addition, the two-engine configuration with CTS-800 engines possesses the potential to exceed key RFP requirements, such as HOGE and OEI ceilings, maximum cruise speed, and load carrying capability. The reason that the final comparison deviated so greatly from the preliminary sizing results (Table 4.1) is because of the superior engine characteristics of the CTS-800 relative to the Model 250 (Table 4.3).

**Table 4.6 - Final Number of Engines Comparison**

<b>No. of Engines</b>	2	3
<b>No. of Blades, <math>N_b</math></b>	4	3
<b>Blade AR (R/c)</b>	17.5	22
<b>Solidity, <math>\sigma</math></b>	0.0728	0.0434
<b>M/R Diameter</b>	12.05 m (39.5 ft)	15.8 m (51.9 ft)
<b>Takeoff Weight</b>	2964 kg (6535 lb)	3047 kg (6718 lb)
<b>Empty Weight</b>	1606 kg (3541 lb)	1641 kg (2618 lb)
<b>PL/MGW</b>	0.189	0.184
<b>Cruise SFC</b>	0.338 kg/kW/h	0.39 kg/kW/h
<b>Fuel Weight</b>	580 kg (1279 lb)	630 kg (1389 lb)
<b>Acquisition Cost</b>	\$2.96 Million	\$3.12 Million

The final result of the preliminary sizing analysis was the selection of a configuration with two CTS-800 engines and a four-bladed rotor of solidity,  $\sigma = 0.0728$ , and a diameter of 12.05 m (39.5 ft).

## **Section 5 - Aircraft Certification**

The RFP stipulates that the design solution is required to meet CFR Title 14, Part 27 or Part 29. To this end, a certification class was selected, based on preliminary weight estimates, and steps were taken to meet the applicable requirements of that class.



**5.1 - Applicability**

FAR regulations group all rotorcraft into two categories: Normal Category Rotorcraft and Transport Category Rotorcraft. Normal Category Rotorcraft are required to have a maximum weight of not more than 7,000 lb and generally have more lenient requirements for certification than Transport Category Rotorcraft. Transport Category Rotorcraft are further divided into two categories. Any rotorcraft weighing over 20,000 lbs, and carrying 10 or more passengers is required to be certified as a Category A rotorcraft. Any Rotorcraft weighing less than 20,000 lbs and/or carrying 9 passengers or less may be certified as either Category A or Category B. Initial sizing estimates of the Condor showed a MGW of just over 7,000 lbs. It was, therefore, decided to design the aircraft under Transport Category requirements.

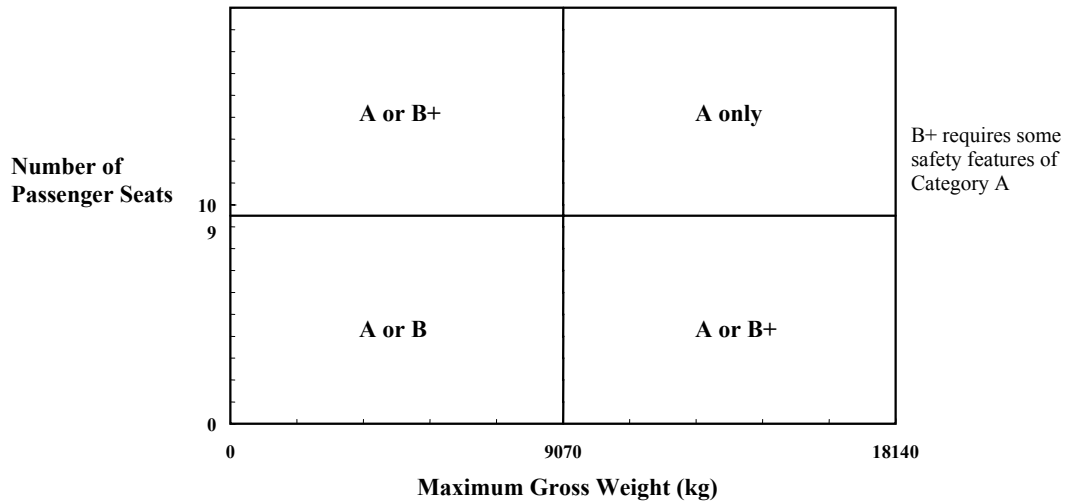


Figure 5.1 - Category Distinctions

**5.2 - Category A Vs. Category B**

Category A rules are generally more strict than Category B rules. The main difference is that the CFR requires Category A helicopters to have a “stay up” capability. This is essentially the ability to climb at a rate of 30.5 m/min (100 ft/min) in forward flight after the failure of a single engine. This obviously eliminates single engine aircraft from being certified as Category A. Although the Condor is light enough to be certified as a Category B aircraft, a Category A aircraft has several advantages that would improve its mission capability. For example, since Category A helicopters have the “stay up” capability, they are permitted to make takeoffs and landings from small heliports such as city-center rooftops and oil rigs. This is a desirable feature since it vastly improves the helicopter’s multi-mission capability. Category A helicopters are also permitted to



fly over residential areas or areas that have no emergency landing sites, where Category B helicopters are not. This is an essential capability for a rescue helicopter, where the victim's life may depend on the aircraft's arrival time. Being able to fly the most direct route to the rescue site is a necessary capability for this mission profile. For these reasons, it was decided to design the Condor for certification as a Category A Transport Rotorcraft.

### **5.3 - Summary of Design Requirements From CFR**

Throughout the design proposal, CFR sections are referenced when pertaining to a requirement applicable to this design. Some of the specific CFR requirements were beyond the scope of this design proposal because of its preliminary nature and were, therefore, ignored. The following section summarizes the main points of the 14CFR29 grouped by subparts:

***Subpart A - General:*** This section outlines the criteria for applicability of the certification categories.

***Subpart B - Flight:*** This section presents the requirements for flight performance of the aircraft. Included in the section are weight and center of gravity limits, main rotor speed and pitch limits, stability requirements, height-velocity envelope, which gives the flight envelope for safe autorotation, and takeoff and landing requirements. This section stipulates the "stay up" capability mentioned previously. Because the aircraft was designed to maintain hover at 3,658 m (12,000 ft) with one engine inoperative, it can easily achieve a climb rate of 30.5 m/min (100 ft/min) at sea-level with one engine inoperative.

***Subpart C - Strength Requirements:*** Requirements presented in this section range from factor of safety to pilot input forces and torques. It outlines the minimum loads the aircraft structure must take for all modes of flight including hard landings and maneuvering limit loads. An important requirement is that the aircraft be able to withstand gust loads of 17.77 knots (30 ft/sec). Because the RFP requires flight in gusts of up to 40 knots, this requirement is easily satisfied.

***Subpart D - Design and Construction:*** This is one of the largest sections in CFR Part 29. It outlines requirements for virtually all aspects of an aircraft design. During each segment of the design process, Subpart D was researched for specific requirements. Among the topics in this section are autorotational control, flutter and divergence, materials, cabin and cockpit layouts, emergency exits, lightning and static electricity protection, and even bird strikes.

***Subpart E - Powerplant:*** This section outlines all requirements for the powerplant system and subsystems. Because the engines used on the Condor are existing engines that are already certified, most of the requirements are satisfied. Subsystems of the engine system such as fuel



tanks, oil system, intake and exhaust, and firewalls were designed to meet the requirements from this section.

**Subpart F - Equipment:** This section deals with the equipment implemented with the helicopter such as flight control, navigational, anti-collision, and autopilot systems. Stipulations for electrical systems, hydraulic systems, and ice protection systems are also included and are referenced throughout the design proposal.

**Subpart G - Operating Limitations and Information:** This section provides information on the absolute operating limits for a certified aircraft. Included are requirements on never exceed speed, rotor speeds, limiting height-velocity envelope, as well as safety equipment information.

## Section 6 - Main Rotor & Hub Design

### 6.1 - Baseline Rotor Design

The main rotor for the Condor was designed for efficient hover at high altitude and good high speed, high altitude cruise performance. The two modes of flight often carry very different requirements, creating the need for design compromises. The rotor diameter, number of blades and solidity were previously selected in the preliminary sizing study (See Section 4). Table 6.1 lists the key design parameters for the main rotor.

**Table 6.1 - Main Rotor Design Parameters**

Diameter	12.05 m (39.5 ft)
No. of Blades	4
Blade Chord	0.34 m (1.1 ft)
Twist	-12 deg (linear)
Sweep	20 deg (from 94%)
Anhedral	20 deg (from 96%)
Taper	10% (from 94%)
Tip Speed	210 m/s (690 ft/s)

#### 6.1.1 Blade Twist

A negative blade twist is beneficial during hover because it redistributes the lift distribution inboard of the blade tips. This tends to reduce the induced power and hence, increases the figure of merit of the rotor [Leis00]. Blade twist also tends to delay the onset of stall on the retreating blade at high speeds. Too much twist, however, degrades blade performance on the advancing side of the disk in high speeds by creating negative lift near the tips. Both modes of flight were important for the design of the Condor. Therefore, a moderate linear blade twist of -12 degrees was selected as a compromise between the hovering and forward flight performance.



### **6.1.2 Airfoil Sections**

The selection of airfoil sections is critical to the rotor performance. The Condor is required to fly at high speeds at high altitudes, making stall and compressibility effects key issues. To delay the onset of stall on the retreating blade, airfoils with high lift to drag ratio and maximum lift coefficient should be used. To prevent the onset of compressibility effects on the advancing side, airfoils with high drag divergence Mach numbers are needed. Unfortunately, these are conflicting requirements, making it necessary to use multiple airfoil sections over the span of the blade for the best performance. Another desirable characteristic for rotor airfoil sections is that the slope of the pitching moment versus angle of attack (AOA) curve be small in order to keep the hub loads and control loads to acceptable levels. To fulfill these requirements, two advanced airfoil sections were selected for the Condor, namely the NASA RC(4) and RC(6) airfoil sections. The RC(4) is a high lift airfoil with low pitching moments [Noon90] and it is used from 0-90% span. The RC(6) is a supercritical airfoil section with a high drag divergence Mach number and good maximum lift capability at high speeds [Noon91]. The RC(6) is used from 90% span to the tip. These particular state-of-the-art airfoils were selected, in part, because of their readily available aerodynamic characteristics. Unlike the advanced airfoils developed by manufacturers, these airfoils and their characteristics are available in the public domain.

### **6.1.3 Tip Speed**

The selection of tip speed has a significant effect on the performance of a helicopter rotor. Higher tip speeds help to delay the onset of retreating blade stall in forward flight. Also a high tip speed allows for good autorotative performance. However, a very high tip speed also promotes compressibility effects on the advancing blade even at lower forward speeds and lead to problems of noise [Leis00]. In addition, higher tip speeds lead to higher centrifugal forces generated by the blades, which increases hub weight. In light of these problems and the fact that retreating blade stall can be delayed with blade twist and advanced airfoil sections, a nominal tip speed of 210 m/s (690 ft/s) was selected for the Condor.

### **6.1.4 Tip Geometry**

A planform sweep of 20 degrees, starting at the 94% span was selected to minimize compressibility effects to cruise speeds of over 170 knots at 3,658 m (12,000 ft). A moderate amount of taper of 10% was also used beginning at the 94% span in order to increase the figure of merit by offloading the blade tips. In addition, 20 degrees of anhedral was used starting at the



96% span, similar to the Sikorsky growth blade tip used on the Blackhawk. Again, anhedral is used to boost the figure of merit by a modest amount.

## **6.2 - Swashplateless Rotor Control**

### **6.2.1 - Trailing Edge Flaps**

The primary flight control in a helicopter is achieved by controlling the rotor thrust vector, which in turn is accomplished by changing the blade pitch as a function of blade azimuth. This can be achieved by two different mechanisms. One approach makes use of a swashplate to change the blade pitch. This is normally achieved by tilting the plane of the stationary part of swashplate system through the use of servo actuators. The other approach involves the use of servo-flaps located at the trailing edge of the rotor blade. Deflecting the servo-flaps in collective and cyclic modes changes the aerodynamic loads over the blades, introducing elastic twist in the blades. To have good flap effectiveness, the blades need to be soft in torsion, which can be achieved with a soft torsional spring (tension-torsion strap). The overall actuation force required for a swashplate system to change the blade pitch is significantly higher than what is required to produce desired flap deflection in a swashplateless system [Chop02]. Consequently, the regular swashplate system is bulky, heavy, mechanically complex and causes a large parasite drag. A swashplateless design is lighter, mechanically simple, and offers up to 15% reduction in parasite drag [Shen03], enabling easy maintenance, improved performance, increased payload ratio and decreased maintenance costs. However, it requires a compact actuation system.

Kaman has been using the servo flaps as primary control devices in their helicopter for more than 50 years [Wei03]. However, an external trailing edge flap system causes some additional drag penalty because of exposed surfaces. The presence of external flaps move the sectional center of gravity to aft positions, hence large ballast weights are required to bring the blade sectional c.g. forward to an acceptable position, resulting in additional overall blade weight penalties. Using an embedded trailing edge flap eliminates some of these problems. A rotor with integrated trailing edge flaps has better aerodynamic performance than auxillary servo flaps (i.e., plane flaps) and superior lift-to-drag ratios. In addition, it has been demonstrated that such flaps can also be used efficiently for individual blade tracking, and active vibration and noise suppression [Roge02], [Roge04], [Shen03], [Strau04].

Because of the enormous potential of embedded flaps, major helicopter manufacturers are investigating possible incorporation of this technology in their aircraft. Boeing has conducted



extensive tests to evaluate performance of smart material actuators; and more recently performed whirl tower tests of the full scale rotor with trailing edge flaps actuated with piezostack actuators. It has been established that the use of smart material actuated flaps offers significant performance and vibration benefits [Strau04]. Sikorsky, as well as Kaman are also examining incorporation of this technology for primary control in their forthcoming designs.

In light of these recent technological developments, a swashplateless rotor with a trailing edge flap actuated by a compact piezo-hydraulic actuator for primary and vibration control was selected for Condor. The design team is quite aware of various methodologies that have been attempted as a replacement for the swashplateless system. A brief discussion of these is presented below.

- (i) Blade camber control - achieved by cyclic excitation with embedded material with different arrangements on top and bottom surfaces of the blade sections. Because of the lack of availability of suitable smart materials with sufficient stroke and stiffness to produce desired deformation, this concept was found to be infeasible [Dado82], [Strau95].
- (ii) Blade twist control - enables blade twist to be generated from embedded active materials by the application of a cyclic differential voltage over the blade span. Such a design requires large actuation power and the structural integrity of the blade is compromised [Buet01].
- (iii) Blade pitch control - individual blades are actuated using hydraulic or smart material actuators in the rotating frame. Hydraulic actuation requires a complex hydraulic slip ring, whereas smart actuation is limited by a relatively small stroke [Ham83], [Chop00].
- (iv) Tilting shaft concept - the control mast is tilted to control the rotor thrust vector. Unacceptably large actuation force and stroke requirements make this concept infeasible for full-scale rotors [Hous98].

### **6.2.2 - Lift Flaps vs. Moment Flaps**

#### ***Lift Flaps***

When the flaps are used to enhance lift on the torsionally stiff blades ( $v_\theta > 4/\text{rev}$ ), the deformation due to aerodynamic pitching moments is negligible and the only effect of the flaps is to increase the sectional lift, which is similar to the effect of changing blade pitch. The primary effect of such flaps is to change the lift characteristics of the blade without significantly affecting the pitching moment characteristics of the blade or the blade pitch dynamics. These flaps are referred to as lift flaps and have significantly large chord ( $> 35\%$  of blade chord) to increase their

efficiency. The amount of deflections required by such flaps is relatively large and consequently results in higher drag, stalled blades and degraded rotor performance. Further, to actuate such flaps for primary controls, large stroke actuators are needed, which is often prohibitive with the currently available smart materials.

### ***Moment Flaps***

Moment flaps on the other hand are smaller in size ( $< 25\%$  blade chord) and are used with torsionally soft blades ( $v_0 < 2/\text{rev}$ ). These types of trailing edge flaps are considered to be more effective in changing the pitching moment of blade section with only a small change in sectional lift characteristics. The induced pitching moment from flap deflection results in a twisting of the blade. The flap deflections required for achieving the primary control using moment flaps is small compared to requirements with lift flaps [Shen03a], and they have been used by Kaman for over 50 years for primary control purposes, as external servo flaps. Because of their smaller size, lower deflections requirements and lower drag penalty, integral moment flaps were chosen for the Condor's rotor design.

### **6.2.3 - Details of Moment Flap Design**

The key parameters that influence the performance of trailing edge flaps are the blade torsional frequency, pitch indexing angle, flap size, spanwise location, and chordwise aerodynamic balance [Shen03], [Shen03a], [Ormi01]. To investigate the effect of these parameters, a mathematical model was developed using a propulsive trim model of a helicopter with active trailing edge flaps for a level flight condition. The coupled pitch-flap equations were solved using the harmonic balance method. The pitch inputs were defined as:

$$\delta(\psi) = \delta_o + \delta_{1c} \cos\psi + \delta_{1s} \sin\psi, \quad \delta_c = (\delta_{1c}^2 + \delta_{1s}^2)^{1/2} \quad \text{and} \quad |\delta| = \delta_o + \delta_c$$

where  $|\delta|$  is the maximum flap deflection and  $\delta_c$  is the maximum cyclic flap amplitude. A parametric study was carried out for a flap chord of 20% blade chord to determine the optimum flap configuration for the current design requirements [Shen03], [Shen03a], [Ormi01]. Figure 6.1 shows that a blade with low torsional stiffness decreases the trailing edge flap deflection requirements. Blades with very low torsional frequency ( $< 1.7/\text{rev}$ ), however, are prone to aeroelastic instabilities, such as pitch-flap flutter and pitch divergence. Torsional frequencies close to  $2/\text{rev}$  may lead to resonance condition and torsional frequencies greater than  $2/\text{rev}$  require large flap deflections and actuation power. The optimum frequency lies between the two extremes, therefore a torsional frequency of  $1.8/\text{rev}$  was chosen for the rotor blades of the current design.

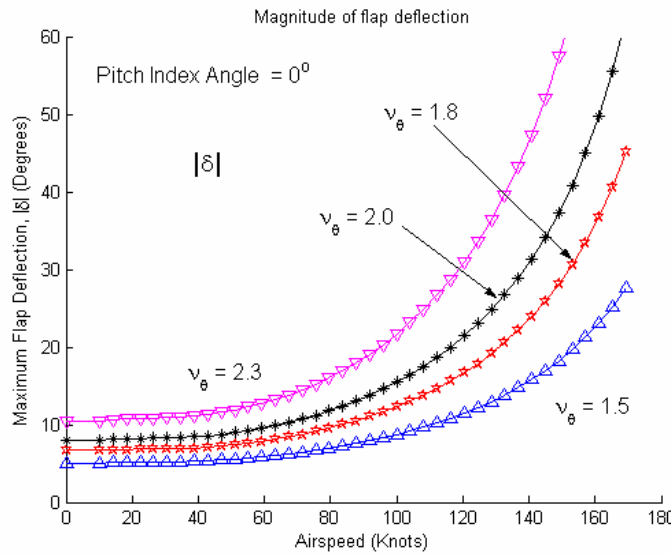


**Figure 6.1 - Maximum Flap Deflection For Level Flight (flap chord = 0.2C)**

The flap deflections required to achieve trim at high speeds are relatively large (Figure 6.1), therefore the blade pitch needs to be indexed. The blade pitch index angle defines the three-quarter radius blade pitch value relative to the hub plane. Pitch index angle is normally selected to be higher than the collective pitch required to trim the helicopter at a selected forward speed. This is done to ensure that positive collective flap deflection is required at all speeds. A downward flap deflection increases lift on the blade, moving the blade airload distribution inboard, and improving the rotor performance.

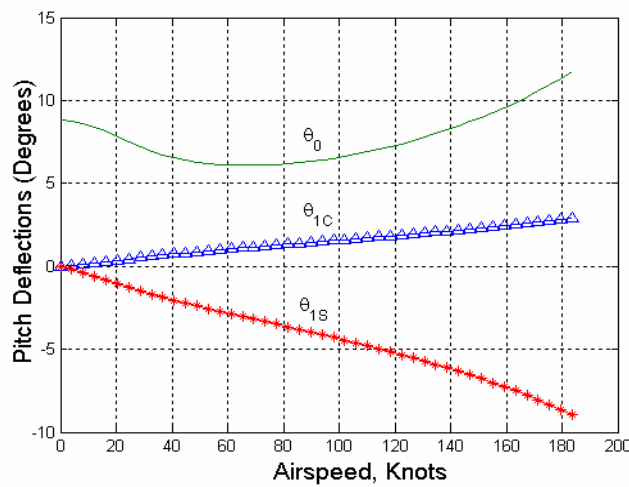


**Figure 6.2 - Blade Pitch Angles Required to Trim (Conventional Swashplate System), Zero Twist**

Figure 6.2 shows the pitch angles required at the blade root to achieve trim for a conventional swashplate system. The required collective pitch angle changes with forward speed, hence the

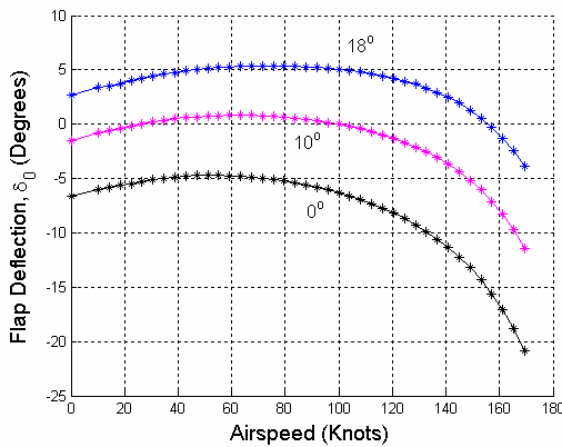


Figure 6.3 - Collective Flap Deflections

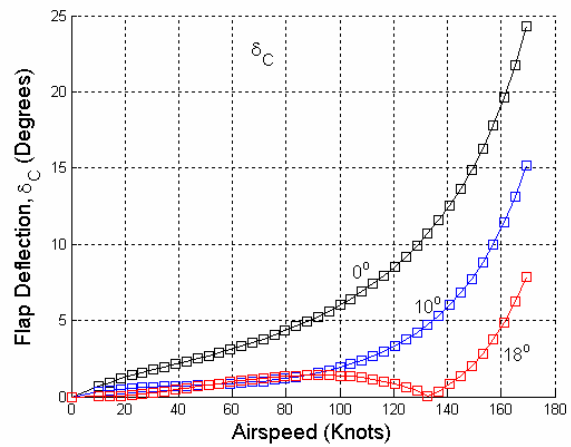


Figure 6.4 - Maximum Cyclic Flap Amplitude

optimum pitch index angle should also change with forward speed. The blades have 12° of negative twist, which translates into 9° of negative twist at 75% radius. From Figure 6.2, it is clear that a collective angle of 8° is required to trim the helicopter at 150 knots. A pitch index angle of 18° appears to be suitable to achieve positive flap deflections for 0 to 150 knots, and requires minimum flap deflection, with a flap of 20% span located at 75% radius, especially near 145 knots, which is the desired cruise speed. Figures 6.3 and 6.4 show, respectively, collective and cyclic flap deflections required to trim the helicopter at different speeds. With an index angle of 18°, the required collective flap deflection is below 5°, and more importantly, the cyclic flap amplitude is also below 5° for speeds up to 160 knots.

### 6.2.4 - Moment Flap: Parametric Design Studies

A flap aerodynamic overhang (flap hinge) of 15% chord was selected as the basis of preliminary analysis. The location and size of the flap was then varied to study the effect on the required flap deflections. Figure 6.5 shows that the smaller flap deflections are required when the flaps are located outboard towards the tip (higher dynamic pressure). However, as the flap is moved outboard, the actuator weight contribution to the blade flapping moment of inertia increases, thereby reducing the Lock number. This means that the inertial forces become relatively large and may affect blade dynamics. Also, placing the flap near the tip will start impairing its effectiveness due to 3-D aerodynamics. Taking these issues into consideration, the flap mid-span location was selected at 75% blade radius, which clearly shows acceptable levels of flap



deflections. Figure 6.6 shows that having a larger flap span is desirable, but hinge moment requirements increase with the flap span. A flap span of 0.2R was selected as the optimum size.

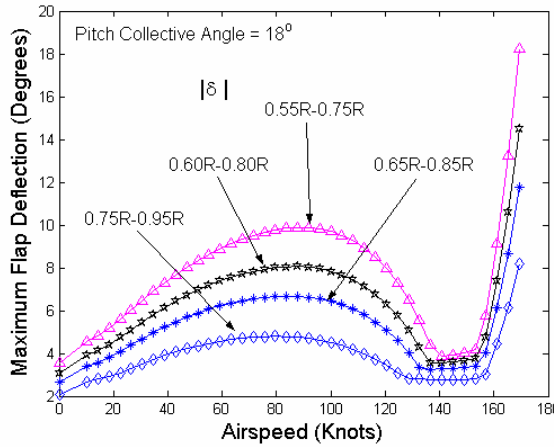


**Figure 6.5 - Effect of Varying Flap Location (Flap Length 0.2R)**

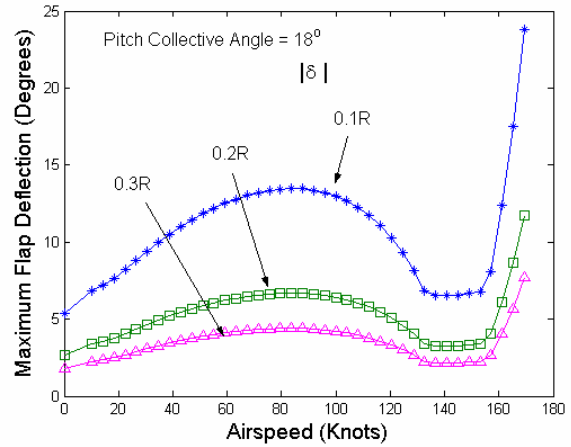


**Figure 6.6 - Effect of Varying Flap Size (Flap Location 0.75 R)**

The details of the final optimized configuration are shown in Table 6.2. The final configuration consists of two flaps each consisting of 10% of the rotor radius. A dual flap design was chosen to provide additional redundancy in the control system as well as low actuation requirements per flap. In case of the failure of one of the flap actuators, the other flap should be able to trim the helicopter in all normal flight conditions. The hinge moments (steady component  $HM_0$  and cyclic components  $HM_{1c}$  and  $HM_{1s}$ ) and blade deflections required for trim are shown in Figures 6.7 and 6.8, respectively. The results displayed in these figures are a clear indication of the superior performance provided by the proposed configuration.

**Table 6.2 - Swashplateless Rotor Design Parameters**

Parameter	Value
Torsional frequency (rotating)	1.80 / rev
Lock number (sea-level)	9.45
Blade feathering moment of inertia	$6.54 \times 10^{-4}$
Flap chord	20% blade chord
Flap spanwise location	1 <sup>st</sup> flap 65-75%; 2 <sup>nd</sup> flap 77-87%
Blade sectional pitching moment coefficient	-0.006
Blade twist	-12 degrees
Pitch index angle at the blade root	18 degrees

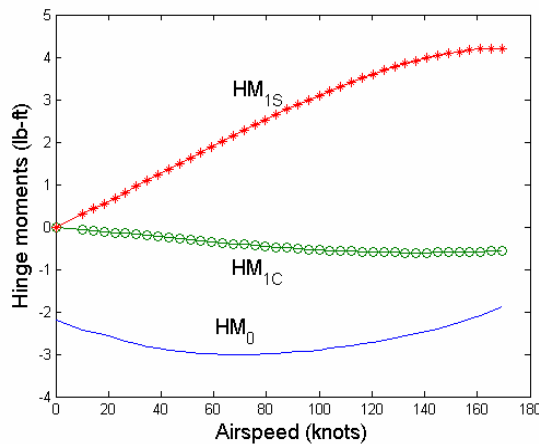


Figure 6.7 - Flap Hinge Moment

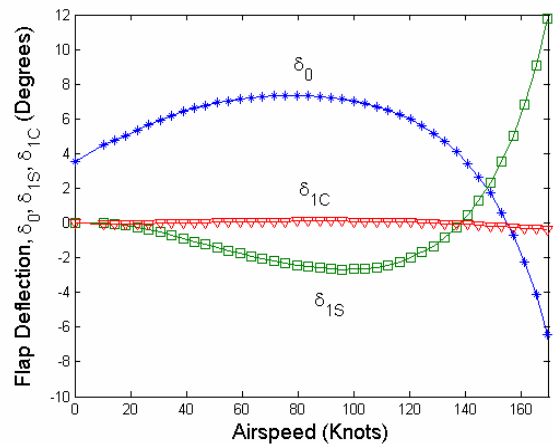


Figure 6.8 - Flap Deflections for Trim

### 6.3 - Compact Flap Actuator

To meet the cyclic and collective flap requirements for primary control of the rotor throughout the flight envelope, a compact flap actuator was designed to be embedded in the rotor blade.

#### 6.3.1 - Actuator Design

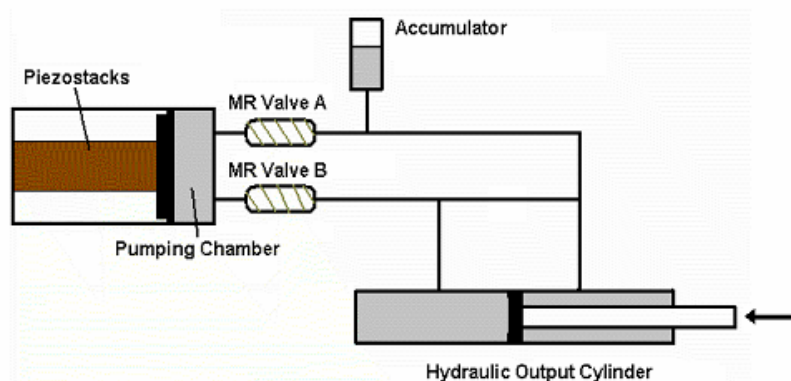
From the flap analysis carried out in the previous section, it was determined that a flap angle range of  $\pm 5^\circ$  would be sufficient to meet cyclic control requirements. Based on a 25 mm offset hinge, this leads to the requirement of an actuator output displacement of  $\pm 2.5$  mm about the neutral point. In addition, the hinge moment requirements lead to an actuator output force of about 111.25 N (25 lb) per actuator, using two actuators per flap. With a rotor RPM of 333, the actuator output frequency required for primary rotor control is about 5.5 Hz. Using these requirements, smart materials were compared for use as the flap actuator in Table 6.3.

Table 6.3 - Comparison of Potential Smart Materials for Actuation

Smart Material	Maximum Strain	Blocked Force	Bandwidth	Evaluation
Shape Memory Alloy	High (8%)	High	Low (<1 Hz)	Bandwidth too low for primary control
Magnetic Shape Memory Alloys	High (6%)	Low	High (~1 kHz)	Magnetic coils are large and heavy; insufficient blocked force
Electrostrictives	Low (0.1%)	Moderate (~2500 N)	High (<100 kHz)	Low operating temp. (<40°C)
Magnetostrictives	Low (0.2%)	Moderate (~2500 N)	High (<10 kHz)	Magnetic coils are large and heavy
Piezobimorphs	Low (0.13%)	Low (~45 N)	High (<100 kHz)	Blocked force insufficient
Piezostacks	Low (0.1%)	High (~4500 N)	High (<100 kHz)	Requires stroke amplification method

Piezostacks were selected as the best smart material for use in the flap actuator because of their high blocked force and bandwidth capabilities. In addition, they do not incur the same weight penalty as magnetostrictive actuators. Magnetostrictives require large coils to produce the magnetic fields needed to actuate the material. Piezostacks are actuated with an input voltage, and therefore, only need electrical wires for actuation. Because the maximum strain of piezostacks is relatively small, it was necessary to use some type of stroke amplification method.

A piezo-hydraulic hybrid pump, recently developed at the University of Maryland was used to amplify the small stroke actuation of the piezostacks [Siro03], [Elli04]. The working principle of the pump is based on frequency rectification of the high frequency, low stroke actuation energy of piezostacks into low frequency, large stroke hydraulic output energy. When actuated at high frequencies (>1 kHz), piezostacks create an enormous amount of energy. The fluid is used to transmit the energy of the piezostacks to a hydraulic output cylinder. Because the fluid in the pump is self-contained, the actuator is compact and does not require hydraulic lines to provide a fluid source. The mechanics of the actuator parts are shown in Figure 6.9:



**Figure 6.9 - Piezo-hydraulic Flap Actuator**

**Piezostacks** - Eight piezostacks with dimensions of (10 mm × 10 mm × 18 mm) are enclosed in an aluminum casing along with a piston and diaphragm assembly. One end of the piezostacks is fixed to the aluminum casing while the other end makes contact with the piston. An AC voltage (< 110 V) is applied to the piezostacks at a high frequency (~1 kHz), producing high frequency, small amplitude fluid displacements in the pumping chamber which are then rectified by magnetorheological (MR) valves.

**MR Valves** - MR valves are used in the flap actuator for both frequency rectification and output directional control. The MR valves work by producing a small magnetic field in the working fluid of the pump. Because the fluid used in the pump (MR Fluid 132 80) has magnetic

properties, its exposure to a magnetic field increases its local viscosity, effectively blocking the valve. The valves are always kept in opposite states and are switched at the same frequency as the piezostacks. So, when the piezostacks expand, fluid is pushed out of the pumping chamber through Valve A. The valves then switch states, and as the piezostacks contract, fluid is pulled into the pumping chamber through Valve B. This frequency rectification process creates a constant flow direction to the output cylinder. The output direction is changed by simply shifting the phase of the valves by 180°. Note: mechanical reed valves were successfully applied initially [Elli04] before implementing MR valves [Yoo04].

**Output Cylinder** - The output cylinder used to actuate the flap has a bore diameter of 14 mm and is 75 mm long. It is a single acting cylinder with a piston rod diameter of 6.5 mm.

**Accumulator** - The accumulator is used to apply a pre-pressure to the working fluid of the pump so that it is insensitive to air entrained in the fluid.

### **6.3.2 - Actuator Mounting and Operation**

The entire actuator assembly is placed behind the blade spar. The heaviest component of the assembly, the pump and MR valve assembly, is rigidly attached to the blade spar. This keeps the chordwise center of gravity of the blade as far forward of the aerodynamic center as possible, reducing the likeliness of blade flutter. The complete actuator assembly weighs about 0.45 kg. The output cylinder is mounted on a support rib in the chordwise direction. The output piston rod is connected to the flap hinge tube using a pitch horn. The flap hinge tube is connected to the blade using two flange mounted roller bearings on each side. A panel above each actuator is provided to allow easy access to the assembly. The panel is secured using countersunk screws so that the complete assembly fits within the airfoil contour.

Cyclic and collective output displacements from the piston rod are translated into cyclic and collective flap deflections. The system uses a feedback signal from a potentiometer mounted on the flap hinge tube to determine the exact position of the flap. Estimated power required for primary control is about 45 W per actuator, or 180 W per blade. Because the actuator can provide output frequencies of up to 4 times that required for primary control, there is the possibility of using the flap for vibration reduction at the 3, 4, and 5 per rev frequencies. Such a pump has already been fabricated and tested under a wide range of load conditions for both static and dynamic loads.



### **6.3.3 - Safety and Monitoring**

The compact piezo-hydraulic pump contains no moving parts and is therefore, extremely reliable. To provide extra redundancy, two actuators are provided for each flap. If one actuator fails, the second actuator has enough authority to execute primary controls and trim the rotor in level and descending flight modes. Strain gauges mounted on the piezostacks of all the actuators will alert the pilot and the HUMS if the system is not functioning properly. In the case of engine failure, the flap actuators are designed to immediately position the flap at the optimum angle to allow rapid entry of the rotor into autorotation as stipulated by 14CFR29.691. The actuator has the ability to provide mean displacement beyond the normal requirements to allow a higher collective for flare when performing an autorotational landing.

### **6.4 - Slip Ring**

Power is supplied to the flap actuators by the electrical system in the helicopter (see Section 12.2.7). It is, therefore, necessary to transfer electrical power from the non-rotating frame to the rotating frame. A slip ring, consisting of stationary housing and brushes in contact with a rotating slip ring, is used for this purpose. Because small dust particles can disrupt contact between the brushes and the slip ring, multiple sets of “long-life” brushes and rings are used. This ensures that power to the actuators will not be lost because of a single loss of contact. Contactless magnetic slip rings were considered an infeasible technology for certification at this point in their development.

### **6.5 - Blade Structural Design**

The blades of Condor were designed to accommodate the flaps, actuators and related hardware, and provide low vibrations using tailored composite blades [Bao04]. The blades have aft c.g. limits imposed by the 14CFR29.629 requirements to avoid pitch-flap flutter and pitch divergence. This is particularly important, as the blades were designed to be soft in torsion to achieve desired flap effectiveness for the swashplateless system. The foreword c.g. limits are imposed by the nose down pitching moments generated by the main lifting section of the blade.

#### **6.5.1 - Blade Design Details**

The use of composite materials in blade manufacturing gives the designer flexibility in tailoring the properties of the blade to meet the stress requirements. In addition, specific elastic coupling can be introduced. Wind tunnel tests on Mach scaled composite tailored rotors of the UH-60

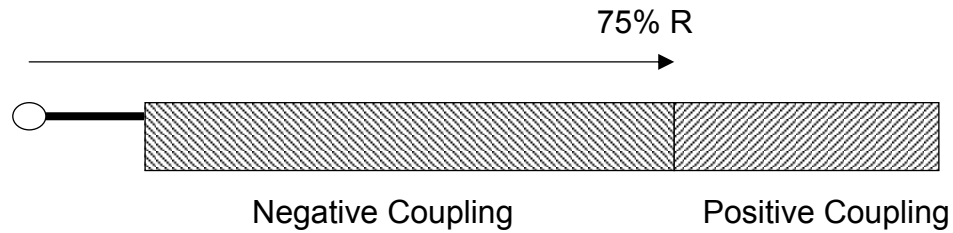


**Figure 6.10 - Layup of Composite Tailored Blade**

Black Hawk with flap-bending/torsion coupling have demonstrated significant effect on the fixed frame vibratory rotor hub loads. A composite rotor with a dual spanwise segmented flap-bending/torsion coupling (FBT-P/N) significantly reduced the 4/rev vibratory hub loads, a key source of vibrations in a four bladed rotor. Tests show that vertical hub forces were reduced by up to 15%, in-plane hub forces were reduced by up to 3%, and the head moment was reduced by up to 14% [Bao04]. The blades used on the Condor make use of this technology to minimize vibration (Note that Sikorsky is also investigating this technology for their current and future rotor systems). The blade structure (refer to Foldout 6.1) consists primarily of a D shaped spar and a skin made out of  $\pm 45^\circ$  graphite epoxy weaver. The FBT coupling is introduced in the D-spar which is made of 26 plies of 0.005 inch graphite epoxy composite. The blade has negative FBT coupling for up to 75% of blade radius and positive FBT coupling beyond 75% (Figure 6.10). Preliminary estimates suggest an unbalanced ply layup, as shown in Figure 6.11.

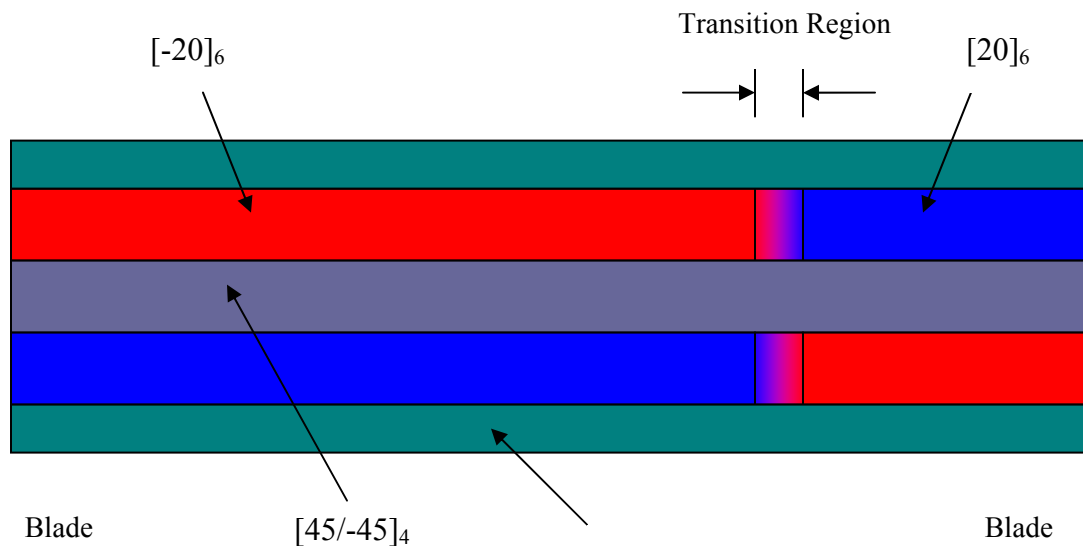
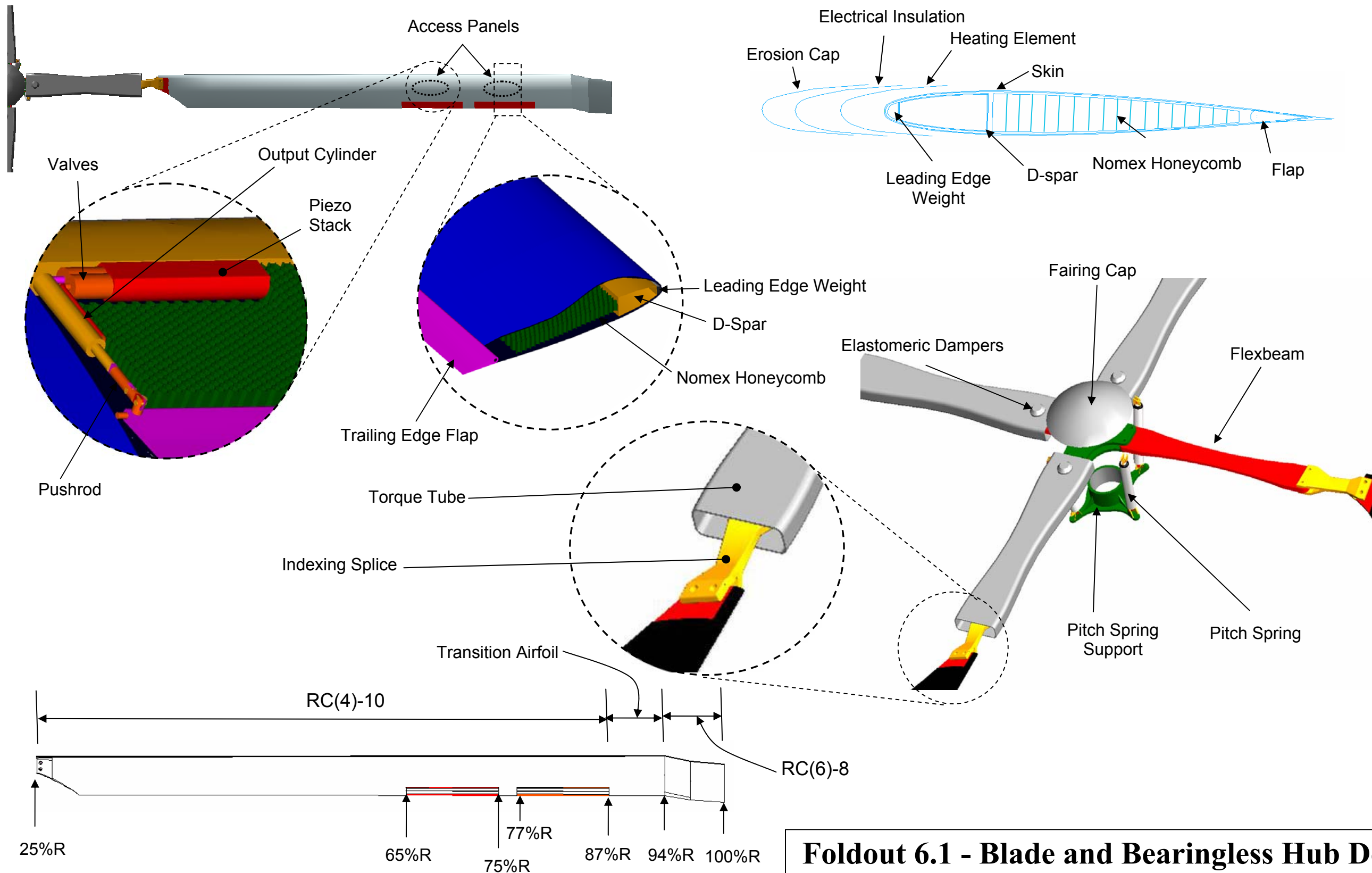


**Figure 6.11 - Spanwise Ply Layup for D-Spar**



**Foldout 6.1 - Blade and Bearingless Hub Details**



A typical section has six unidirectional sub-laminates for axial & bending stiffness, four balanced ([45/-45]) sub-laminates for shear stiffness, and remaining twelve layers to introduce desired coupling. An optimized ply layup may be further refined using a more detailed analysis [Gang94]. Tungsten mass ballast weights were used in the inner nose cavity of the blade to move the center of mass of the blade forward to the quarter chord location. Erosion strips are mounted over the blade leading edge and electrically insulated heating element (de-icing blanket) is placed beneath the erosion strip. The remaining internal blade structure is made of Nomex honeycomb since it bonds well with the skin and has low moisture absorption. Table 6.4 summarizes the properties of the primary structural materials used in the design of the blades.

**Table 6.4 - Properties of Materials Used in Blade Structure**

Material	Density (lb/in <sup>3</sup> )	Young's Modulus (msi)	Shear Modulus (msi)	Nominal ply thickness (in)
±45° Graphite epoxy	0.055	2.1	4.55	0.018
Nomex Honeycomb	0.00116	0.0105	0.0042	-
Tungsten	0.70	40	19.2	-

**6.5.2 - Lightning Protection and Electromagnetic Shielding**

Helicopter blades are required to withstand a 200 kA lightning strike and still permit the helicopter to land safely [Alex86]. Lightning strikes may cause delamination in the composite spar due to high heat, and the large current flow could damage the actuators. To protect these components, blade sections that are susceptible to heating and large currents are covered externally with doublers made of conductive materials that conduct the current to a titanium abrasion strip. The current flows spanwise to the root end attachment of the blade to avoid any electrostatic charge build up. The actuator housing is wrapped in a nickel/iron alloy foil to shield it from stray low frequency electromagnetic signals. The design conforms to the requirements stipulated in 14CFR29.610 for lightning and static electricity protection.

**6.6 - Hub Design**

The hub for the Condor was designed to ensure low aerodynamic drag, low weight, structural simplicity, and superior handling qualities. The trailing edge flap design imposes low torsional stiffness of the rotor blades to ensure adequate flap effectiveness. Hence a bearingless soft in-plane hub was selected, which ensures greater control power and therefore better handling qualities than articulated designs [Prou89]. A soft in-plane hub design was selected to minimize in-plane loads.



The bearingless hub for the Condor (refer to Foldout 6.1) has four primary elements: a flexbeam (through which flap, lead-lag, and pitch motions are achieved), a torque tube (for the blades to react against the pitch spring), an elastomeric damper (to provide lead lag damping), and a pitch spring (low frequency adapter).

**Flexbeam** - The flexbeam was tailored to the required stiffness and structural properties, and provides virtual flap and lead-lag articulations. The flexbeam is cantilevered to the hub support structure at one end and is bolted to the pitch indexing splice at the other end. The flexbeam is fabricated from uni-directional S-glass/epoxy tapes. The length of the flexbeam is 20% of blade radius.

**Torque Tube** - The torque tube in this design reacts against the pitch spring and elastomeric damper, instead of transmitting the pitch input as is done in a conventional design. The torque tube is fabricated from carbon fiber filaments to which uni-directional tape is added to provide high chordwise stiffness.

**Pitch Spring** - The pitch spring or frequency adapter is a soft compression spring that was designed to adjust the fundamental torsional frequency of the blades to 1.8 /rev. It carries the 1/rev oscillatory loads and provides reaction forces to achieve required pitch angles for trim of the helicopter. The stiffness of the spring was calculated using UMARC and was designed to allow a maximum blade pitch of  $\pm 20^\circ$ . The spring parameters are presented in Table 6.5.

**Elastomeric Damper** - Because the soft in-plane hub design was selected, lead-lag damping is required to avoid ground and air resonance. Therefore, a Silicone-rubber elastomeric damper consisting of alternate layers of elastomer and metal shims was used to augment lead-lag damping. These dampers have long service life, high reliability, low maintenance/inspection requirements, and are effective in temperatures from  $-65^\circ\text{F}$  to  $+200^\circ\text{F}$  [Lord04].

Table 6.5 - Spring Design Details

Length (mm)	Turns	Coil diameter (mm)	Coil wire diameter (mm)	Ultimate fatigue shear stress (GPa)	Shear Modulus (GPa)
210	20	45	4.8	0.35	82.7

### 6.7 - Autorotation Characteristics

All helicopters are required to demonstrate autorotation capabilities for CFR certification. Autorotation capabilities of a new design can be compared with existing helicopters using an autorotative index. A comparison of the current design to existing helicopters using the Sikorsky autorotative index, which is defined as the kinetic energy of the main rotor divided by the product



of gross weight and disk loading, is given in Table 6.6. It is clear that the Condor will have excellent autorotation characteristics with an index of nearly twice that of the S-76A.

**Table 6.6 - Autorotation Index Comparison**

Helicopter	GTOW (kg)	Polar moment of inertia (kg-m <sup>2</sup> )	Rotor speed (RPM)	Disk loading (N/m <sup>2</sup> )	Autorotation index (m <sup>3</sup> /kg)
Condor	3,343	941	333	255	1.34
S-76A	4,672	2,562	293	333	0.77
SA365N	4,000	2,091	349	360	0.97

**6.8 - Active Vibration Control**

Vibration is a serious problem in all helicopters and the main rotor is a key source of vibratory loads. Vibration inducing oscillatory airloads are caused by a highly unsteady flow field, complex wake structure, coupled blade motion, and time-varying blade pitch inputs. For identical blades (tracked rotor), only  $kN_b/\text{rev}$  harmonics of blade loads are transferred from rotating frame to fixed frame ( $N_b$  is the number of blades,  $k$  is an integer). However, if the blades are not identical, non- $kN_b/\text{rev}$  harmonics (mainly  $1/\text{rev}$ ) are also transferred to the fuselage. Currently, to overcome this problem blades need to be tracked periodically resulting in a significant operating cost. Further, to minimize blade dissimilarities, tight manufacturing tolerances are imposed leading to high manufacturing cost. The blades of the Condor have been tailored using composites to suppress  $kN_b/\text{rev}$  vibrations using flap-bending-torsion coupling. However, to completely minimize vibrations and suppress non- $kN_b/\text{rev}$  loads as well IBC is used.

IBC involves the calculation of optimal control input for each blade separately to minimize both the  $kN_b/\text{rev}$  and non- $kN_b/\text{rev}$  loads. To achieve the control of individual blades, the rotor hub loads are measured in fixed frame in real time. Once the steady-state has been established, the hub loads are sampled for one revolution and the system identification is performed (Figure 6.12), which involves the calculation of uncontrolled hub forces, and transfer matrix (which relates the flap deflection on each blade to hub loads). Once the state estimates are obtained, the optimal control inputs can be determined by minimizing a performance function involving vibratory hub loads and flap control angles (higher harmonics). A robust Kalman filter based adaptive control methodology was adopted to implement IBC [Roge04]. This is a computationally efficient algorithm designed to update parameter estimates recursively on the basis of a single measurement. The controller is implemented by sampling the hub loads and control inputs on a per rev basis. It performs both vibration reduction and system identification in real time.

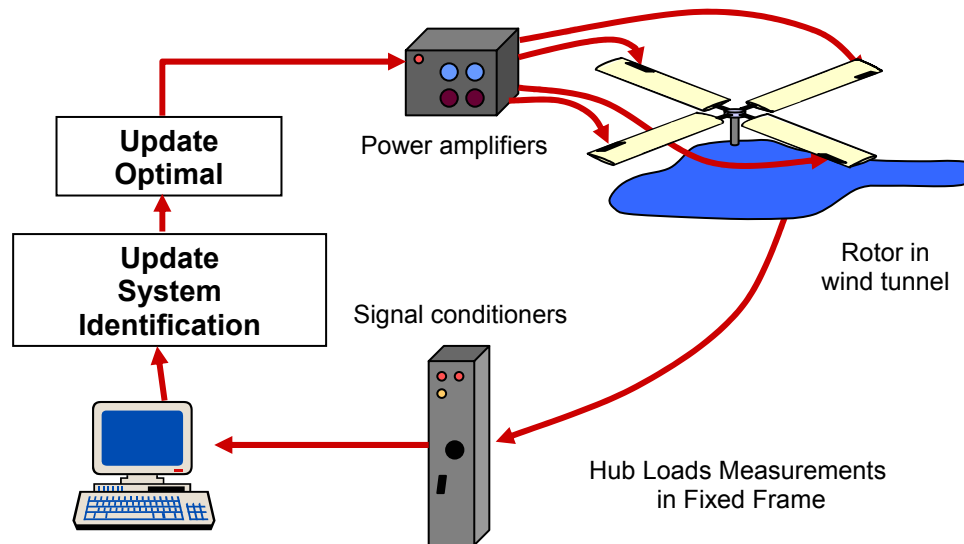


Figure 6.12 - Scheme for Active Vibration Control

A flap located outboard of the blade (at 77-87% of blade radius) was employed for this purpose in present design because it has better flap effectiveness (refer to Section 6.2.4). Recent wind tunnel tests conducted in the Glenn L. Martin wind tunnel on Mach scaled rotors revealed that flap deflections of  $2.8^\circ$  or less were sufficient to reduce the 3, 4 and 5/rev harmonics of root flap bending moments by 40%, 91%, and 91%, respectively, when targeted alone [Roge04], [Roge02]. This, and previous wind tunnel tests, demonstrated the robustness of this time-domain IBC control methodology. Significant 1/rev vibration reduction was also demonstrated. Therefore, the trailing edge flaps of the Condor will not only be used for primary control but also for active vibration control and in-flight tracking.

## **6.9 - Rotor Dynamics**

The main rotor system is soft inplane bearingless design with blades that are soft in torsion. Hence, its dynamics characteristics were carefully examined to ensure proper frequency placement to avoid aeromechanical instabilities.

### **6.9.1 - Dynamic Analysis**

The fan plot was obtained by using UMARC. The blade was modeled using 13 finite elements for the blade, 4 finite elements for the flexbeam, and 3 elements for the torque tube. The blade and flexbeam stiffness were optimized to appropriately place the blade frequencies. The blade stiffness and mass distribution is shown in Figure 6.13. The small spike in the blade mass distribution in the outboard section is due to the presence of the piezo-hydraulic actuators,

provided for flap deflection. The rotor frequencies are well separated as seen from the fan plot (see Figure 6.14). The first six natural frequencies are given in Table 6.7.

**Table 6.7 - Main Rotor Blade Natural Frequencies**

Mode	Flap	Lag	Torsion
First	1.04	0.65	1.80
Second	2.76	4.15	-
Third	4.68	-	-

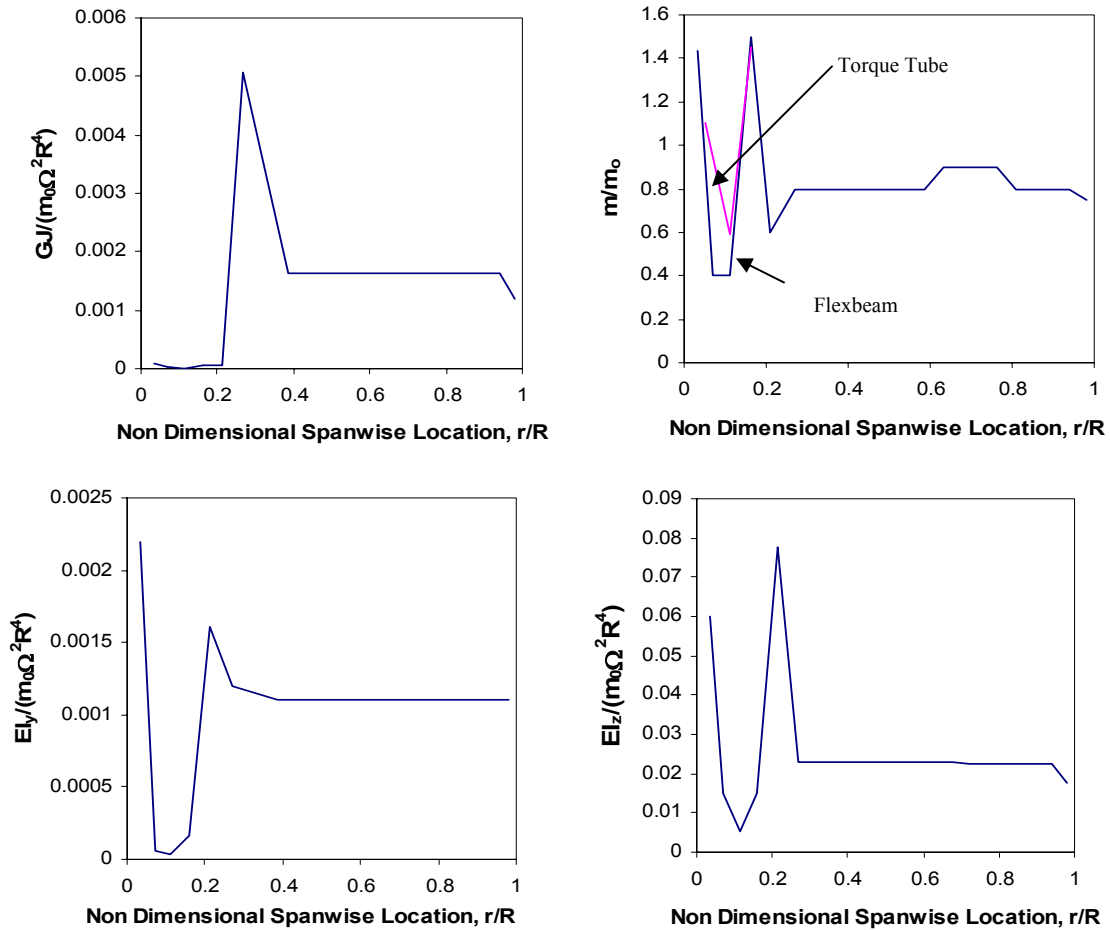


**Figure 6.13 - Blade Stiffness & Mass Distribution**

**6.9.2 - Aeroelastic Analysis**

To ensure that the rotor is free from any aeromechanical instability, an aeroelastic analysis was carried out. A pitch-flap flutter analysis (see Figure 6.15) indicates that the critical c.g. offset to avoid pitch-flap flutter and pitch divergence, is aft of the quarter chord at nearly 28% of the chord from the leading edge. Ballast weights were used in the blade tips to move the c.g. ahead of



quarter chord to 22% of chord. This provides adequate margin to avoid pitch-flap flutter and divergence. A comprehensive aeroelastic analysis was carried out (see Figure 6.17) and all rotor modes were found to be stable over the entire flight regime.

**6.9.3 - Ground & Air Resonance**

Because the Condor rotor is a soft in-plane bearingless design, a ground resonance analysis was performed. It can be seen from the Figure 6.16, that all the modes, including rotor in-plane modes, are stable and adequately damped. Soft in-plane rotors are also susceptible to air resonance which occurs due to interaction of rotor flap and lag modes with the fuselage pitch and roll modes. A comprehensive air resonance analysis was performed (see Figure 6.18), and it can be seen that the rotor lag mode remains stable even in the absence of elastomeric damper at all advance ratios. The inclusion of the elastomeric dampers would further augment the stability of the lag modes.

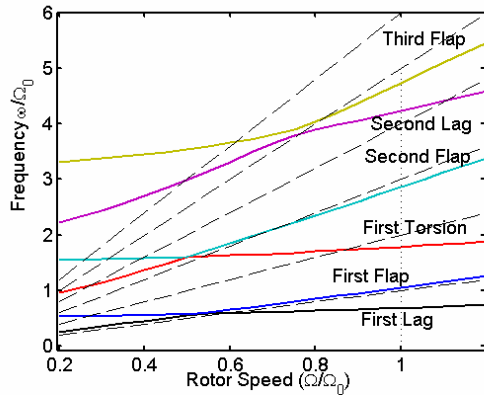


**Figure 6.14 - Rotor Fan Plot**

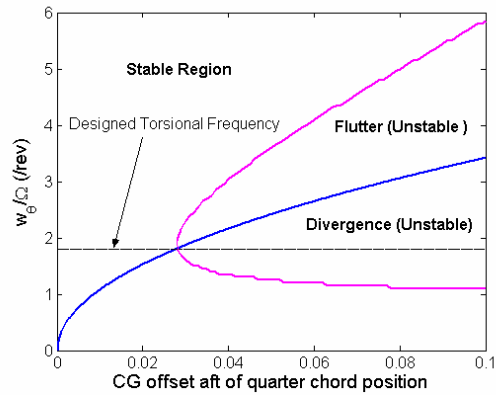


**Figure 6.15 - Pitch Flap Flutter/Divergence Stability Boundary**

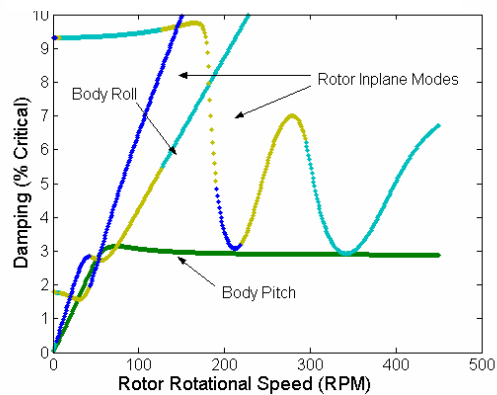
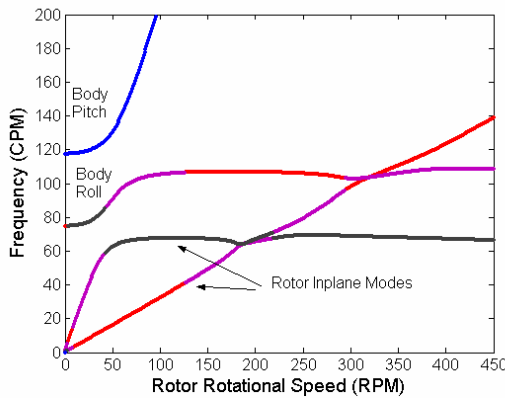


**Figure 6.16 - Ground Resonance Analysis**

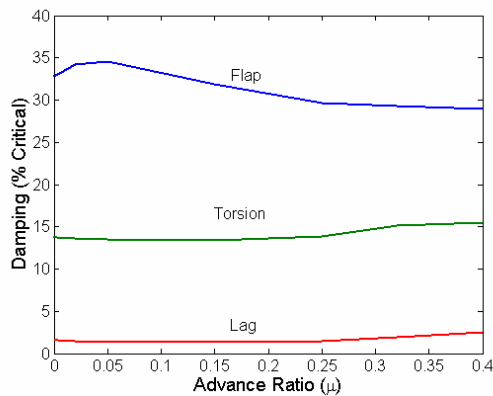


Figure 6.17 - Flap/Lag/Torsion Analysis

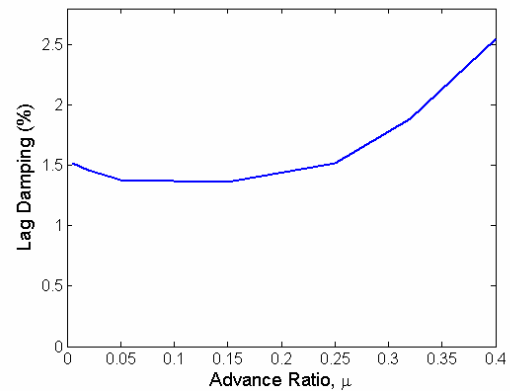


Figure 6.18 - Air Resonance Analysis

## Section 7 - Fan-in-Fin Anti-Torque System

### 7.1 - Anti-Torque System Trade Study

The configuration of the anti-torque system was decided after a trade study between the conventional tail rotor and the fan-in-fin concept.

**Safety on ground and in flight** - Because the Condor is designed as a mountain rescue helicopter, operational safety is of prime concern. The exposed, and often unseen rotor blades of a conventional tail rotor are potential hazards for people on the ground, while a fan-in-fin design, with a protective duct around the rotor, is safer and more visibly apparent. Additionally, for the same thrust capability, a fan-in-fin design usually needs about half the disk area of a conventional tail rotor. This is an important consideration in rescue operations because greater usable space around the helicopter means faster and safer unloading of patients. The duct around the fan prevents the tail rotor blades from striking obstacles such as mountain ledges or tree branches during flight operation in confined spaces.

**Maneuverability** - A mountain rescue helicopter needs to have sufficient yaw maneuverability and handling qualities for negotiating turns in tight spaces and withstanding high sidewinds. A fan-in-fin design is expected to have both of these qualities. The RFP requires capability of the helicopter to maintain heading with a cross wind of 40 knots from any azimuth. Cross winds directed against the downwash of the tail rotor are the most critical design conditions. If the ratio of crosswind to induced velocity of the tail rotor is high enough, there is a possibility of vortex ring state developing. Typically, fan-in-fin designs operate at higher induced velocities than conventional tail rotors designed for the same thrust capability. This means that a fan-in-fin design needs a higher side wind to induce vortex ring state than a conventional tail rotor.



Furthermore, the structure surrounding the fan prevents the establishment of air re-circulation, thus delaying the onset of the vortex ring state [Moui86].

**Hover efficiency** - From momentum theory, a fan-in-fin produces a thrust equivalent to that produced by a conventional rotor of twice the disk area. This is mainly due to two factors. First, a conventional tail rotor loses about 10% of its thrust capability from vertical fin blockage [Vuil86]. The fan-in-fin design eliminates this problem. In addition, about 50% of the anti-torque produced by a fan-in-fin comes from thrust generated by a negative static pressure at the duct inlet [Moui86]. In general, the fan-in-fin design is a more efficient anti-torque system in hover.

**Forward flight** - Due to the fact that the vertical fin in a fan-in-fin design can be made large without the penalty of blocking the rotor downwash, there will be substantial offloading of the fan-in-fin in forward flight. It should be noted, however, that the drag experienced by a larger vertical fin will add profile drag during cruise. Overall, a properly sized fan-in-fin requires less power in cruise than a conventional tail rotor.

**Noise** - Noise emanating from the tail rotor can be a major component of the total aircraft noise. Noise levels in a fan-in-fin design are lower than conventional tail rotors for several reasons. Firstly, the higher number of blades produces noise at higher frequencies, which is attenuated in the atmosphere at a much faster rate. Secondly, the largest component of the tail rotor noise occurs when the tail rotor is operating at high advance ratios during cruise. For a fan-in-fin, the tail rotor duct blocks the forward velocity component keeping the tail rotor at low advance ratios throughout cruise. Unequally spaced fan blades help to further attenuate noise [Niwa98].

**Weights and Cost** - The fan-in-fin design shows a substantial reduction in weight and cost when compared with a conventional design. A conventional design would require placement of the tail rotor at the top of the vertical fin for safety, requiring an intermediate gearbox and increasing weight and cost by about 20% [Moui86].

## **7.2 - Fan-in-Fin Detailed Design**

Based on the previous trade study, it was decided that the Condor will use a fan-in-fin anti-torque system. There are several components to a fan-in-fin anti-torque system: the duct (inlet lip, fan hub, diffuser), fan blades, and vertical fin. A diagram of the duct is given in Figure 7.1.

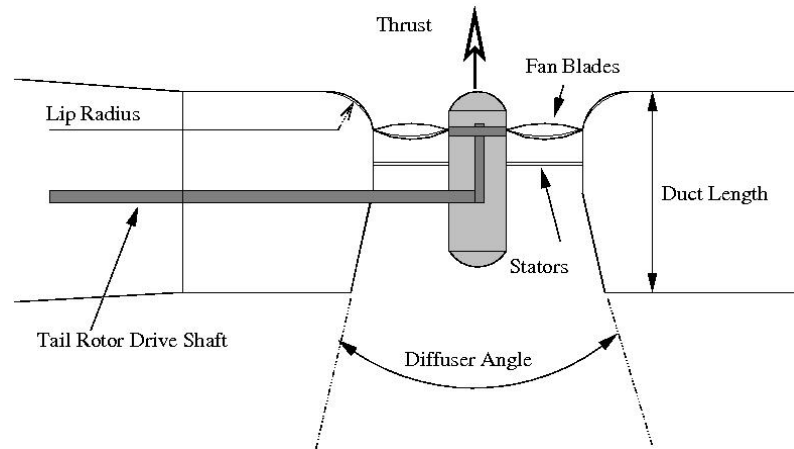


Figure 7.1 - Duct Cutaway Layout (Plan View)

### **7.2.1 - Duct/Shroud Design**

Designing the duct is an essential part of the fan-in-fin design and is optimized to maximize hover and low speed performance using the smallest duct size possible. The duct is comprised of three main sections - the inlet lip, fan hub and the diffuser.

**Inlet lip** - The inlet lip is a rounded section that creates a suction force from the inflow of the tail rotor. Experimental results from scaled tests performed at United Technologies Research Center (UTRC) have shown that a lip radius of 5-7% of fan diameter enables the duct to produce almost as much thrust as the fan itself [Kuche53, Keys91]. A survey (Table 7.1) of existing fan-in-fin designs shows that lip radii normally chosen for fantail systems are within this range. A lip radius of 7% fan diameter was chosen for the Condor to take advantage of these benefits.

**Fan hub** - The fan hub includes the fan blades and stator vanes, which are downstream of the fan. The hub also houses the mechanisms for control of the collective pitch. Stator vanes help to reduce the swirl flow component induced by the rotating blades and recover energy from the downstream flow field, thus increasing thrust. In Eurocopters, typically 8-11 stator vanes are used to straighten the flow. Full scale experiments have shown the advantages of stator vanes [Vuil86].

**Diffuser** - The effect of the diffuser is to prevent the wake from contracting, as in the case of a conventional rotor. Tests show that the maximum thrust generated by this wake expansion occurs at a diffusion angle of 20°. [Moui86] However, in practice, the diffusion angles are limited to 10°, because of instabilities that may occur from higher diffuser angles in forward flight [Keys91]. The diffuser angle used in the Condor is 10°.

Table 7.1 - Survey of Existing Fan-in-Fins

Parameter	SA342	EC130	EC135	EC120	XOH-1	SA365N	EC155	RHA66	Ka 62
Weight (kg)	1900	2400	2500	2800	3550	3849	4850	5800	6000
$D_{MR} / D_{TR}$	15.1	10.72	10.2	13.3		10.9	11.5	8.7	9.7
$V_{tip,TR}$	172	185	185	180	201	221	220	205	202
$\sigma_{TR}$	0.46	0.4	0.42	0.39	0.56	0.4	0.4	0.622	0.6
$(CT / \sigma)_{TR}$	0.12	0.11	0.13	-	0.1	0.12	-	0.11	0.09
$N_{b,TR}$	13	10	10	8	8	13	10	8	11
Chord (m) <sub>TR</sub>	0.04	0.06	0.05	0.06	0.12	0.04	0.06	0.16	-
Lip radius (% fan diameter)	-	-	-	-	7	10		7.5	-
Twist (deg) <sub>TR</sub>	-7	-	-	-	-11	-7	-	-7	-

### 7.2.2 - Fan Design

Fan design primarily looks for high aerodynamic efficiency. Research results from Aerospatiale and Boeing have been used for this design [Keys91,Moui86].

**Fan Diameter** - Historical trends shown in Table 7.1 show that the ratios of main rotor diameter to tail rotor diameter for fan-in-fin designs range from 8.7 for the Comanche to 15.1 for the SA342. The fan has to be large enough to provide efficiency during hover while incurring a low weight penalty. Moreover, the diameter has to be large enough for the tip speed to remain low, limiting noise. Considering all these factors, a value of 10 was chosen for this ratio and the diameter of the fan was determined to be 1.2 m. With this, the length between the main rotor hub and the fan hub becomes 6.7 m.

**Fan tip Mach number** - The fan tip mach number was decided by noise considerations. The tip speed is 180 m/s and is comparable to other fan-in-fin designs.

**Fan blade spacing** - The fan blade spacing influences the noise generated by the tail rotor. It has been reported that an asymmetrical fan blade arrangement can be used for reducing noise [Niwa98]. These results have been used to determine the fan blade spacing of the Condor as a 26°/36° arrangement. The blades were spaced to ensure that there was no mechanical interference of the blade pitch links.

**Fan blade airfoil** - A highly cambered airfoil is ideal for fan blades. Because fan blades are small and have a high torsional stiffness, it is unlikely that they will twist considerably. Therefore highly cambered airfoils are used for fan blades. Considering these factors, NACA63A312 airfoil was chosen as the airfoil section for the fan-in-fin blades.



**Blade Solidity** - The selected solidity of the fan was based on high altitude considerations. Because the fan blades operate at low Reynolds numbers, it is important to choose lower values of  $C_T/\sigma$  (blade loading coefficient) to prevent the onset of stall. The fan was sized to provide anti-torque during hovering at 4,572 m (15,000 ft). A value of 0.115 was chosen for  $C_T/\sigma$  of the fan at this design point. Because  $C_T$  is known, a rotor solidity of 0.606 and a blade chord of 0.11m can be obtained. It can be seen in Table 7.1 that this value is typical of other fan-in-fin designs.

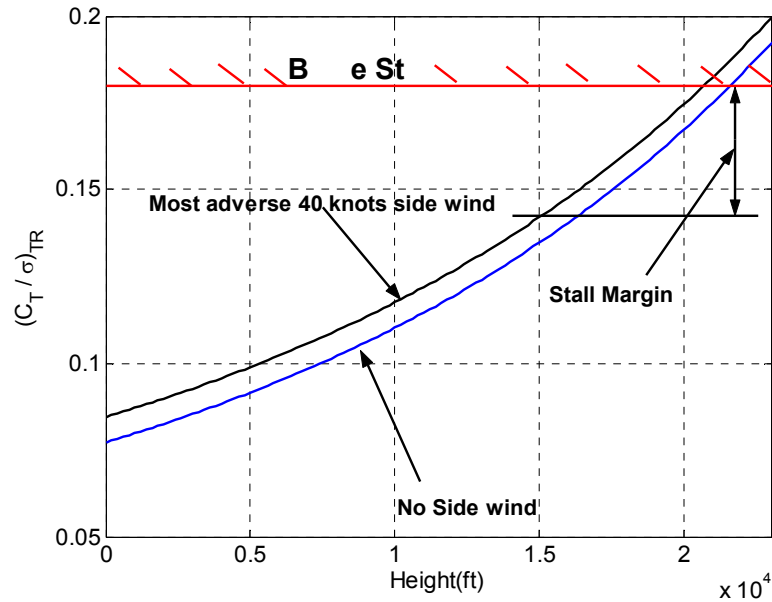


**Figure 7.2 - Blade Loading Coefficient (with and without sidewind) at Altitude**

**Stall Margin** - Stall margin for the fan-in-fins becomes an issue for trying to maneuver while resisting side wind. Figure 7.2 shows the blade loading that is required for hovering at different altitudes with and without side wind. Side winds affect the tail rotor in two ways. Firstly, there is an increase in the torque (that the tail rotor has to counter) generated from fuselage side force, and secondly, the inflow in the duct is altered by the side wind. The major contribution to the extra torque generated by the fuselage side force comes from the side force on the vertical tail. This is what has been considered in Figure 7.2. It can be seen that there is a considerable stall margin at 4,572 m (15,000 ft) even during the most adverse 40 knot side wind. This ensures the Condor will have sufficient tail rotor authority to maneuver at 4,572 m (15,000 ft) in the presence of a 40 knot side wind.

### 7.2.3 - Vertical Fin Design

As mentioned earlier, the vertical fin is sized to provide all the anti-torque necessary at cruise, so offloading the fan completely and increasing the life of the fan mechanisms. Offloading the fan has many advantages. Because the dynamic strains on the hub components are minimized during cruise, fatigue loads are reduced, increasing the life of the hub and mechanical linkages. In addition, the drag penalty that occurs as a result of operating the fan during cruise is reduced. Experiments have shown that the drag penalty of an unloaded fan can be reduced by 30% [Keys91]. Finally, a safe return to base and landing can be performed with an inoperative fan in case of a tail rotor failure. This feature was demonstrated in flight by the Dauphin, which landed safely after one hour of flight without the tail fan [Moui86].

A highly cambered airfoil section with a high thickness-to-chord ratio was chosen for the vertical fin. A high camber is chosen to provide maximum lift coefficient at a low AOA, so reducing the drag produced by the fin. The high thickness-to-chord ratio is necessary to have a smooth transition from the duct to the fin. The airfoil chosen was a NASA63<sub>3</sub>A618 positioned at an angle of incidence of 4°. The lift-to-drag ratio at this angle of incidence is 145. Simple airfoil theory was used to analyze the lifting force generated by this airfoil. As per the RFP requirement, the fin was sized for cruising at 3,658 m (12,000 ft) and the area of the fan is 1 m<sup>2</sup>. Figure 7.3 shows the fraction of the required anti-torque thrust that is generated by the fan and the fin at different cruise speeds. At a cruising speed of 145 knots, the fin unloads the fan completely of thrusting requirements except for directional control. Figure 7.4 shows power required by the fan at different cruise speeds. Once again, we can see the fan is off-loaded completely at a cruising speed of 145 knots.

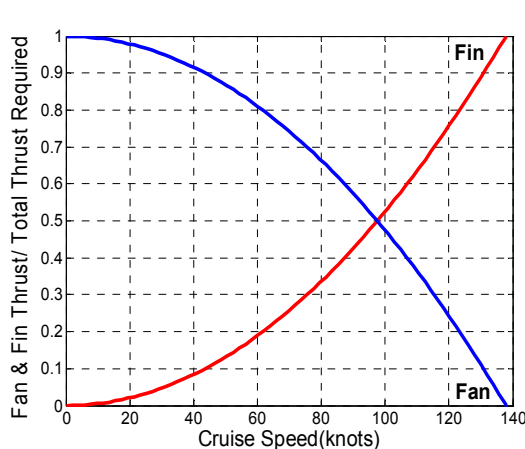


Figure 7.3 - Thrust to Total Thrust Ratio

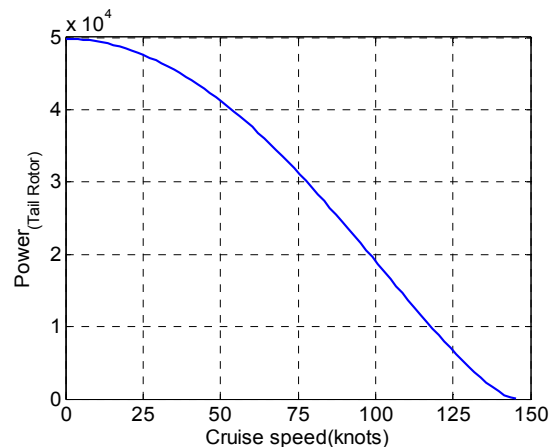


Figure 7.4 - Fan Power vs. Speed

## **Section 8 - Airframe/Landing Gear Design**

### **8.1 - Airframe Design**

The structural layout of the Condor consists of three modules: the cockpit, the central fuselage, and the tail boom. There are seven primary bulkheads which serve to inter-connect the modules, bear the loads and bending moments, and to support the engine and transmission deck. In addition, there are secondary bulkheads to maintain shape and frame openings. Two keelbeams and the transmission/engine deck provide structural integrity and support to the cockpit and cabin floor. See Foldout 8.1 for structural details.

#### **8.1.1 - Structural Details**

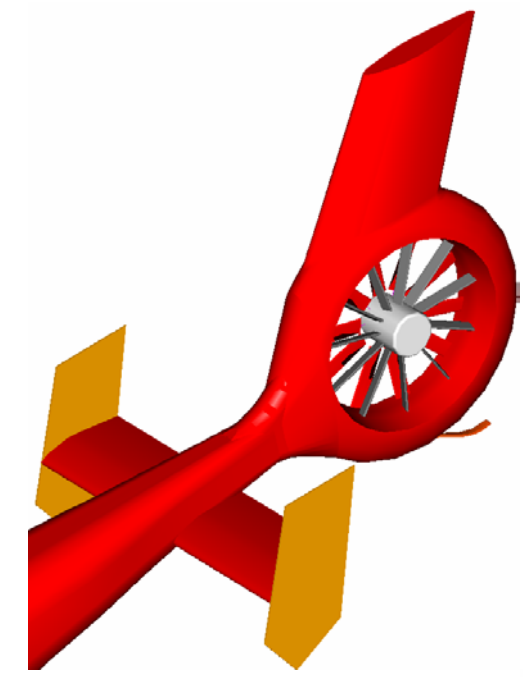
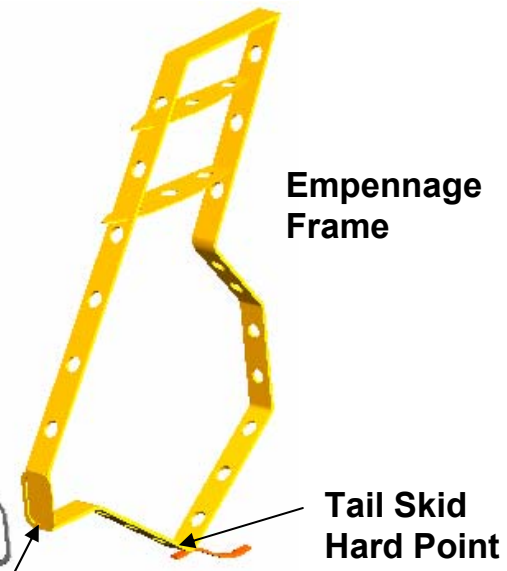
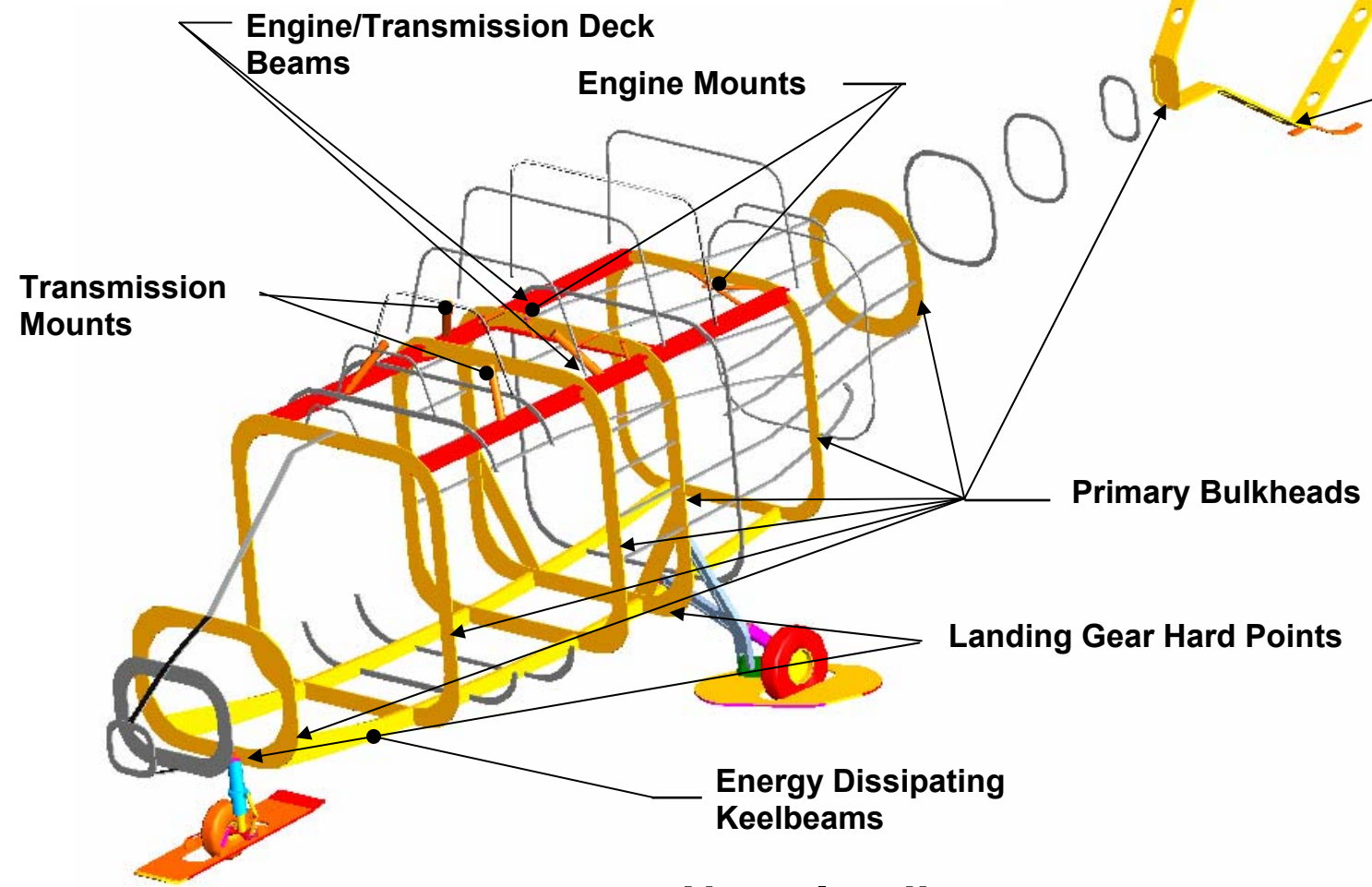
The first primary bulkhead connects the nose to the cockpit, and houses the nose landing gear attachment bracket. The second primary bulkhead connects the cockpit to the central fuselage and is the forward support of the transmission deck. The third and fourth bulkheads offer intermediate support to the transmission deck. The main landing gears are attached to the fourth bulkhead. The fifth bulkhead is the aft most support of the transmission deck, and the sixth bulkhead connects the central fuselage to the tail. Between the first and the sixth bulkheads, keelbeams and stringers augment the bulkheads, so that a major part of the airframe is semi-monocoque. Aft of the sixth bulkhead, the tail section is fully monocoque. The seventh primary bulkhead connects the empennage to the tail boom.

The cabin cross section of the Condor is a rounded square from bulkhead #2 to bulkhead #5. This shape maximizes useable interior space in the central fuselage, and leads to bulkheads that have simple geometries making each module easy to manufacture and assemble. Furthermore, this fuselage shape allows for placement of two large sliding doors. Maintaining a consistent cross section also produces an exterior surface that is aerodynamically clean and aesthetically pleasing.

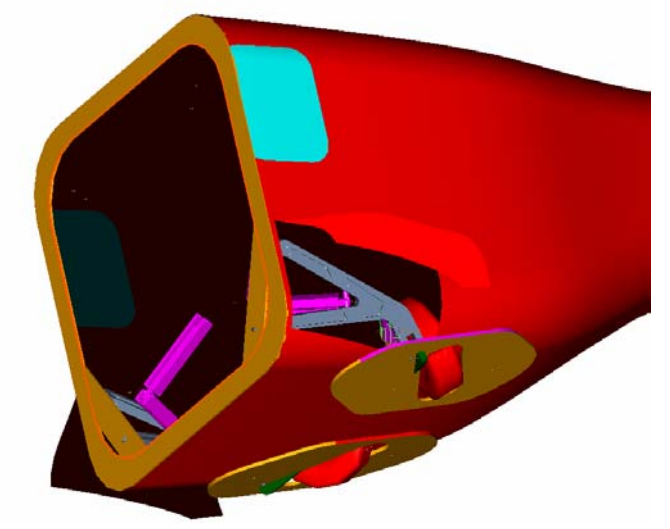
Each of the primary bulkheads has been designed to have a safety factor of 1.5 over the limit loads. These loads come from five main categories: landing, flight, takeoff, ground handling, and rotor operations. Landing loads in particular were scrutinized carefully for the Condor, because unprepared landing areas and adverse weather conditions are primary contributors to this category, and are likely to be encountered during mountain rescue missions. Fatigue loads are an additional source of concern for helicopters, and hence every structural element of the Condor has been designed to meet or exceed the requirements of 14CFR29.571.

# Foldout 8.1 - Structural Layout

Note: Empennage connected to fuselage via monocoque composite tail boom

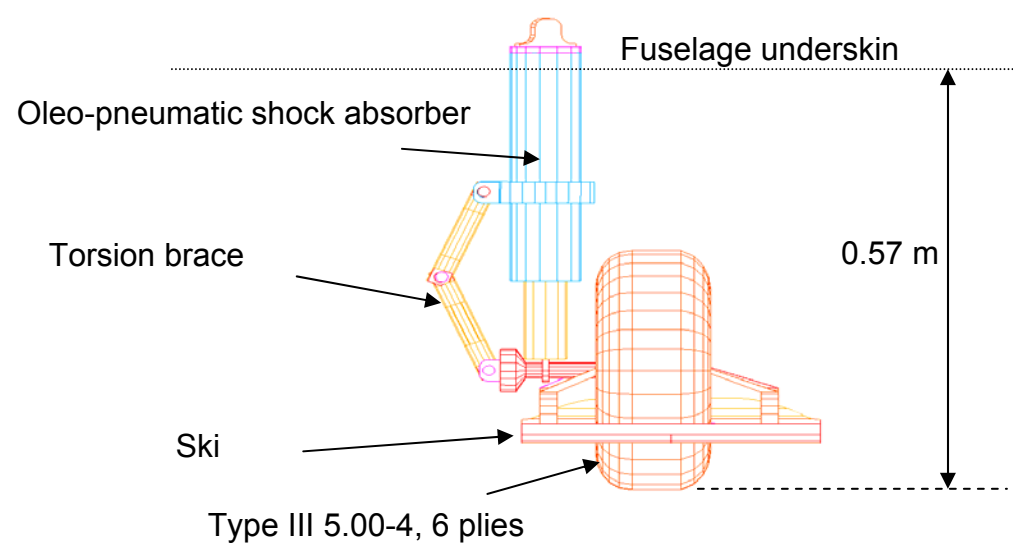


**Fan-in-Fin**  
 Fan-in-Fin anti-torque system provides good yaw control to 20,000 ft with side winds of 40 knots. The 'Fin' offloads the fan completely in cruise.

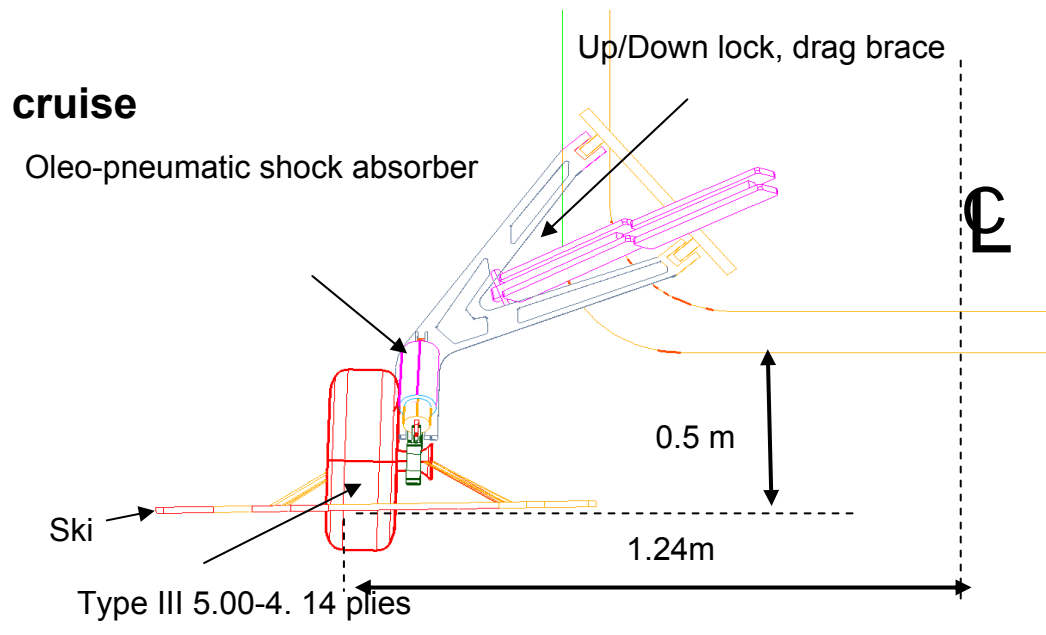
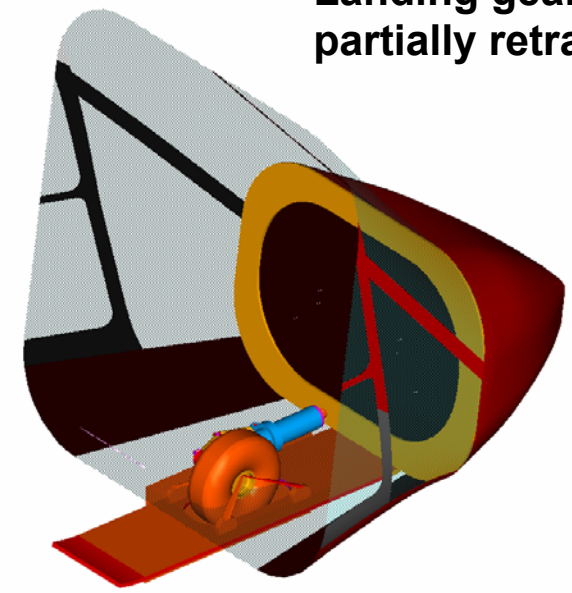


Rear landing gear

Nose landing gear



Landing gear can be partially retracted during cruise





### **8.1.2 - Crash Resistance**

The mountain rescue mission of the Condor makes encounters with rough terrain and adverse weather very probable. Therefore the airframe is rugged and designed to protect its occupants during high load events such as rollover or obstacle strike. Throughout the airframe, structural members have been sized and arranged to maximize survivability by emphasizing energy absorption and dissipation. The webs of the two keelbeams have been designed to absorb energy by collapsing in a high buckling mode; this pattern increases the amount of energy which is absorbed during an emergency landing. The bulkheads and stringers are arranged to collapse progressively when subjected to high inertial loads so that those loads are substantially reduced before reaching passenger/crew accommodations like seats and litters. During blade-ground strike events, the primary danger to occupants is that the high bending moments and torsion transmitted to the rotor mast can cause the transmission to intrude into the cabin. The transmission of the Condor is designed to prevent this type of movement through high strength ceiling support. To allow for rapid exit from the helicopter, all doors have been designed to remain operable after a high load event.

### **8.1.3 - Materials, Manufacturing, Construction**

The bulkheads, stringers and keelbeams of the airframe are aluminum-lithium alloy. Lithium being the lightest metallic element, it can reduce the weight of an aluminum alloy by about 3% for every 1% of lithium added. Most commercially available Al-Li alloys contain about 2% lithium, offering a 7-10% reduction in density, and a 10-15% increase in elastic modulus. This type of alloy also has good resistance to the growth of fatigue cracks, making it advantageous for rotorcraft airframes. These elements are also overlaid by a Kevlar/graphite/epoxy skin. Graphite fibers have superior strength and stiffness, but the material is susceptible to impact damage. Kevlar is more resistant to impact damage, making it an ideal external skin.

The engine/transmission deck is made from titanium alloy plate. Titanium was selected over aluminum-lithium and composite sandwich construction for its resistance to heat and fire, as well as oil corrosion.

The three modules of the Condor airframe are manufactured separately, and fitted with required subsystems. Final assembly is made easier by the consistency of the cross section and simplicity of interior structure.



**8.1.4 - Doors**

The cockpit doors are large and hinged on the forward side. The hinge placement precludes the possibility of the doors being blown open if improperly latched. Sliding doors are located on both sides of the fuselage, and are wide enough to facilitate hoisting operations and litter embarkation. All doors are braced to prevent jamming in the event of airframe warping, and can be jettisoned in emergencies (14CFR29.783).

**8.2 - Landing Gear Design**

A trade study was completed to decide the configuration type for the Condor landing gear. The options considered were the skid landing gear and the tricycle type retractable wheeled landing gear. The prominent considerations are given in Table 8.1.

**Table 8.1 - Landing Gear Configuration Comparison**

Parameter	Skid Configuration	Retractable Wheeled Configuration
Weight (% of MGW)	1.2 %	2.4 %
Flat Plate Area (% of total)	15 %	4 %
Technical Complexity	Simple	Complex
Snow Operation	Yes	Needs ski attachment
Adaptability	Poor	Good
Hoisting Hindrance	Some interference	No interference

Skid landing gears are usually preferred for use in light and middle weight category helicopters because they are light and less mechanically complex to design than wheeled landing gears. They also offer the ability to land and operate on snow, a necessary feature for mountain operations. A wheeled landing gear provides ground maneuverability and has the advantage of being easily adapted for multi-mission capability, a key feature considering the Condor is a high-powered aircraft and could be valuable for a variety of missions. Another important criterion is the drag penalty associated with each configuration. Skid landing gears offer larger flat plate area and greater drag than the wheeled configuration. The additional ski attachments required for snow operation prevent the landing gears from being retracted completely into the fuselage. However, as can be seen in Foldout 8.1, they have been designed to fit closely to the fuselage profile, reducing parasitic drag. The skis were designed in accordance with 14CFR29.737 to withstand aerodynamic and inertial loads during flight. It is shown in Figure 8.1 that the power penalty associated with a skid landing gear versus this retractable wheeled landing gear is approximately 30 kW (for cruise at 145 knots), or alternately, 4 knots in cruise speed for the same cruise power required. The final factor in selecting the landing gear type was the interference of the gear with

hoisting operations. Skid landing gears could hinder rescue operations by obstructing the litter’s hoisting path. A wheeled configuration, however, would be positioned beneath the fuselage and would not cause any interference. Considering these factors, a retractable wheeled configuration with attachable skis for snow landings was the landing gear arrangement chosen for the Condor.

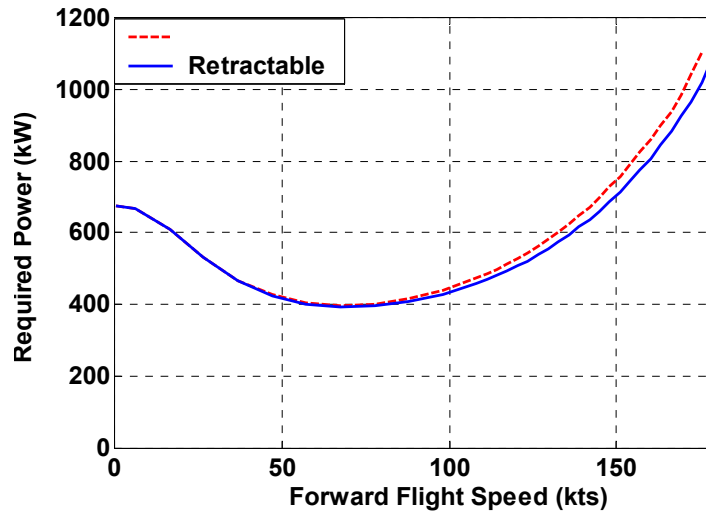


Figure 8.1 - Required Power with Fixed and Retractable Landing Gear

**8.2.1 - Configuration**

The position of the main and nose landing gears were decided to cater to the variations in the c.g. experienced by the helicopter. For ground handling qualities, the recommended values for landing gear static loads are 80% for the main landing gear and 20% for the nose landing gear [Curr88]. The Condor has a wheel track of 2.2 m and a wheel base of 3.6 m. Under static conditions, 77% of the load is carried by the main gears while 23 % is taken by the nose landing gear. The lateral position of the rear landing gears was calculated to account for the rollover angle requirements. A rollover angle of 57° was adopted for the design, a value well within the recommended value [AMCP74].

Disc brakes are installed in the rear wheels to park the helicopter when grounded. The steering control is implemented using a push pull system that incorporates a shimmy damper. The pilot controls the helicopter using rudder pedals linked to the nose wheels. The maximum turning angle of the wheel is 60° which allows for all required ground maneuvers.



### **8.2.2 - Tire Sizing**

Tire pressures were kept low to allow operations on both prepared and semi-prepared runways. The wheels of the main landing gear were designed for a maximum static load of 45% of MGW (1,350 kg). The tires chosen were Type III 5.00-4 with 14 plies and a bottoming load capacity of 3,129 kg. The inflation pressure of the main landing gear wheels was 620.5 kPa (90 psi). The nose wheel was sized for dynamic loads using a dynamic load factor of 2.5. For this wheel, a Type III 5.00-4 with 6 plies was chosen. This wheel has a bottoming load of 1,450 kg and an inflation pressure of 379 kPa (55 psi).

### **8.2.3 - Oleo Sizing**

Single oleo-pneumatic shock absorbers were used for the main and nose landing gears. The shock absorbers were designed to satisfy the drop test requirements of 14CFR29.723. Each gear must be able to withstand a vertical drop height of .3 m (12 in) or a drop velocity of 2.5 m/s for the reserve energy absorption drop test. Assuming a tire stroke 1/3 of the tire radius, shock absorber and tire efficiencies of 0.85 and 0.47, respectively, a dynamic load factor of 3, and a stroke margin of 0.013 m, the total stroke length of the oleo-pneumatic shock absorber was found to be 0.114 m. An internal pressure of 12410 kPa (1800 psi) was chosen for the absorber as this would enable the use of standard compressors to be used for servicing. The external diameter of the oleo is typically 1.3 times the internal diameter and the length of the strut is typically 2.75 times the required stroke. The resulting dimensions of the oleo-pneumatic shock absorber are 0.27 m in length with an outer diameter of 0.05 m.

## **Section 9 - Details of Cockpit/Cabin Systems**

### **9.1 - Crew Station Features**

In addition to the instruments required for single pilot IFR flight, the Condor cockpit includes several state-of-the-art systems. The Condor features programmable FMZ20001 Flight Management System (FMS), which utilizes GPS as its primary navigation sensor, a Northrop Grumman LN-100G2, which represents one of the most advanced embedded GPS Inertial Navigation System (INS) available in the market, and a limited cabin crew hover control. To assist in search operations, the Condor utilizes a retractable searchlight and Star SAFIRE II FLIR camera, as well as Night Vision Goggle (NVG) compatibility. In addition, a hoist mounted video camera provides the pilots with a view of the hoisting operations.



## **9.2 - Cockpit Layout**

### **9.2.1 - Cockpit and Cabin Access**

Access to the cockpit is provided by two hinged doors on either side of the cockpit. Large sliding doors are provided on both sides of the fuselage to facilitate cabin access and to provide sufficient room for winching operations. The doors can be jettisoned in case of emergency.

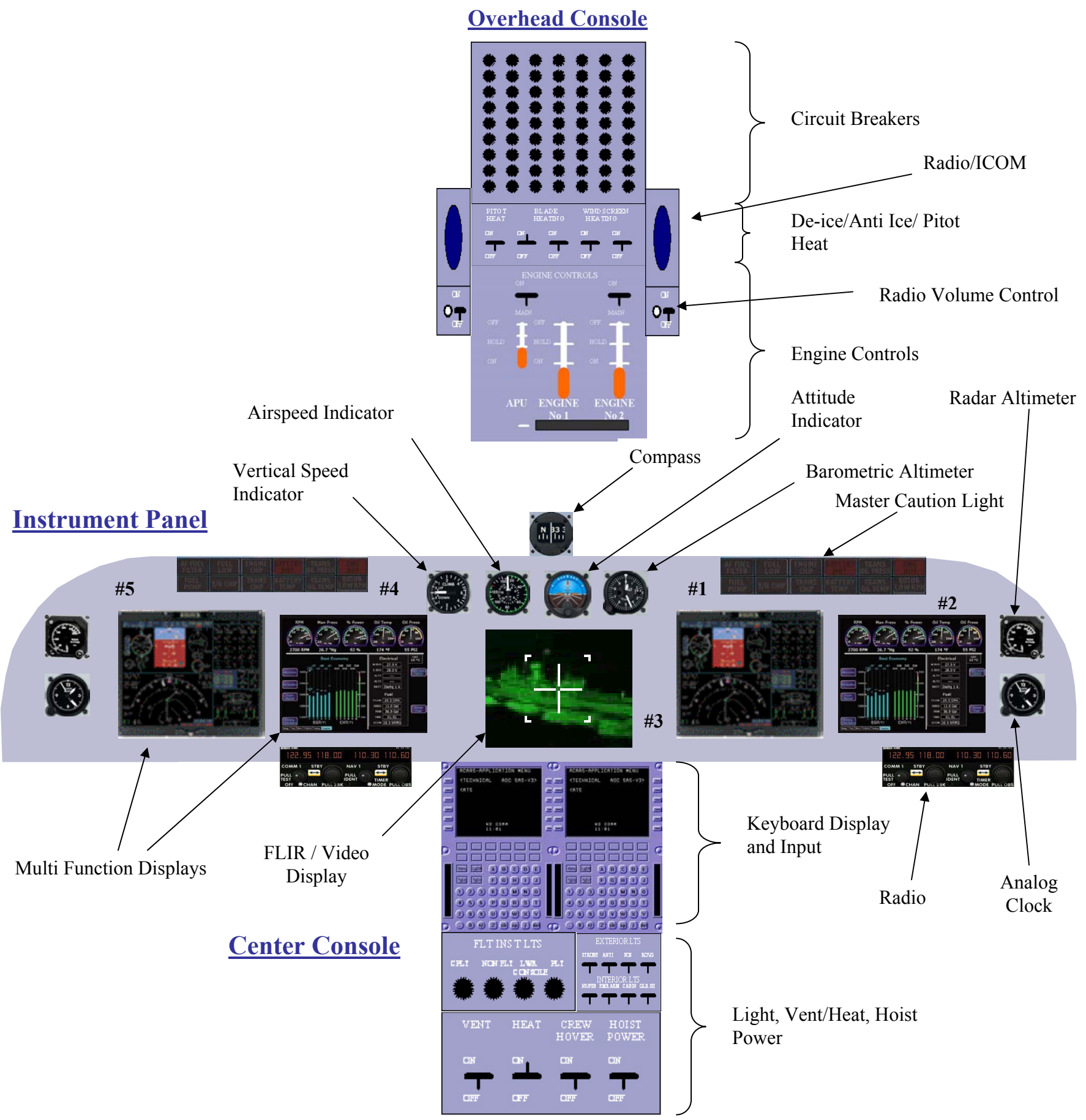
### **9.2.2 - Pilot/Copilot Stations**

The pilot station is located on the starboard side of the cockpit while the copilot seat is on the port side. Both pilot and copilot have full access to the full complement of flight instruments and controls. Although a state-of-the-art glass cockpit was selected for the baseline design, the Condor also offers an alternate less expensive avionics package. The details of this package are presented later in this section.

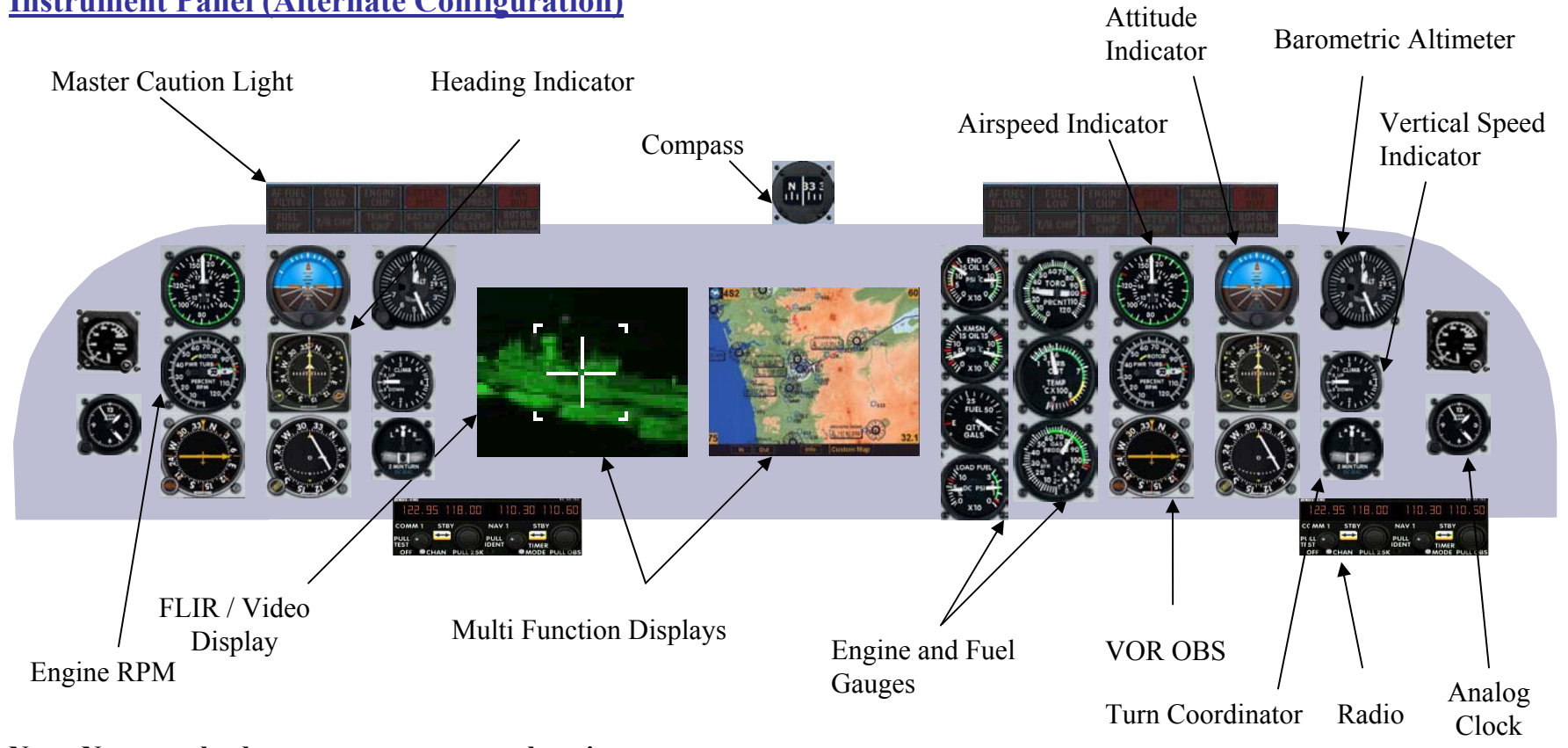
The instrument panel (refer to Foldout 9.1) consists of five smart Multi-Function Displays (MFDs), as well as standby attitude indicator, altimeter, airspeed indicator and vertical velocity indicator. Also provided on the instrument panel are two backup radios, two analog clocks, two radar altitude gages, a compass, and two master caution light panels. The radios can be operated using a keyboard on the control display units (CDUs) or via the backup radio display/dials. An analog backup clock is used in preference to a digital clock, to provide a visual feel for the time elapsed. The caution lights installed on the instrument panel provide visual indications of failure(s) in the engine and/or drive train lubrication system, hydraulic systems, auxiliary power unit (APU), generator, and low fuel warning. These warnings are generated by the HUMS and are displayed on the MFDs.

The overhead console (refer to Foldout 9.1) houses the aircraft system controls which include circuit breakers, engine controls, pilot heat switches, anti-ice system controls, and two radio/Inter-Communication Select (ICS) panels. The center console contains two CDUs, console light controls, external light controls, crew hover control selector, and main hoist control panel. The CDUs provide the interface with the FMS, and can also display weather related data and can work with Enhanced Ground Proximity Warning System (EGPWS) software, to provide a graphical display of origin or destination terrain information, the terrain data provides crew awareness of landing or take-off location.

# Foldout 9.1 - Cockpit Layout



## Instrument Panel (Alternate Configuration)



Note: Not to scale, does not represent actual equipment.



The collective stick has controls to turn the searchlight and FLIR on and off, to control the direction of the searchlight/FLIR, and to operate the searchlight retraction mechanism. The cyclic stick is equipped with the hoist release/cable shear switch (shielded switch to avoid accidental release), hoist fixed speed control roller, stick trim button, trim release button, moding cursor control (coolie hat), and ICS call trigger.

### **9.3 - Cockpit Systems**

#### **9.3.1 - Sensor Suite**

The Condor is equipped with LN-100G embedded GPS inertial system, which provides inertial, GPS, and hybrid navigation solutions. It combines the Zero-lock Laser Gyroscope with the latest electronics, and GPS to provide enhanced position, velocity, and heading reference. The output is available in digital form which is fed directly to MFDs. The INS/GPS unit provides true heading, pitch, roll, position, velocities and accelerations which are also sent as an input to the FMS. The unit is located near the c.g. to provide accurate measurements. The accuracy of the GPS receiver can be improved by providing differential corrections from a Differential GPS (DGPS) reference station located nearby.

#### **9.3.2 - Multi-function Displays**

The Condor's instrument panel has a total of five Northrop Grumman Colorsmart MFDs. All the MFDs are identical, interchangeable, and fully reconfigurable for changing roles and missions. Two MFDs are provided on the pilot's side and two on the copilot's side. In addition, a fifth central MFD is provided for the FLIR display during the flight. During rescue, this will be used as a video display for the pilot to monitor the hoisting operation.

Based on open system architecture, each MFD has a separate processor which allows it to communicate independently with the data bus rather than through a main mission computer. The advantage of such a system is that an individual chip failure would only affect a single MFD, and will not compromise the mission capability. The increased redundancy of this type of system outweighs the increased cost incurred by having a separate processor for each display [Nort04b].

The main pages of the MFDs include the Primary Flight Displays (PFDs include attitude indicator, airspeed indicator, vertical velocity indicator, barometric pressure, turn coordinator etc.), navigation pages, fuel and engine related information, sensor pages, FLIR page, system status page, and the Warning/Caution/Advisory (WCA) page. The interchangeability and

configurability of the displays makes it possible to have a wide range of information displayed in the cockpit panel.

### **9.3.3 - Communication Systems**

The communication systems of the Condor include cockpit-to-cockpit, cockpit-to-cabin, cockpit-to-rescuer and over the horizon channels to aid in the rescue operations. The equipment provided includes VHF-FM ground and airborne radios, a VHF-AM radio, a UHF-AM radio and a high frequency radio for non-line-of-sight communications. An intercom system is provided to facilitate hands off communication with the aft crew. Throat microphone and earpiece are provided to the rescuer involved in ground operation to communicate with the crew. Chemlights are also provided in case of a communication system failure and/or to minimize voice traffic being relayed to the helicopter crew.

### **9.3.4 - Mission Systems Equipment**

The mission system equipment includes NVG filters and dimmers, Primus 700 SAR/Weather RADAR system, a Star SAFIRE II FLIR camera, a data loader, a retractable SX-5 Starburst Searchlight, and IFR equipment (Stability Augmentation Systems (SASs), Attitude Retention Systems (ATTs), Autopilot Systems (APs), Flight Director Systems (FDs); see Section 11).

#### ***FLIR, Searchlights, and Radar System***

The NVGs, FLIR, searchlights, and weather radar can be combined together to enhance search and rescue at night. Star SAFIRE II [Flir01] provides enhanced thermal sensitivity and powerful optics for superior range performance. A SX-5 Starburst Searchlight [Spec01] is located in the nose of the helicopter alongside the FLIR system. It is equipped with a 500W short arc Xenon lamp which delivers a minimum of 15 million candle power. The searchlight is retractable to minimize parasite drag when not in use. The Condor is equipped with a Primus 701A SAR/Beacon/Weather radar system that is integrated with color weather radar and personal beacon detection. With high resolution precision surface mapping, minimum detection range as low as 450 ft and Doppler turbulence detection, Primus 701A is tailor-made for the operations in mountainous environments, where sudden exposure to turbulence can be hazardous. The Primus701A can also be used to locate and



**Figure 9.1 - FLIR**



identify personal locator beacons, a commonly used safety tool for today's mountain climber/hiker [Hone04c].

### ***Enhanced Ground Proximity Warning System***

The Condor is equipped with a Honeywell Mark XXII - Enhanced Ground Proximity Warning System (EGPWS). EGPWS provides a real-time situational awareness display of surrounding terrain and obstacles in relation to an aircraft's altitude and flight path. The system is designed to visually and audibly alert the flight crew of potential terrain/obstacle conflict. It includes a high-resolution built-in terrain database designed to help eliminate controlled-flight-into-terrain (CFIT) type accidents [Hone04b]. A Traffic Alert & Collision Avoidance System (TCAS) (Honeywell CAS-100 4MCU) is included as well, to increase traffic and terrain awareness of the crew. The TCAS system interacts with the EGPWS system to retrieve terrain data and provide traffic solutions that optimize separation from terrain and other aircraft [Hone04d].

### **9.3.5 - Flight Management System**

The flight management system uses the position information obtained from the GPS/INS system and combines with the information from its internal database to guide the helicopter along the optimized flight path for the specific mission. The Honeywell FMZ-2000 Flight Management System provides this feature on the Condor. With Honeywell's SmartPerf (Smart Performance) software option, the FMS learns the performance characteristics of a specific aircraft and provides the crew access to numerous performance calculations. Using its performance database along with atmospheric data, SmartPerf provides pilots with the following performance calculations:

- (i) Time, fuel and predicted altitude at all waypoints.
- (ii) Time and distance to step climb.
- (iii) Predictions for stored or active flight plans.
- (iv) Equal Time Point.
- (v) Point of no return.
- (vi) One engine performance data.

SmartPerf logic originates with the baseline performance information for the type of aircraft and fine-tunes to the performance characteristics of the aircraft when installed [Hone04a]. A data loader is used to help reduce the mission start times. If the exact location of the target is available then the related information can be directly downloaded from a disk carried with the crew from their point of origin, or can be updated via uplinks from a data-stream whilst en route to the rescue area. From this information, the FMS can propose the optimized flight path.



### **9.3.6 - Alternate Avionics Package**

The design team is aware of the fact that the current design faces a very competitive, cost-conscious market, and every effort has been made to keep the cost to a minimum without compromising the mission capability. For this reason, the Condor can be equipped with an alternate, less expensive avionics package that has two MFDs, with primary flight information being provided using mechanical gages. In addition, the INS/GPS system would be replaced by a less costly unit, and if the mission does not require operation in mountainous regions, the EGPWS may not be required. To facilitate this, the elements of the avionics package are installed in accessible areas and can be removed or replaced easily to fit the client's needs.

### **9.4 - Cabin Systems**

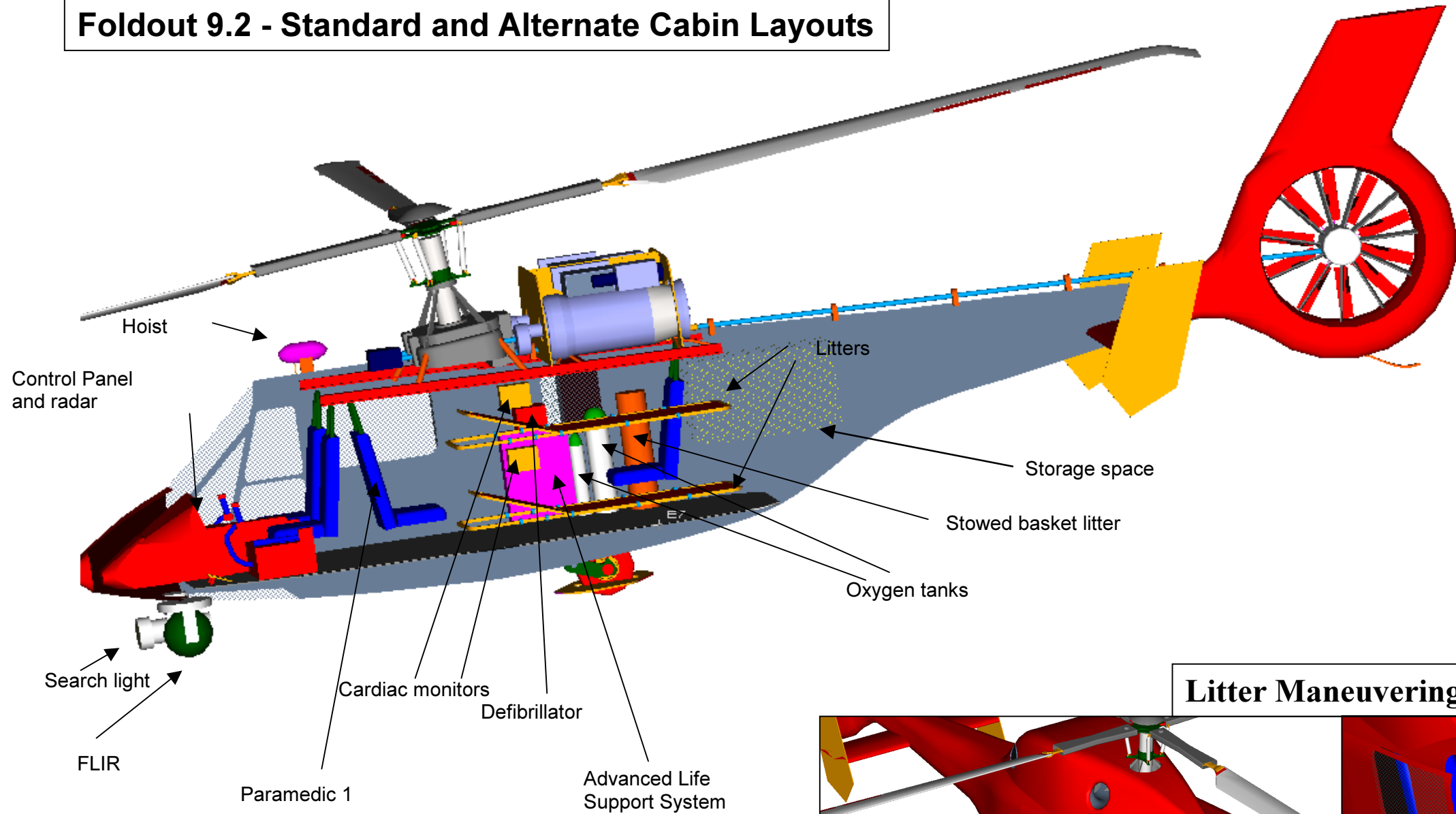
The hoist control panel is located to the right of the starboard cabin door. It contains control for the hoist power and motion. It also has a cable fault sensor light and a cable position indicator. A tethered portable hoist control is also available near the crew station, which can be used to perform the hoisting operation while leaning out of the cabin door, a safety belt provides a secure harness to the crew member manning the hoist.

### **9.5 - Cabin Equipment Layout**

The cabin of the Condor is arranged to maximize the amount of usable working space for the crew. The SAR mission provides the cabin crew two priorities: loading passengers, and caring for patients. Loading an immobile patient into the helicopter requires maneuvering the rescue litter through the sliding door and onto the appropriate rack, as shown in Foldout 9.2. When the helicopter is on the ground, an external crew member can help to fit the rescue litter through the door. During hoisting operations, however, the rescue litter must be brought through the door while suspended from the hoist and moved into position.

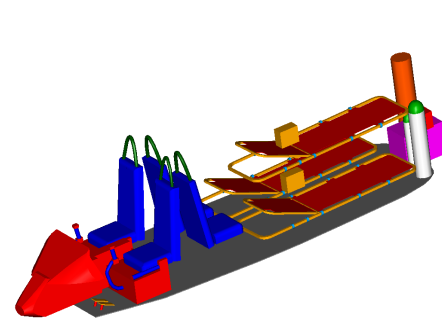
To maximize working space in the cabin, the two litters in the supine position are stacked vertically on the port side of the cabin. This allows adequate room for the crew to maneuver the rescue litter into the desired position and to provide medical attention to the patients once they are loaded. The first litter is 160 mm (6.3 in) above the cabin floor, allowing accessibility to the patient for a seated crew member. The second is 640 mm (25.2 in) above the first, locating the patient at about waist height, and providing accessibility to a standing crew member. This layout provides an additional height of 640 mm (25.2 in) above the top litter to the cabin ceiling. The

# Foldout 9.2 - Standard and Alternate Cabin Layouts

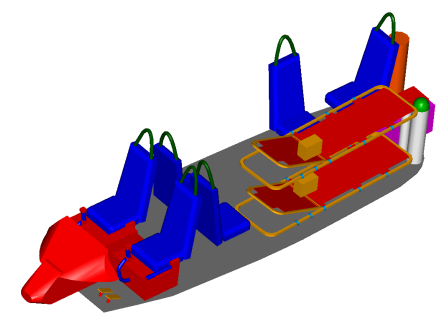


Note: Search light and FLIR cannot be extended with deployed nose landing gear

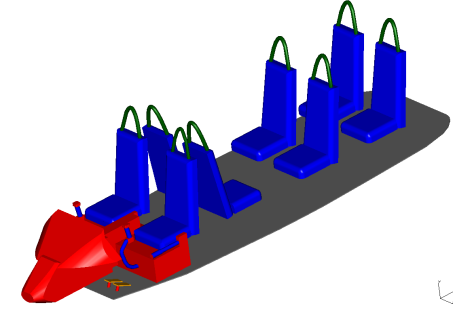
**3 Patients + 2 Paramedics**



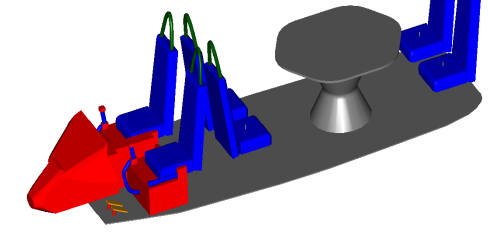
**4 Patients + 2 Paramedics**



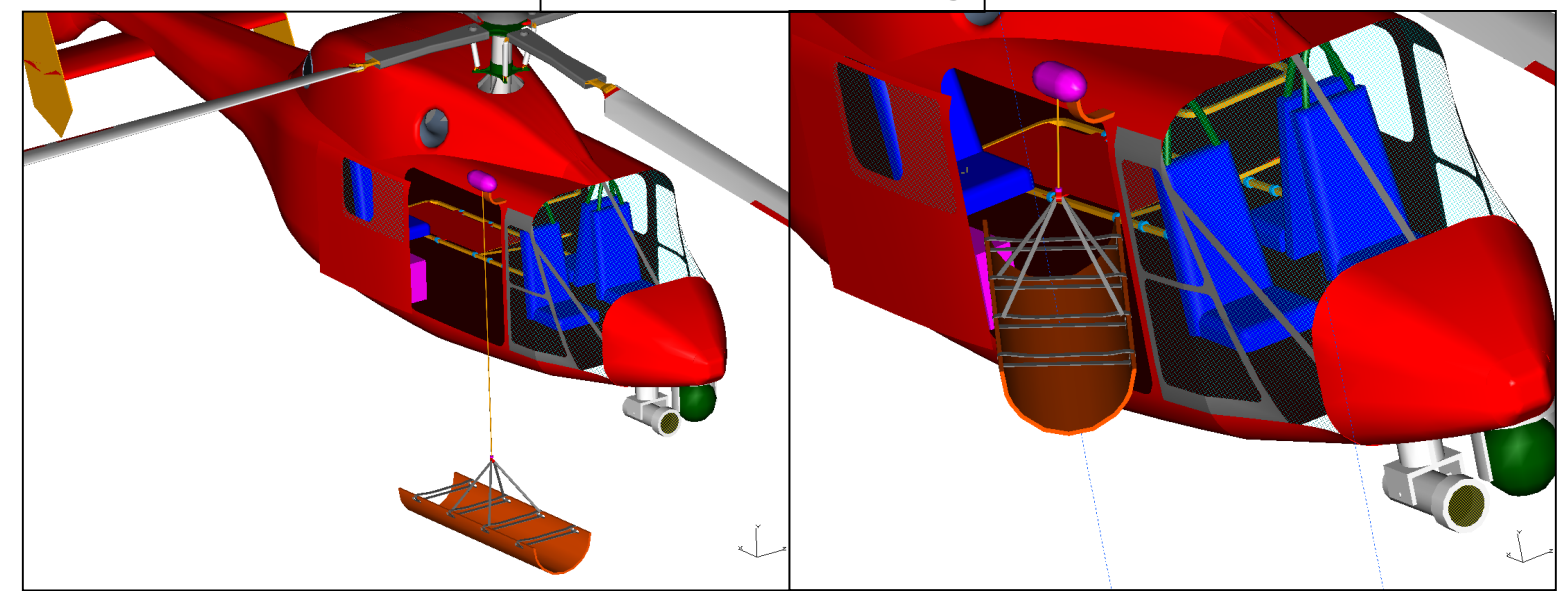
**Passenger Transport**



**Business Class**



## Litter Maneuvering



height of the top litter is low enough to allow the crew to easily load a patient onto it, and for the patient to come down unassisted, if he/she is mobile. The starboard side of the cabin is open, leaving room for the crew to move. Inertial reels allow the crew members to move about the cabin while maintaining a secure tether to their seats. The crew seats are arranged at the head and side of the litter bay, so that one paramedic is positioned for patient airway management while the other can assist with other tasks. The medical equipment is stowed against the walls of the cabin, with the monitor/defibrillator units close to the chests of the patients. Rescue equipment and the large oxygen cylinder are located in the aft storage space, which also holds modular avionics bays (standard and alternate cabin layouts can be seen in Foldout 9.2). There is an access hatch into these bays for easy maintenance, installation, and replacement of avionics.

## **Section 10 - Mission Equipment**

The specified mission task of the Condor, in addition to the flight profile, requires two distinct in-flight operations. The first is a hoisting rescue of stranded victims from a hazardous environment. The second is the application of life-saving medical aid for the rescued victims during the return from the rescue site. Both operations are indeed critical, and so a considerable research effort was made to ensure that the Condor was outfitted with state-of-the-art search and rescue and medical equipment for a high rate of mission success.

### **10.1 - Rescue Gear**

#### **10.1.1 - Retrieval Gear**

The Condor is equipped with rescue equipment that enables it to retrieve various combinations of ambulatory and immobile patients. The Sked<sup>®</sup> Basic Rescue System is a highly compact rescue stretcher which allows horizontal or vertical hoisting. Although it provides rigid support when a patient is strapped in, it can be rolled up and packed away when not in use. Patients who do not need to be supine during hoisting can be retrieved with either the rescue basket, which has a loading capacity of 272 kg, or with the rescue seat.

The rescue seat can lift or lower two people at a time, and is an update of the forest penetrators used by the United States Army.



**Figure 10.1 - Rescue Litter [Sked04]**



**Figure 10.2 - Two-person Rescue Seat [Life04]**



**Figure 10.3 - Rescue Basket [Life04]**

**10.1.2 - Hoist**

The Condor’s external hoist is a model 42325 from Goodrich Hoist and Winch Company. An electric version was chosen for ease of installation, maintenance characteristics, and reliability. Goodrich hoists feature translating drum technology, which permits an unlimited angle between the helicopter and the load to be lifted. This is an essential feature in uneven terrain or in the presence of obstacles, both of which are known to be factors in mountain rescue operations. The hoist has a 272 kg lifting capacity, a cable length of up to 88.4 m, and a hoisting speed of 38 m/min. An accessory cable cutter is mounted in the cabin behind the pilot seat. This device is an improvement on the included internal cutter, because it allows the cable to be spliced after cutting, so that interrupted rescue operations can be resumed. This is not possible when the cable is cut inside the hoist housing.



**Figure 10.4 - External Hoist [Good04]**

**10.1.3 - Additional Rescue Equipment**

During rescue operations, it is essential that the pilots and crew have good views of the hoisted payload. Accordingly, the Condor is equipped with a video camera and a full-color display that gives a continuous, real-time view of the rescue operation.

**10.2 - Medical Equipment**

The Condor is well-equipped to handle medical emergencies. The cabin floor is an integral unit that is leak-proof, protecting the underlying structure and fuel tanks from any medical effluvia. Supine patients are strapped into stretchers which are installed so that they do not shift under normal or most high-load conditions, as required by 14CFR29.785. The litters allow the patient’s head to recline at a range of angles, facilitating the paramedic’s access to the airway. There are two litters for supine patients, each of which is locked into a rack cantilevered by two of the fuselage structure’s primary bulkheads.



**Figure 10.5 - AED [Card04]**



**Figure 10.6 - CCT Monitor, Pacemaker, & Defibrillator [Zoll04]**

The primary medical equipment is located in close proximity to the chests of the patients. This includes two of the Zoll CCT combination cardiac monitor, defibrillator, and pacemaker. These devices feature full color displays and hospital quality monitoring. A battery-operated automatic external defibrillator (AED) is available for additional patients, or can be deployed outside the helicopter. Two advanced life support kits are stowed in cabinets on the starboard side of the cabin. These kits contain various airway, diagnostic and trauma supplies. The cabin is fitted with conveniently placed hooks for intravenous bags and tubes. There is a distribution system for oxygen; an E-size oxygen cylinder is located next to the forward facing paramedic and a larger M90 oxygen cylinder is racked in the aft stowage space.

Emergency packs are carried on board the Condor in case any person can not be immediately transported. These packs contain a space blanket, signaling devices such as a mirror and personal locator beacon, a light and flares, potable water, water purification tablets, and high-energy food rations. First-aid kits are included, and the AED can be left for treatment of an injured patient. Rescue equipment is stored aft of the main cabin, where it is readily accessible to the crew.

**Table 10.1 - Rescue and Medical Equipment Weights**

Rescue Item	kg	Medical Item	kg
Basket Litter	8.6	Advanced Life Support (x2)	22.7
Rescue Basket	18	Monitor Defibrillator (x2)	16.8
External Hoist	45	Portable AED	3.1
Rescue Seat	8.1	Stretcher System (x2)	17

Weight has been considered in the selection of the medical equipment for the Condor (see Table 10.1), but quality and utility were the primary drivers. Every item is state-of-the-art for helicopter EMS, and enables the crew to provide quality care to the patients.



## **Section 11 - Flight Control System**

Flight control in the Condor is achieved by using trailing edge flaps on the rotor blades to produce the required collective and cyclic pitch. The fan-in-fin uses conventional controls. The Flight Control System (FCS) for the Condor was designed to optimize performance and handling qualities. A triple redundant, digital fly-by-wire (FBW) system was selected for the design. Signals to the actuators and servos of the main rotor and fan-in-fin blades are generated by the two subsystems: the Primary Flight Control System (PFCS), and the Automatic Flight Control System (AFCS). Another subsystem, a Neural Network Hardware Processor is provided to perform onboard fault diagnosis for the rotor flaps. The dual, self-checking, triple redundant PFCS electronically connects the pilot's control inputs to the actuators and servos for safe operation of the aircraft, and is a digital equivalent of the traditional mechanical linkages. The AFCS provides command shaping, control mixing, a suit of holds, and the necessary level of stability and control augmentation required for reliable mission performance.

The FBW system, which represents the state-of-the-art in FCS, was selected in place of a mechanical system it presents potentials for weight savings, enhanced handling qualities, flexibility to accommodate changes (which requires a mere change in the software), improved fault tolerance and ease of incorporating onboard fault diagnostic systems. The digital FBW control system has automatic maneuver envelope protection, as the flight computer rejects maneuvers outside the operational flight envelope.

### **11.1 - Design of FCS**

#### **11.1.1 - Details of Flight Control System**

The FCS architecture for the Condor is shown in Figure 11.1. The core of the Condor's flight control system is the triplex Flight Control Computers (FCCs), which provide flight control law processing and also perform redundancy management for the FCS [Kubo01]. The design provides dual CPUs for each FCC, and an analog backup channel to maintain the control capability in worst case scenarios of failure or malfunction of all FCCs. There are four types of flight control laws for the Condor FCS: RD (Rate Damping), RCAH (Rate Command Attitude Hold), ACAH (Attitude Command Attitude Hold), and TRC (Translational Rate Command). In addition, turn coordination and side slip suppression can be provided to reduce pilot workload [Satt01]. The rate damping mode is a stability augmentation system (SAS) that provides damping





The Actuator Control Computers (ACCs) drive the actuators to deflect the embedded trailing edge flaps and to drive the fan-in-fin servos in accordance with the actuator position commands from the FCCs. When a failure of all the FCCs is detected, ACC automatically switches the control to an analog backup channel to maintain the minimum control capability [Kubo01].

Automatic flight and Flight Director flight in Condor is accomplished by coupling FMS with FCC, as shown in Figure 11.1. The autopilot coupling function and the guidance function is provided for the purpose. The autopilot coupling function provides automatic guidance and control, according to the autopilot commands calculated in the Flight Management Computer (FMC), to follow the flight path defined in the flight plan. The guidance function judges the condition of the helicopter from state flags and waypoint data, and determines the command gain necessary for calculating the guidance command. The guidance command is generated by multiplying the error calculated from the preset courses by command gain. The attitude mode being the most stable mode is used for automatic flight and FD flight [Kubo01]. The flight director system provides pre-programmed paths and furnishes the steering commands necessary to obtain and hold a desired path to preprogrammed destinations. The pilot can select out of preprogrammed destinations using the keyboard of the control display unit.

### **11.1.2 - Neural Network Based Fault Detection**

The current design proposes to use Neural Network hardware processors, which offers an efficient and cost-effective method to install fault diagnostics in flight systems, permitting on-board diagnostic modeling of very complex subsystems. In the current design, neural network hardware processor is used to monitor the performance of trailing edge flaps, the normal functioning of which is critical for mission success. The neural network hardware performs the functions of subsystem modeling to support the fault diagnostics, and aircraft parameter modeling that is used in the controller algorithm to optimize the control input. The neural network models the normal operation and failure modes of the flaps, and can predict their failure. This requires training which involves the collection of data that characterize normal and failure modes of operation of the trailing edge flaps. This data can be generated either using a simulation or from test operation of the system [Urne96]. The information regarding possibility of a failure would be displayed on the MFDs, which gives pilot ample time to take corrective measures.



**11.2 - Stability and Control Analysis**

A simplified linear model was developed based on the methods of Padfield & Prouty [Padf96], [Prou86], to carry out stability and control analysis. Stability and control derivatives were estimated from first principles, and using simplifying assumptions for the aerodynamic characteristics of the fuselage. The stability and control derivatives for two flight conditions (hover and forward flight at 145 knots) are given in Table 11.1. The force derivatives and the moment derivatives are normalized by the design gross weight and the moment of inertia respectively. The pitch damping,  $M_q$  and the roll damping,  $L_p$ , are important derivatives, because of their close relationship to the short-term and moderate amplitude response, which influences the handling qualities of a helicopter. Larger magnitudes of these derivatives indicate a stable helicopter. Table 11.1 suggests that Condor has good roll and pitch damping. This is because of the use of a bearingless hub, which gives us greater effective hinge offset than articulated rotor.

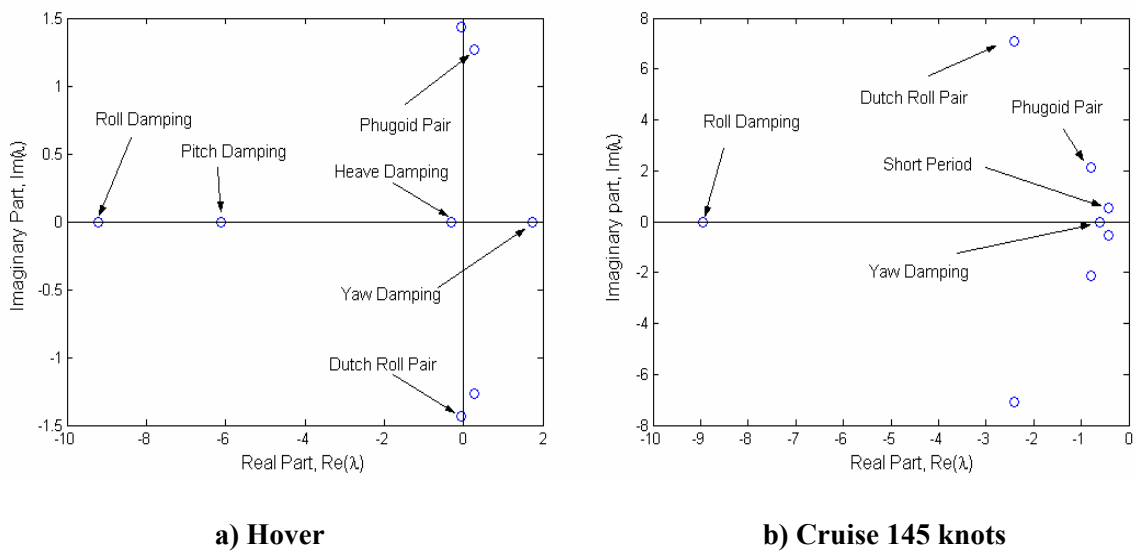


**Figure 11.2 - Longitudinal and Lateral Flight Stability Poles**

**11.2.1 - Lateral & Longitudinal Modes**

Figure 11.2 shows the estimated longitudinal and lateral poles for two different flight conditions, hover and cruise at 145 knots. Like any other helicopter, the phugoid mode of Condor is unstable in hover, however the stability increases with forward speed so the instability is not critical. During hover, the pitch and heave modes are uncoupled since the  $M_w$  derivative is zero. In forward flight they are coupled and form a short period mode which is stable. Due to significant high damping, the roll subsidence is the most stable mode.



As seen from Figure 11.2 the dutch roll mode is neutrally stable in hover and becomes more stable with forward speed. Dutch roll is highly dependent on the coupling of roll and yaw, where the dihedral effect ( $L_v$ ) and yaw due-to roll rate ( $N_p$ ) are the main contributors. Again, because of the bearingless design both of these derivatives are found to be large and negative in cruise. A negative value of  $N_p$  tends to destabilize the Dutch roll oscillation, however, the strong dihedral derivative is sufficient to stabilize this mode.

### **11.2.2 - Tail Sizing**

The size of the horizontal stabilizer is decided by two conflicting requirements, the stability of the phugoid mode and the stability of speed modes. The phugoid mode becomes unstable with increased horizontal stabilizer size, while decreasing the stabilizer size makes the speed mode unstable. A balance was achieved by selecting a horizontal stabilizer size of 1.4 m<sup>2</sup> (15 ft<sup>2</sup>), which gave adequate stability to both the modes.

### **11.3 - Handling Qualities**

The ADS-33 (Aeronautical Design Standard - Performance Specification) establishes the criteria for acceptable handling qualities for rotorcraft. These requirements are based on open-loop Bode plots in roll, pitch, and yaw. The bandwidth and phase delay are calculated from these Bode plots to determine the handling quality levels. An aircraft with high bandwidth and small phase delay would have a quick, crisp response, which is preferred by the pilots. The handling quality of the bare airframe with AFCS off and on needs to be investigated [Celi04]. A preliminary analysis was performed on the frequency response between the pitch attitude and longitudinal cyclic control of the bare airframe for small amplitude changes in attitude at a cruise speed of 145 knots. The short term response was observed to have a bandwidth of 1.4 rad/sec and a phase delay of 0.03 sec, which implies a Level 2 handling quality. The use of a flight control system with RCAH, ACAH, and RD (available with Condor AFCS) would decrease the pilot workload and improve the handling qualities.



**Table 11.1 - Stability Derivatives**

Derivative	Hover	Cruise	Units	Derivative	Hover	Cruise	Units
$X_u$	-1.01	-0.48	1/sec	$L_u$	0.03	0.03	rad/sec-ft
$X_v$	-0.05	0	1/sec	$L_v$	-0.07	-0.68	rad/sec-ft
$X_w$	0	-0.18	1/sec	$L_w$	0	-0.11	rad/sec-ft
$X_p$	-5.44	-2.88	ft/rad-sec	$L_p$	-9.2	-8.97	1/sec
$X_q$	13.65	21.03	ft/rad-sec	$L_q$	-3.66	-1.9	1/sec
$Y_u$	0.04	0.2	1/sec	$L_r$	0	0.1	rad/sec-ft
$Y_v$	-1.02	-0.63	1/sec	$M_u$	0.27	0.07	rad/sec-ft
$Y_w$	0	-0.16	1/sec	$M_v$	0.01	0	rad/sec-ft
$Y_p$	-13.65	-19.36	ft/rad-sec	$M_w$	0	-0.21	1/sec
$Y_q$	-5.44	-2.56	ft/rad-sec	$M_p$	1.45	0.83	1/sec
$Y_r$	0	-242.5	ft/rad-sec	$M_q$	-3.66	-4.51	1/sec
$Z_u$	0	0.02	1/sec	$N_u$	0	-0.12	rad/sec-ft
$Z_w$	-0.32	-0.64	1/sec	$N_v$	0	0.02	rad/sec-ft
$Z_p$	0	0.41	ft/rad-sec	$N_w$	-0.44	0.07	1/sec
$Z_q$	0	243.2	ft/rad-sec	$N_p$	0	-0.3	1/sec
$Z_r$	0	-7.96	ft/rad-sec	$N_r$	1.74	-0.92	1/sec

**Table 11.2 - Control Derivatives in Hover and Forward Flight**

Derivative	Hover	Cruise	Units	Derivative	Hover	Cruise	Units
$X_{\theta_0}$	-3.56	-144.6	ft/sec <sup>2</sup> -rad	$L_{\theta_0}$	0	0	1/sec <sup>2</sup>
$X_{\theta_{1c}}$	-36.29	-22.28	ft/sec <sup>2</sup> -rad	$L_{\theta_{1c}}$	-121.2	108.52	1/sec <sup>2</sup>
$X_{\theta_{1s}}$	239.9	154.5	ft/sec <sup>2</sup> -rad	$L_{\theta_{1s}}$	24.45	16.53	1/sec <sup>2</sup>
$Y_{\theta_0}$	0	-0.14	ft/sec <sup>2</sup> -rad	$M_{\theta_0}$	-5.87	34.18	1/sec <sup>2</sup>
$Y_{\theta_{1c}}$	-239.9	149.06	ft/sec <sup>2</sup> -rad	$M_{\theta_{1c}}$	9.73	6.45	1/sec <sup>2</sup>
$Y_{\theta_{1s}}$	36.29	22.71	ft/sec <sup>2</sup> -rad	$M_{\theta_{1s}}$	-64.34	-44.9	1/sec <sup>2</sup>
$Z_{\theta_0}$	-176.2	-320.8	ft/sec <sup>2</sup> -rad	$N_{\theta_0}$	11.09	10.66	1/sec <sup>2</sup>

## Section 12 - Mechanical Subsystems (Engine/Transmission)

### 12.1 - Engines

The CTS800 engine (see Section 4.5) is the civil version of the T800 engine that was to power the RAH-66 Comanche. Specifically, the CTS800-0 is the basic model, while the CTS800-4N includes an optional nose gearbox which reduces the RPM from 23000 to 6402. The engine has an envelope diameter of 0.55 m (21.7 in) and without the optional nose gearbox, is 0.86 m (33.7 in) long. The CTS-800-4N has a pressure ratio of 14 and weighs 185 kg (408 lb). The Full Authority Digital Electronic Control (FADEC) system provides automatic starting control of the engines. If taking off from an area with ground support, the engines can instead start using a temporary umbilical power connection which saves their battery power. The collector gear in the main gearbox drives a power takeoff gear that provides power to a generator (see Section 12.2.7). An APU provides pneumatic starting of the engines.

#### 12.1.1 - Engine Structural Integration

Two CTS800-4N engines are installed side by side, separated by a distance of 0.76 m (30 in), and located behind the main gearbox. The tail rotor drive shaft is routed between the engines. In accordance with 14CFR29.903, firewalls are installed to isolate the engines from each other and from other systems. Each engine is mounted using two A-frame supports in the front and one in the rear. Elastomer shock mounts located where the A-frame support is connected to the engine to isolate the engine from excess vibrations. The optional original equipment manufacturer (OEM) nose gearboxes which supply a reduction of 3.5926 were used. Using these reduction stages reduces gearbox certification costs and lowers research and development costs. Flexible couplings connect the output shaft of the OEM gearboxes to clutches mounted at the input of the gearbox.



**Figure 12.1: LHTEC CTS800-4N**

**Table 12.1 - Power Ratings for CTS-800-4N**

	<b>Power kW (shp)</b>
<b>Max Continuous</b>	955 (1281)
<b>Takeoff</b>	1014 (1361)
<b>Continuous OEI</b>	1014 (1361)
<b>2 Min OEI</b>	1108 (1487)
<b>30 second OEI</b>	1208 (1621)



**12.1.2 - Engine Performance**

The CTS800-4N power ratings for each engine are shown in Table 12.1. The loss in power for both engines with altitude is plotted in Figure 12.2. Total installation power losses are assumed to be 5% of the total maximum continuous power.

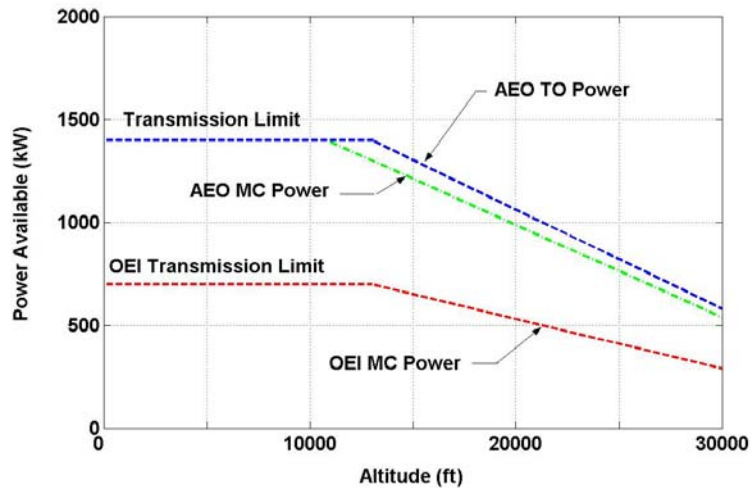


**Figure 12.2 - Power Variation With Altitude**

**12.1.3 - Engine Subsystems**

The oil tank capacity of the CTS800-4N is 3.2 liters (0.83 gal). Independent oil systems are integrated into each engine. These oil systems also lubricate the OEM reduction gearbox, eliminating the need for a dedicated lubrication system which would add weight. The CTS800-4N is manufactured with an inlet particle separator and therefore meets the requirements of 14CFR29.1091 regarding foreign object ingestion without the use of a separate aircraft inlet protection system. The Full Authority Digital Engine Control System communicates with the flight control system to ensure optimal engine performance. In addition, condition and usage information is relayed to the cockpit multifunction display and is recorded by the HUMS.

**12.2 - Transmission Design**

**12.2.1 - Design Baselines**

Because of the OEI requirement for high altitude hover, the main rotor transmission must transmit a proportionally larger amount of power than transmissions in helicopters of a comparable gross weight. Taking this design specification into account, care was taken to minimize gearbox weight while maximizing compactness. Once a basic design was selected, consideration was given to overall simplicity, ease of assembly/disassembly, noise minimization,

fatigue, and manufacturability issues. Table 12.2 lists the baseline parameters the transmission is required to satisfy.

**Table 12.2 - Design Baselines [Heat93]**

Design Baseline Parameters	
Engine Shaft Speed:	23,000 RPM (LHTEC03)
Main Rotor Desired RPM:	332 RPM
HP to Main Rotor (each path):	680 kW (912 hp)
Allowable Stresses	
Max Hertz Compressive Stress:	1,310 MPa (190,000 psi)
Bending Stress:	413.6 MPa (60,000 psi)

**12.2.2 - Configuration Study**

***Standard Gearbox Configuration***

The first option considered for the transmission design (shown in Figure 12.3) is representative of a more standard gearbox configuration. This concept contains a spiral bevel stage, a collector gear stage, and a planetary stage. This design, similar to the AH-64 Apache’s main gearbox, is considered to be a proven design, but the additional reduction stage and absence of torque-splitting results in a larger weight for the desired power rating. The configuration chosen for the gearbox of the Condor was a split-torque design utilizing face gears and a collector gear. This design is preferable over the standard design in many ways. The split-torque design lowers individual gear weight and size resulting in a more compact layout. The combination of face gears and collector gear provides the necessary reduction in as few stages as possible. Using fewer stages and components results in lower probability of failure, lower overall noise, easier and cheaper maintenance, and is easier for the HUM system to monitor (see Section 12.3). The chosen design also allows for weight savings in terms of necessary bearings and oil.

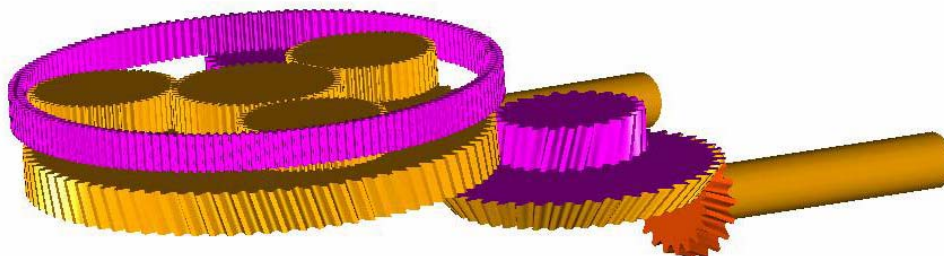


**Figure 12.3 - Standard Gearbox Design**



**Split-Torque Gearbox Configuration**

The main gearbox was sized to be capable of operation in all possible flight regimes of the mission profile. To hover with one engine inoperative at 3,658 m (12,000 ft), the helicopter requires 680 kW (912 hp) of power. Because this is the case that results in the highest torque loading, this is the power rating each torque path in the gearbox was designed to accommodate. In an emergency situation, the gearbox will be able to operate safely close to 800 kW (1073 hp) for approximately 2 minutes. After any scenario involving torques higher than the rated maximum, the drive system must undergo a complete inspection to approve the helicopter for further flight time. The necessity of right-angle nose gearbox assemblies was averted because the weight distribution of the helicopter allowed the engines to be located directly behind the main gearbox. It was deemed appropriate to utilize the OEM provided gearboxes for the first state of reduction. This stage brings the engine output shaft speed of 23,000 RPM down to 6,402 RPM before entering the gearbox. The output shafts from both OEM gearboxes are parallel to each other and to the transmission deck structure. Flexible couplings at this point allow for some shaft misalignment and structural flexing. Lucas Aerospace flexible couplings were chosen due to their single piece design that is light weight, highly reliable, and easy to maintain. Spring-type overrunning clutches are located at the point of gearbox entry to allow for shaft disengagement. Each input shaft of the gearbox drives a 21-tooth spur pinion with a pitch diameter of 88.9 mm (3.5 in) and a face width of 33.6 mm (1.4 in). At this point, the input torque is split between two face gears, meshing on opposite sides of the pinion. Each face gear has a pitch diameter of 321.8 mm (12.67 in), 76 teeth, and a tooth face width of 33.6 mm (1.4 in). The reduction ratio for this stage is 3.619:1. The face gear shafts are supported by bearings at the top and bottom of the

**Table 12.3 - Final Transmission Details**

	<b>Stage 1</b>	<b>Stage 2</b>	<b>Stage 3</b>
	<b>OEM gearbox</b>	<b>Face Gears</b>	<b>Double Helix</b>
<b>Number of Teeth (Pinion/Gear)</b>	-	21/76	21/113
<b>Reduction Ratio</b>	3.5926	3.619	5.38
<b>Diametrical Pitches (Pinion/Gear)</b>	-	6	5
<b>RPM (Pinion/Gear)</b>	-	6,402/1,769	1,769/332

housing. Double helix pinions, each mounted on the face gear shafts, drive a double helix collector gear, resulting in the final stage of reduction. The double helix pinions each have 21 teeth and a pitch diameter of 106.7 mm (4.2 in). The collector gear has 113 teeth and a pitch diameter of 574 mm (22.6 in). Both have tooth face widths totaling 61 mm (2.4 in). The main rotor is attached to the collector gear via a spline mount. The tail rotor drive shaft is driven by a



bevel gear off of the collector gear. Foldout 12.1 shows the final configuration and the other details are listed in Table 12.3.

### **12.2.3 - Optimization Considerations**

#### ***Split-Torque Configuration***

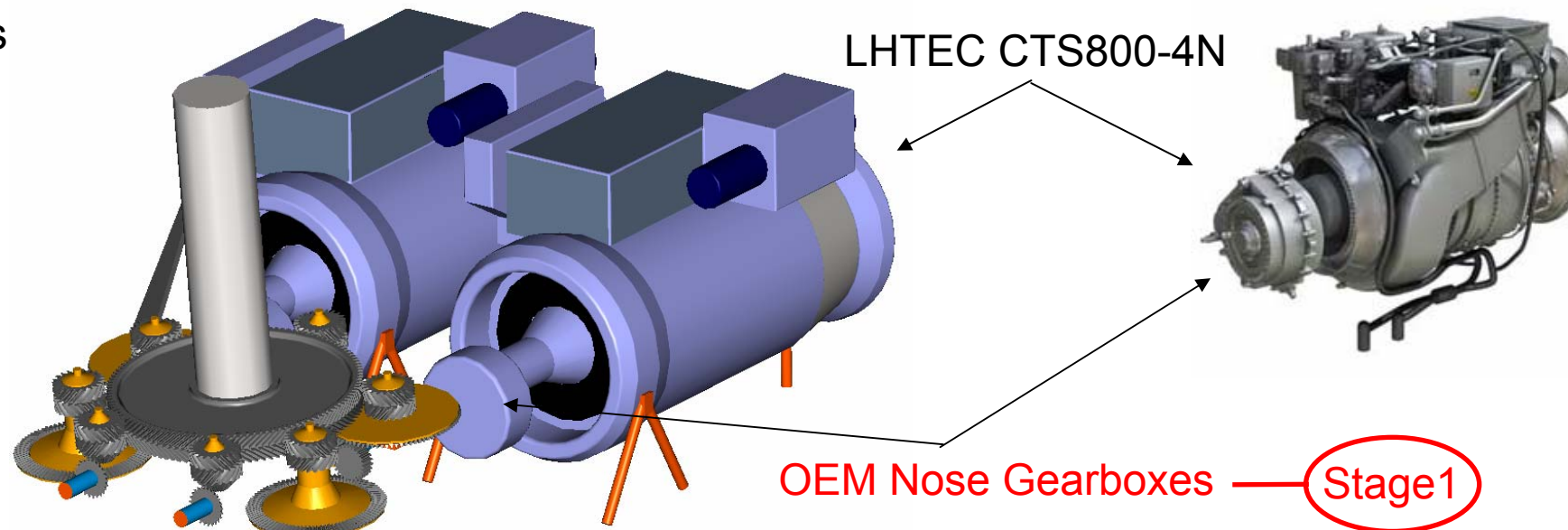
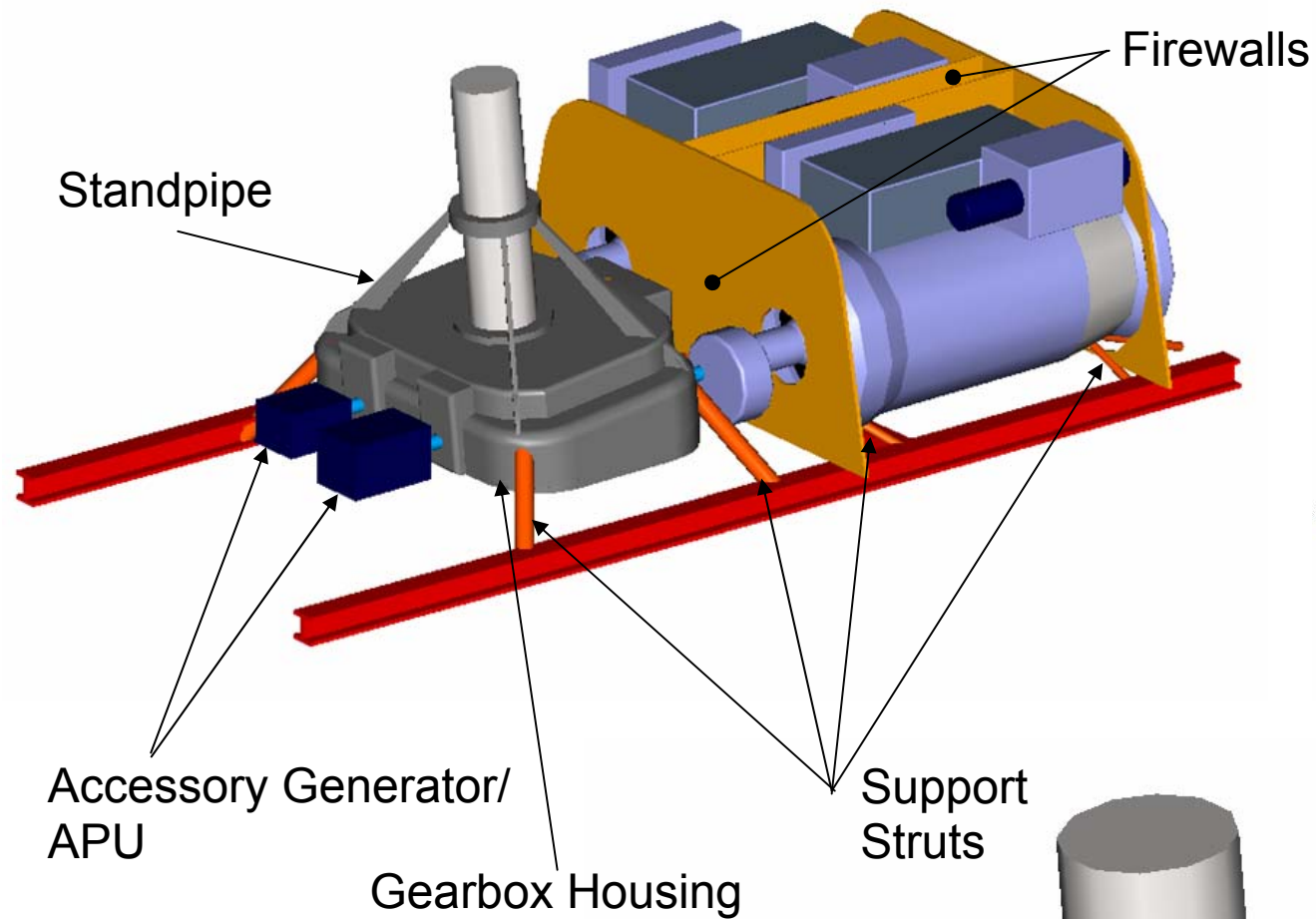
A split-torque configuration was chosen to be a primary design focus after a preliminary gear stress analysis revealed an exceptional reduction in the weight and size from that of a standard configuration. The torque-splitting approximately halves the bending and compression stresses seen on any one tooth of a gear allowing a smaller pitch diameter and face width, or more teeth.

#### ***Face Gear Validation***

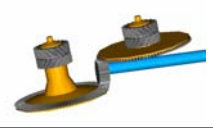
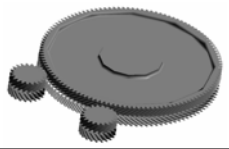
The method of splitting the torque in the proposed Condor transmission is the usage of two face gears being driven by a single pinion. The use of face gearing in a helicopter transmission was first proposed by McDonnell Douglas Helicopter Company in a proposed Advanced Rotorcraft Transmission Report in 1993 [Heat93]. Since then, actual proof-of-concept testing has indicated that face gears could indeed be used at high speeds and loads just as spiral bevel gears [Hand92]. Tests conducted by Boeing showed the relative torque loads between upper and lower face gears to be 48% and 52%, respectively, for a test rig setup similar to the proposed Condor transmission [Fill02]. Other tests performed at NASA Glenn also demonstrate the feasibility of using face gear technology [Tan03], [Lewi99], [Litv00]. The gearbox input pinion driving both face gears is subjected to an approximate net shear force of zero by nature of the design. Additionally, because of this bending load cancellation, bearings at the pinion root do not need to be as heavy as otherwise necessary to counter the bending moments. With this background, the design team is confident that the face gear concept will not pose any problems for certification.

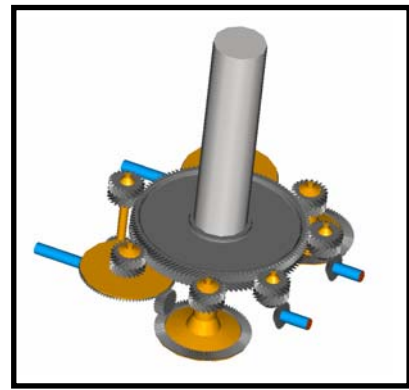
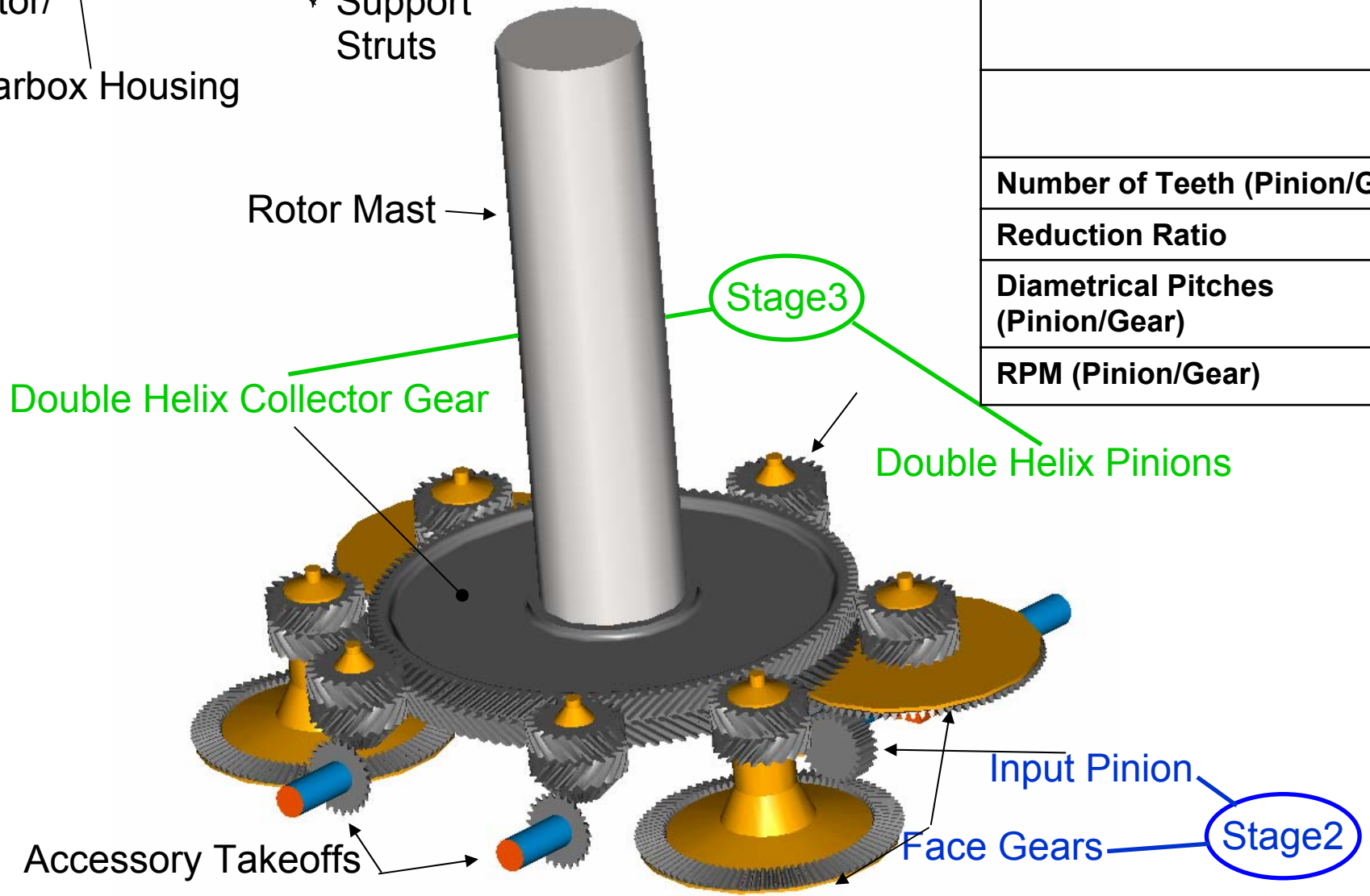
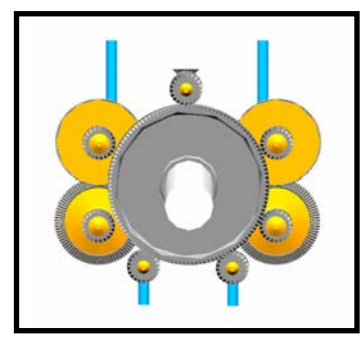
#### ***Noise Minimization***

One of the methods of reducing noise in a pair of meshing gears is to increase the contact ratio of the gear mesh by increasing the number of teeth. A higher contact ratio results in a higher meshing frequency. A higher contact ratio attenuates at shorter ranges, reduces backlash, and induces smoother meshing, resulting in reduced noise. However, increasing the number of teeth also increases the bending stresses seen on an individual tooth. The number of teeth on a pinion that was found to best balance the tradeoffs between these two factors was 25. For both pinion designs in the proposed transmission, the torque requirement limited the number of teeth to 21. Additionally, all gear teeth in this design employ a 20 degree pressure angle, which represents the best tradeoff between tooth surface contact stress and smoothness of meshing [Dudl84].



**Foldout 12.1 - Drivetrain Details**

			
	OEM gearbox	Face Gears	Double Helix
Number of Teeth (Pinion/Gear)	-	21/76	21/113
Reduction Ratio	3.59	3.62	5.38
Diametrical Pitches (Pinion/Gear)	-	6	5
RPM (Pinion/Gear)	23000/6402	6402/1769	1769/332



Stage1 (red circle)    Stage2 (blue circle)    Stage3 (green circle)



**Hunting Tooth Ratio**

For all instances in the transmission where one gear meshes with another, the number of teeth between the two was ensured to have a hunting tooth ratio between the pinion and gear so that a given tooth of the pinion will mesh with every tooth of the gear before meshing with the same gear tooth twice. This pattern of meshing promotes even wear over time. The equation that gives the number of revolutions of the pinion before the gears reset to a given orientation is given as:

$$n_{Reset,input} = \frac{LCM(N_{input}, N_{output})}{N_{output}}$$

The lowest common multiple of the numbers of teeth of both gears divided by the number of gear teeth should be equal to the number of teeth on the pinion for the gears to have a hunting tooth ratio.

**12.2.4 - Structural Integration**

In general, rotor mast moments, side forces, and thrust are transferred to the transmission deck structure through the gearbox housing. In the proposed configuration, a four-shafted truss structure supports the rotor mast through bearings above the gearbox, and transfers the moments and side forces to the reinforced corners of the gearbox. From the gearbox, each corner is attached to the transmission deck through a vibration isolator. Using this arrangement, there is less dependence on the housing which is created by casting metal, and more dependence is placed on extruded materials of a finer tolerance. The cast housing is sized to comply with 14CFR29.621 allowing a safety factor of 1.6. Under this rating, the gearbox inspection routine includes an additional particle analysis as well as a visual inspection.

**12.2.5 - Stress Calculations**

Gears were sized according to stress design formulas presented by Dudley [Dudl84]. Two primary parameters used for calculations were the K factor, a non-dimensional measure of tooth compressive stress, and the Unit Load stress, Ul, a measure of tooth bending stress. The forms for the K factor and Ul are given by the following equations:

$K = \left( \frac{126050 * HP * (RR + 1)}{RPM * PD^2 * F * RR} \right)$	HP: Horse Power RR: Reduction Ratio RPM: Revs/min PD: Pitch Diameter F: Face Width #teeth: # Teeth on Pinion of gears set
$Ul = \left( \frac{126050 * HP * (\#teeth)}{RPM * PD^2 * F} \right)$	



Hertz compressive stress is related to the K factor by the following equation:

$$S_c = 5715 * \sqrt{K}$$

The values calculated for the proposed design are included in Table 12.4.

**Table 12.4 - Calculated Stresses and Weight Estimation**

		Stresses			Weight
		Max K factor	Max Unit Load, <i>U</i> , MPa (psi)	<i>S<sub>c</sub></i> stress, MPa (psi)	kg, lb
Stage 2	Pinion	725	82.3 (11,934)	1061 (153,880)	60.75 (134 lb)
	Gear	200	82.3 (11,934)	557.2 (80,820)	
Stage 3	Pinion	988	120.6 (17,495)	1239 (179,640)	95.25 (210 lb)
	Gear	182	120.6 (17,495)	531.6 (77,100)	
<b>Total:</b>					156 (344 lb)

**12.2.6 - Weight Estimation**

The weight of the OEM gearbox is included with the weight of the engine. The weight of the remaining two stages and the gearbox housing is estimated using parameters and techniques from Dudley [Dudl84], Schmidt [Schm76], and Dyess [Dyes91]. The average Hertz stress index, a function of Hertz compressive stress, is calculated to be:

$$S_a = (800 + K) / 2000 \text{ for spur gears or } S_a = (670 + K) / 2000 \text{ for bevel gears.}$$

Using this value, the weight of each gearbox reduction stage is given by:

$$150 * \left( \frac{Q * HP * A * U * B}{S_a * RPM} \right)^{0.8}$$

where  $Q = 1 + 1/(2 * RR) + RR/2$ , and A, U, and B are correction factors that depend on the structural support characteristics and special features. From these equations, the weight breakdown is given in Table 12.4. Lubrication weight is estimated using the following equation:

$$26 * \left( \frac{\sum P}{1000} \right)^{0.73}$$

where  $\sum P$  is the sum of the HP of the main stages. Using this equation, the weight of lubrication system for the main gearbox can be estimated to be 18.1 kg (39.9 lb).

**12.2.7 - Generator and APU**

One generator is installed that is dedicated to powering the anti-icing system, and an installed APU, acting as an independent power source, provides power for all other electrical needs



including the active flap actuators, medical equipment, hoist, etc. It was chosen to use an APU/generator combination instead of two generators so that the helicopter would be able to perform pre-flight diagnostics checks without the necessity of turning on the main engines. The direct drive style of generator was chosen for its advantage in efficiency over air-bleed generators. The generator is ahead of the main transmission and is driven off of the main collector gear. This placement allows operation of the generator in the one engine inoperative condition. Placement of the APU in a similar location allows easy access to both the generator and APU. Additionally, if it is decided that only one device is necessary for a different mission profile, the modular design of the accessory power takeoff points allows all of the gearing associated with the accessory drive to be modified to suit an alternate configuration.

#### **12.2.8 - Tail Rotor Drive and Gearbox**

The tail rotor drive shaft is sized to operate at a supercritical speed to avoid resonant vibrations. A KAflex coupling is located just after the engines along the longitudinal axis. This coupling allows the necessary slight change in angle without adding the weight of a gearbox. KAflex couplings were chosen as a result of their ability to operate continuously with no lubrication. The shaft was designed according to 14CFR29.931, which states that if a drive shaft is operating at a critical speed, it must be capable of withstanding the induced stresses at that condition.

#### **12.2.9 - Power Losses**

Based on the transmission configuration, an efficiency of 98% is estimated. Assuming the maximum input of 1342 kW (1,800 hp), this amounts to approximately 26.8 kW (36 hp) of lost power that manifests itself as generated heat to be dissipated by the oil system.

#### **12.2.10 - Oil System**

The lubrication system must provide sufficient oil flow directed at the points of gear meshing to prevent metal-on-metal contact and to dissipate heat generated from the meshing. 14CFR29.1011 states that 1 gallon of usable oil is required for every 40 gallons of fuel. This relation suggests a total usable oil capacity of 3.5 gallons (13.25 L). The input oil temperature can be allowed to be as high as 110°C (230°F) while the outlet temperature can be as high as 204.4°C (400 °F). The estimated heat generation is 26.9 kW (1530 BTU/min). The corresponding mass flow of oil is

found by:

$$\dot{m} = \frac{q}{c_p * (T_{in} - T_{out})}$$



where  $q$  is the power dissipated,  $c_p$  is the constant pressure specific heat, and  $T_{in}$  and  $T_{out}$  are the oil inlet and outlet temperatures, respectively. From this simple heat transfer analysis, the necessary oil flow rate for the main gearbox is 6.7 L/min (1.77 gal/min). An inductive oil debris monitor is mounted in the oil return line to detect ferrous and non-ferrous particles. The information from this is monitored and recorded in the central HUMS. As required in 14CFR29.1019, a pressure sensitive oil bypass allows oil to flow in the event the filter is blocked.

### **12.3 - Health and Usage Monitoring**

Typically, helicopter maintenance can be broken down into three distinct processes [Irvi00]:

- (i) **Hard-Time**: Preventative maintenance is performed at fixed intervals. A complete overhaul is performed, replacing all components with a non-infinite lifespan, particularly the non-redundant components.
- (ii) **On condition**: A less rigorous inspection also occurring at fixed intervals in which only suspect components are replaced and the aircraft is approved for continued operation.
- (iii) **Condition monitoring**: The non-preventive process in which information regarding the status of a particular system or component is collected on a continuous basis in order to apply corrective measures if necessary.

Safety and reliability of the helicopter as a whole is enhanced by the addition of an integrated HUMS. Such a system provides global condition monitoring of performance and usage, the recording and measurement of dangerous loads, and identification of incipient faults. Some of the maintenance benefits that have been reported include: a simplified rotor track and balance procedure, reduced airframe vibration levels, more pro-active maintenance, better targeted maintenance, and as a result of the aforementioned, reduced disruption in operating schedules due to unscheduled maintenance [Lard99]. In addition, secondary benefits include increasing the perceived safety of rotorcraft and lower insurance costs, which are leading factors in making helicopters more acceptable to the public as a means of transportation. All of these benefits translate into an overall decrease in direct operating costs for the helicopter.

These benefits have not gone unnoticed by the various global certification organizations. The International Civil Aviation Organization has recommended in Amendment 26 to ICAO Annex 6 that aircraft in excess of 20,000 kg utilize a flight data analysis program, while requiring aircraft in excess of 27,000 kg to use them. The European Commission, Joint Aviation Authorities, and the FAA all responded favorably to this amendment. While the gross weight of the Condor does not come close to the weight put forth in the Amendment, the interest in HUM systems is evident.



The fact that an Advisory Circular introduced by the FAA has been introduced in 1999 to provide details on certifying HUM systems indicates that as soon as practical and feasible, HUM systems will become mandatory on all rotorcraft.

Many HUM systems are currently installed after their host helicopters are already in the field. By integrating the necessary sensors and hardware at the design stage, the cost for installation and certification is reduced, and newly developed HUM systems will integrate with minimal modifications to the existing systems. The HUM system aboard the Condor is organized into two elements, the on-line element and the off-line element. The on-line processing element, to be used by the pilot during flight, condenses data collected that do not require extensive processing, such as average torque usage or flight regime characteristics, into a simple intuitive display that will inform the pilot of the current aircraft status, and any necessary warnings. The off-line ground processing element saves data pertinent to determining the next necessary hard-time overhaul to a flight recorder. These data are then analyzed and processes between flights.

Various sensors are required to monitor the status of the rotor components, bearings, shafts, gears, and couplings. These data collected would be ineffectual for the pilot or ground crew in completely raw form. The HUMS is programmed with how much and at what scan rate the data should be collected and recorded. If practical, the raw data is processed or synchronously averaged on-board.

### **12.3.1 - Rotor**

Rotor blade flaps are monitored for actuator failure or the loss of a flap. Should such a failure occur, the HUM system alerts the flight control system to this changing status. The flight control system is already equipped with a neural network hardware processor which provides the system the capability to automatically compensate for a change in control effectiveness (see Section 11.1.2), but the additional confirmation from the HUMS would allow the control system to home in on a corrected control scheme quicker. Furthermore, the HUM system monitors ply delamination of flexbeams and spliced blade stations using strain sensors.

### **12.3.2 - Engines**

Each engine is equipped with a FADEC system which includes independent monitoring of engine system components. This information can be delivered to the HUMS, where the HUMS would

record and display pertinent information, such as the time spent above the torque experienced at takeoff power, oil filter status, and fault monitoring.

**12.3.3 - Main Gearbox**

Monitoring of the main gearbox is done using two distinct methods:

- (i) **Oil-Based Monitoring:** Individual gearbox components are monitored using in-line oil debris monitors and vibration-based health monitoring. Several MetalSCAN units from Gastops [Gast04] are inserted into the oil return lines. These units use an inductive sensor to detect the size of ferrous and non-ferrous particles. After these units, the metal particles are trapped in a filter, which is analyzed offline between flights.
- (ii) **Vibration Based-Monitoring:** For each shaft connected to a gear, an accelerometer and tachometer is mounted. These vibrations are synchronously averaged using the tachometer pulse train and the averages are periodically saved. The synchronous averaging mitigates noise and other vibrations unrelated to the meshing of the gears of interest. Statistical diagnostic metrics such as FM4 [Stew77], NA4 [Zakr93], NA4\*[Deck94], and a diagnostic algorithm developed at the University of Maryland [Samu99], will be applied to the averaged signals to produce a single value for each metric which provides a measure of health for that component. The typical vibration sensor data flow is shown in Figure 12.4.

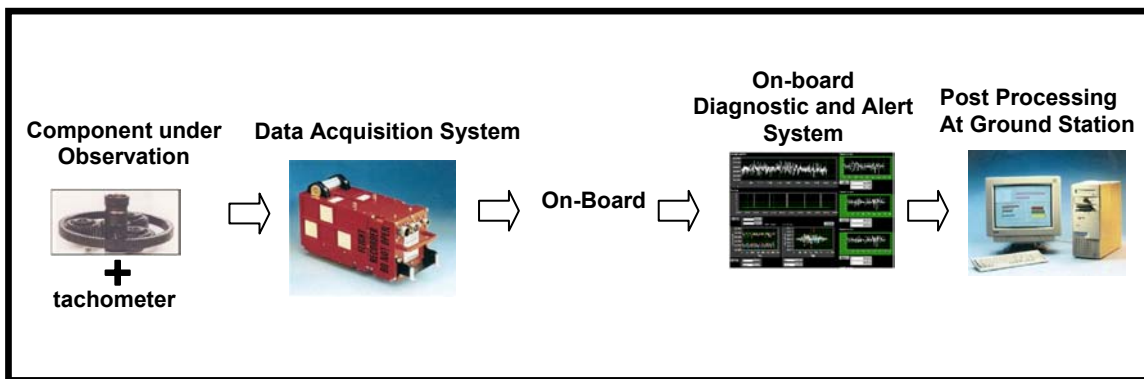


**Figure 12.4 - Typical Sensor Integration Scheme**

**12.3.4 - Tail Gearbox**

The tail rotor gearbox is monitored using a dedicated inductive oil debris monitor. In addition, an accelerometer and tachometer are mounted outside of the bearings of each gear.

**12.3.5 - Structure**

Accelerometers mounted in the pilot seats periodically monitor lateral and vertical acceleration to ensure the pilot is subjected to an acceptable amount of vibration. Should the HUMS detect an



amount of acceleration outside of the acceptable levels, the appropriate warning is displayed on the multi-function display. This measure is of particular important since a deviation of the vibratory levels above normal is often an indicator of component damage. Ruggedized strain gages are mounted at critical stress points where the standpipe truss structure is attached to the gearbox casing. These are monitored to indicate unacceptable fatigue and stress levels.

### **Section 13 - Weight Analysis**

#### **13.1 - Historical Trends**

The weight estimates are based upon empirical data from existing helicopters, and are modified to account for advanced and emerging technologies. The initial data are based upon Prouty’s regression formulae, and are cross-checked with Tischenko’s equations from the Mil Design Bureau [Tish04]. The Condor’s mountain SAR mission task requires a variety of features that

**Table 13.1 - Preliminary Weight Estimates**

<b>Description</b>	<b>Mass, kg</b>	<b>% Mass</b>	<b>l.c.g., mm</b>	<b>v.c.g., mm</b>
Airframe and Cowling	278	16.66%	2571	700
Engines	370.2	22.18%	3275	1784
Transmission System	132.9	7.96%	2239	1722
Main Rotor System	214.6	12.86%	2239	2600
Avionics (incl. search equip.)	182	10.91%	1115	186
Unconsumed Fuel	11.6	0.70%	1912	20
Landing Gear	86	5.15%	2909	-434
Fuel System	49.7	2.98%	1912	20
General Furnishings & Equipment	50	3.00%	645	700
Cooling System	25.6	1.53%	2355	1784
Fire Protection System	19.9	1.19%	2150	1784
Control System	40.8	2.44%	2239	1784
Hydraulics	18.6	1.11%	1955	1784
Electric System	56.2	3.37%	2571	1784
Fan-in-fin & Empennage	36.6	2.19%	9000	1436
De-icing System	10	0.60%	2239	2600
Crashworthiness	63.1	3.78%	2571	700
Empty Weight (Equipped)	1645.8	100%	2581	1267
Fuel Weight	650		1912	20
Passengers	191		2648	616
Paramedics	191		2272.5	485
Pilot	95.5		645	485
Copilot	95.5		645	485
Transmission & Engine Oil	15.4		2155	1784
Rescue & Medical Equipment	139.3		4000	1059
Gross Weight	3024		2263.7	852



have been included in these estimates, such as medical supplies, search and retrieval equipment and crash resistance features in the structure and in the furnishings.

Early estimates of the weight savings made possible by using advanced technologies and materials were approximately 20% to 30% [Unsw84, Shin84] for components of the airframe and main rotor hub. Unfortunately, these estimates have proven to be over-optimistic, and current analyses show that compared to conventional configurations, weight reductions of 12% to 17% are more realistic [Kay02]. Appropriate correction factors have been applied to the groups of the weight estimate to reflect this new approximation. See Table 13.1 for weight estimates.

### **13.2 - Preliminary Weight Estimates**

The groups in the weight breakdown conform to the requirements of MIL-STD-1374. Centers of gravity refer to an origin located at the ground plane and the centerline of bulkhead #1. MIL-STD-1374 weight breakdowns for the Condor are given in Appendix A. In the following sections, brief descriptions are given for the primary groups of the weight estimate.

### **13.3 - Component Weights**

#### **13.3.1 - Fuselage and Cowling**

The fuselage and cowling of the Condor are constructed from Kevlar/graphite/epoxy panels and aluminum-lithium metal alloy. At some high-demanding critical stations such as the engine deck, titanium has been used. Every effort has been made to streamline the design and construction of this group to minimize weight while not compromising structural integrity. Accordingly, the weight of this group as a whole has been adjusted by 15% to 278 kg.

#### **13.3.2 - Fan-in-fin and Empennage**

Aft of primary bulkhead #5, the structure of the Condor is monocoque Kevlar/graphite/epoxy composite panels and aluminum-lithium ring bulkheads. Both the horizontal and vertical stabilizers are fully composite, as is the fan-in-fin assembly. The weight of this group is estimated at 36 kg.

#### **13.3.3 - Engines**

The engines used in the Condor are the culmination of years of advanced research on weight reduction and performance improvement. Although future engines will certainly improve on this



new baseline, the LHTEC CTS-800 offers a very high power to weight ratio. Each engine has a weight of 185.1 kg.

#### **13.3.4 - Transmission**

The incorporation of face gears to provide a split-torque transmission arrangement lowers the stresses seen on any one tooth of a gear. Therefore, the gears can be downsized accordingly. Furthermore, the incorporation of a standpipe structure to route loads through the reinforced corners of the gearbox allows less casting material to be used resulting in lowers weight. The estimated weight of the transmission system is 156 kg.

#### **13.3.5 - Rotor System**

The main rotor blades of the Condor are constructed primarily from Nomex honeycomb and graphite/epoxy composite. These advanced materials provide a lightweight base for the necessary addition of a de-icing system and lightning strike protection.

#### **13.3.6 - Avionics**

The Condor takes advantage of the most recent innovations in avionics technology; consequently the avionics bay contains many line replacement units (LRUs) for the wide range of digital systems that are utilized. The avionics system is subject to change as new equipment is added and obsolete items are removed; the position of the avionics bay behind the pilots' seats reduces the impact of these weight changes on the center of gravity. The total weight of the avionics group is estimated at 182 kg.

#### **13.3.7 - Landing Gear**

The landing gear is estimated to weigh approximately 3% of the design gross weight of the Condor. The main gear supports the primary landing loads, and uses 80% of this weight allotment (86 kg).

#### **13.3.8 - Fuel and Fuel System**

The mission fuel requirement is approximately 650 kg (802 liters or 212 US gallons), including a 20 minute reserve. Approximately 2% of the mission fuel is trapped in the tanks and feed lines, and is unusable. The fuel tanks are provided with expansion space of 2% tank capacity, in accordance with 14CFR29.969, and are located under the cabin, between primary bulkheads 2 and 4. Each tank supplies fuel to one engine. The fuel system weight is estimated at 50 kg.



### **13.3.9 - Electric System**

The weight of the engine starter batteries is included in the weight of the engine, as it is part of the engine's FADEC. Two generators are driven off of the main transmission, providing power for the de-icing system, the active flap actuators, medical equipment, and all other power requirements. The generators weigh a combined 56 kg.

### **13.3.10 - Crashworthiness**

The fuel tanks are designed not to leak when filled with water and dropped from a height of 15.2 m (50 ft), and are fitted with self-sealing breakaway couplings to prevent leakage during impact events (14CFR29.952). Tank to fuselage attachment is accomplished with frangible attachments designed to prevent rupture or local breaks of the tanks at the point of attachment. The fuselage is supported with structural elements designed to deform in higher buckling modes to maximize energy dissipation. The cabin furnishings have been selected for crashworthiness, including seats with long-stroke energy attenuation systems. The weight of the crash-resistance mechanisms are estimated to add a total of 2.1% to the gross weight of the helicopter.

### **13.3.11 - Passengers and Crew**

The RFP specifies two pilots, two paramedics, and two patients of 95.5 kg (210 lb) each.

### **13.3.12 - Rescue and Medical Equipment**

The rescue and medical equipment has been chosen to enable the Condor to fulfill its mountain SAR mission while minimizing equipment weight. Each of these items represents the current state-of-the-art, so weight correction factors were not applied. This group is estimated at 139 kg.

## **13.4 - Weight Efficiency**

This initial weight estimate gives an empty weight fraction of approximately 50%, when the search equipment is counted as payload, instead of empty weight. This compares well to existing SAR helicopters.

## **13.5 - Weight and Balance**

The longitudinal c.g. travel envelope of the Condor is plotted in Figure 13.1. In this plot, the copilot has been treated as optional crew; his effect on longitudinal c.g. travel can be seen clearly



for both forward and aft loading. The extremes of the longitudinal c.g. are 75mm (3 in.) forward and 279 mm (11in.) aft of the rotor shaft.

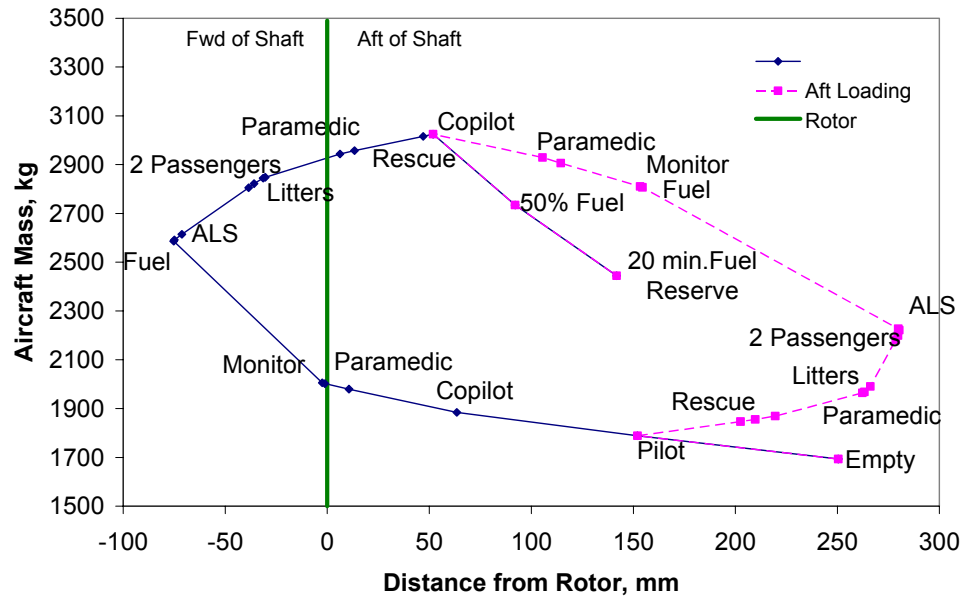


Figure 13.1 - Longitudinal c.g. Travel

## Section 14 - Performance Analysis

The Condor was specifically designed for operating at high altitudes. Therefore, the hover ceiling and high altitude cruise performance are of the greatest importance in this analysis. Table 14.1 is a summary of the Condor’s high altitude performance.

Table 14.1 - High Altitude Performance Summary

<b>Design Gross Weight</b>	3,024 kg (6,668 lb)
<b>Speed for Minimum Power (3,658 m)</b>	130 km/h (70 knots)
<b>Speed for Maximum Range (3,658 m)</b>	270 km/h (145 knots)
<b>Maximum Cruise Speed (3,658 m)</b>	315 km/h (170 knots)
<b>HOGE Ceiling (Continuous Power)</b>	6,700 m (22,000 ft)
<b>OEI Ceiling (OEI Continuous)</b>	3,658 m (12,000 ft)
<b>Maximum VROC (3,658 m)</b>	13.1 m/s (2,585 ft/min)
<b>Max Range (3,658 m w/ Reserve)</b>	1,270 km (690 nm)
<b>Max Endurance (3,658 m w/ Reserve)</b>	4.7 hours

The RFP requirements for a maximum cruise speed of 145 knots at 3,658 m (12,000 ft), HOGE ceiling of 4,572 m (15,000 ft) at continuous power and an OEI ceiling of 3,658 m (12,000 ft) at the highest engine rating. The Condor greatly exceeds all of these requirements with a maximum



cruise speed of 170 knots at altitude, a HOGE ceiling of 6700 m (22,000 ft) at continuous power and an OEI ceiling of 3658 m (12,000 ft) on continuous OEI power - or up to 4572 m (15,000 ft) at the 2 minute OEI rating.

**14.1 - Drag Estimation**

The parasitic drag was estimated using methods developed by Prouty [Prou86]. A component breakdown of the equivalent flat plate area is given in Table 14.2. Frontal areas for the various components were calculated from the drawings and combined with empirical factors given by Prouty to calculate the flat plate area of the entire helicopter. A factor of 20% was then added to the total as recommended by Prouty for more realistic results. Efforts were made to streamline the helicopter. However, the large amount of installed power and the relatively low maximum cruise speed requirement made aerodynamic cleanliness less critical. While the searchlight and FLIR system are fully retractable, the hoist remains fixed outside of the helicopter in cruise. While the landing gear is partially retractable, it is still a source of drag due to the attached skis. Combined with the large engine cowling for the CTS-800 engines, the equivalent flat plate area for the Condor is not low for its weight class. The rotor mast incidence angle was set to six degrees in order to minimize the angle of attack and therefore fuselage drag at the design cruise speed of 145 knots.

**Table 14.2 - Component Drag Breakdown**

Component	Flat Plate Area (m <sup>2</sup> )	Flat Plate Area (ft <sup>2</sup> )
Fuselage & Cowling	0.325	3.49
Main Rotor Hub & Shaft	0.269	2.89
Landing Gear	0.128	1.38
Horizontal Stabilizer	0.006	0.06
Vertical Stabilizer	0.006	0.06
Rotor/Fuselage Interference	0.065	0.70
Exhaust Drag	0.050	0.54
Miscellaneous Drag	0.050	0.54
FLIR	0.065	0.70
Hoist	0.034	0.36
<b>Subtotal</b>	<b>0.997</b>	<b>10.73</b>
20% Growth	0.199	2.15
<b>Total Flat Plate Area</b>	<b>1.197 m<sup>2</sup></b>	<b>12.88 ft<sup>2</sup></b>

**14.2 - Hover Performance**

The mission requirements of a high altitude hoisting operation placed great importance on the hovering performance of the Condor. The hovering power requirements were estimated using a



modified momentum theory, factoring in the tail rotor power requirements as they varied with altitude. Additional power was allotted for powering the deicing system and mission equipment.

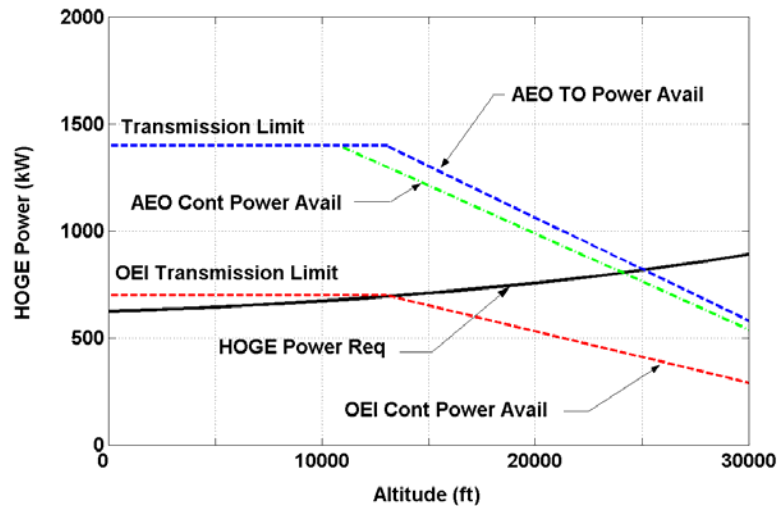


Figure 14.1 - HOGGE Power Required @ MGW and Power Available vs. Altitude

Of particular interest in this analysis were the hovering ceilings of the helicopter with continuous power and with one engine inoperative. The OEI transmission limit was set such that the Condor would have an OEI HOGGE ceiling of just over 3,658 m (12,000 ft) as shown in Figure 14.1. It should be noted that the ceiling of OEI 3,658 m (12,000 ft) is achieved at the OEI continuous engine rating and the maximum continuous transmission rating. Operating at the emergency ratings of the transmission and engine, the Condor can operate as high as 4,572 m (15,000 ft) OEI at MGW for up to two minutes.

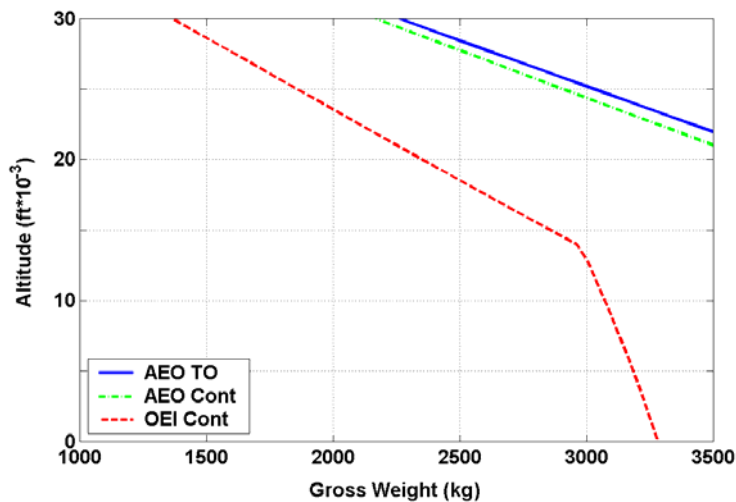


Figure 14.2 - HOGGE Altitude vs. Gross Weight for Various Engine Ratings



It can also be seen in Figure 14.1 that the AEO hover ceiling is approximately 7,320 m (24,000 ft) at maximum continuous power. However, the operating hover ceiling for the Condor at MGW is at 6,700 m (22,000) ft because of the stall limits of the fan-in-fin. Figure 14.2 shows the HOGE ceiling vs. gross weight for the Condor at various power ratings. The HOGE ceilings are seen to increase greatly with decreases in gross weight. At 50% fuel (~2,700 kg), the OEI continuous hover ceiling is increased to over 4,572 m (15,000 ft) and the AEO continuous ceiling is raised to 27,000 ft. To operate at these high altitudes, the main rotor was designed to have low values of blade loading ( $C_T / \sigma = 0.0675 @ \text{sea-level}$ ), delaying the onset of stall to altitudes of over 25,000 ft at MGW. In addition, the selection of a low blade loading at sea-level optimized the rotor for best figure of merit at high altitudes. The maximum vertical rate of climb vs. altitude is shown in Figure 14.3. The Condor achieves high values of rate of climb even at a high altitude as a result of the abundance of available installed power. This will also prove beneficial for maneuvering in mountainous terrain.

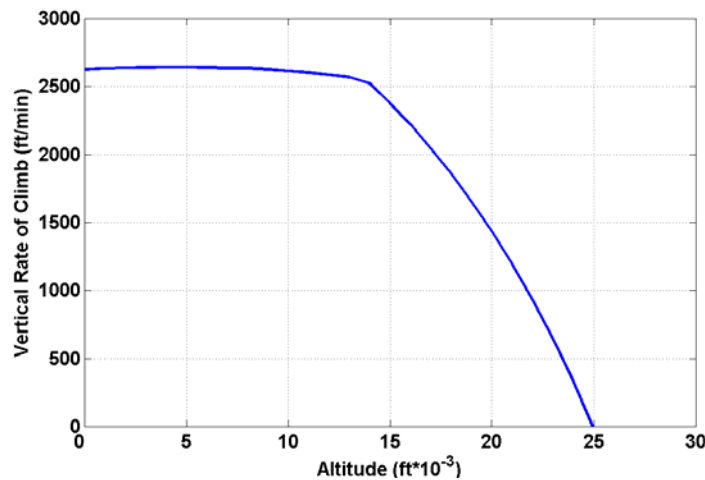
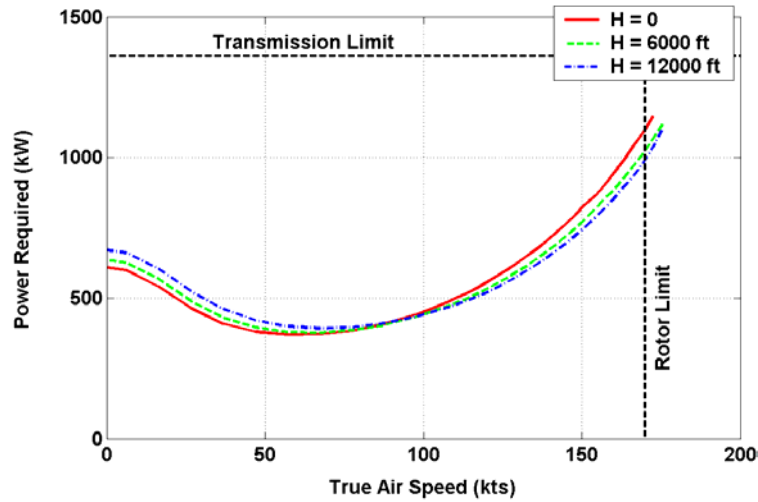


Figure 14.3 - Maximum Vertical Rate of Climb vs. Altitude @ MGW

### 14.3 - Forward Flight Performance

In addition to the high altitude hovering performance, the Condor was designed for high speed, high altitude cruise. The main rotor was designed such that compressibility and stall limits would be delayed to beyond 170 knots at 3,658 m (12,000 ft). The power requirements in forward flight were calculated after trimming the helicopter at each speed, taking into account the drag due to the angle of attack of the fuselage and blades. It was found that for altitudes up to 3,658 m (12,000 ft), power is not a limiting factor in the maximum cruise speed of the Condor because of the large amount of installed power and high transmission rating, as shown in Figure 14.4.



**Figure 14.4 - Power Required in Forward Flight for Various Altitudes (H)**

Figure 14.4 shows that the power requirements at higher altitudes are lower than those at sea-level for high speed forward flight. This is because of the lower parasitic drag experienced at higher altitudes, where the density of the air is decreased. However, it can be seen that the power requirements increase with altitude at low speeds where the influence of induced power is more prevalent. If one engine fails, the available continuous power will be 680 kW according to the OEI transmission limit. For this available power, it is seen that cruise speeds of up to 140 knots can be achieved, meaning that the Condor has the ability to fly safely home in the event of an engine failure. The rotor limits shown in Figure 14.4 are plotted versus altitude in Figure 14.5.

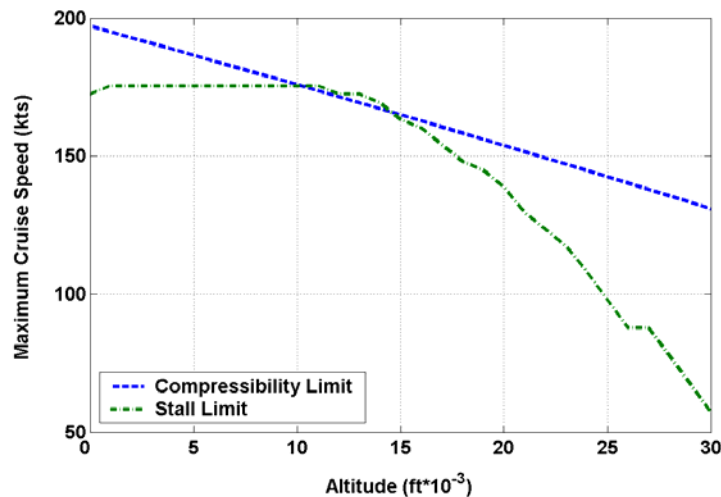


**Figure 14.5 - Maximum Cruise Speed vs. Altitude @ MGW**

The stall limit is seen to be the largest limiter for the majority of the altitude range and the compressibility and stall limits are seen to coincide at over 170 knots for the design cruising

altitude of 3,658 m (12,000 ft). The fuel flow at 3,658 m (12,000 ft) was calculated and plotted in Figure 14.6 using the power curves and the known variation in specific fuel consumption with engine power. It can be seen that the speed for minimum power (maximum endurance) is 70 knots and the speed for maximum range is 145 knots, which was selected as the design cruise speed. There is a small variation in these values at sea-level. The speed for maximum endurance becomes 60 knots and the speed for maximum range becomes 140 knots.

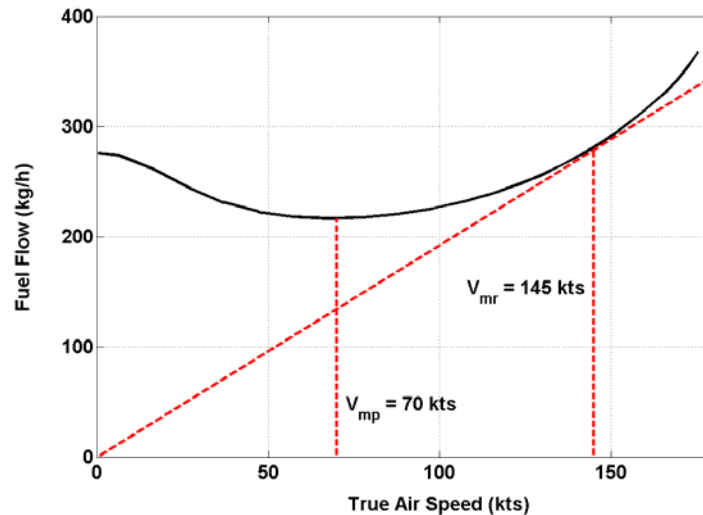


Figure 14.6 - Fuel Flow vs. Air Speed @ 3,658 m (12,000 ft)

#### **14.4 - Mission Capability**

For this analysis, payload included patients, paramedics, medical equipment and any additional seats. The search and rescue equipment such as the searchlight, FLIR system, and hoist are considered to be part of the standard equipment installed in this aircraft. The pilot and copilot are also considered to be installed weight. Thus, the payload for the mission specified in the RFP is approximately 520 kg. The payload-range capability of the Condor at sea-level and at 3,658 m (12,000 ft) is plotted in Figure 14.7. It can be seen that the payload-range capabilities at sea-level and at altitude are very similar, with the maximum range being slightly higher at altitude. This is, in part, because both cases used the cruise speed for maximum range (140 knots for sea-level and 145 knots at altitude). It can also be seen that the design payload of 520 kg can be carried a distance of approximately 600 km (320 nm) without refueling. For a nominal range of 200 km, the Condor is capable of carrying over 800 kg of payload, which could include up to 7 passengers (patients and paramedics) in addition to the required medical equipment. This capability, however, does not factor in the hover time necessary for a rescue operation. Figure 14.8 shows



the payload-range capability at 3,658 m (12,000 ft) with 20 minutes of hover at altitude as detailed in the RFP.

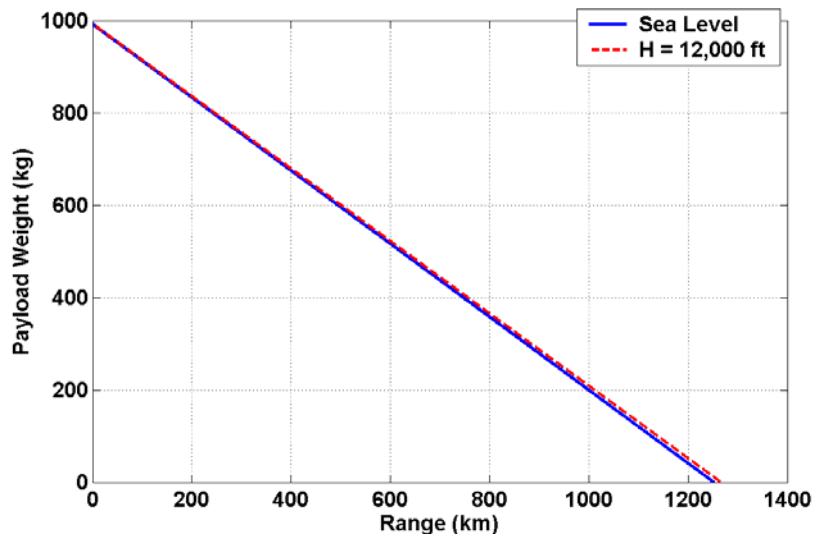


Figure 14.7 - Payload-Range at Sea-level and at Altitude (20 min. Reserve)

It can be seen in Figure 14.8 that 20 minutes of hover time greatly reduces the payload-range capabilities, which is because of the large amount of fuel required to hover at high altitudes. Under this condition, the design payload of 520 kg can then be carried approximately 400 km

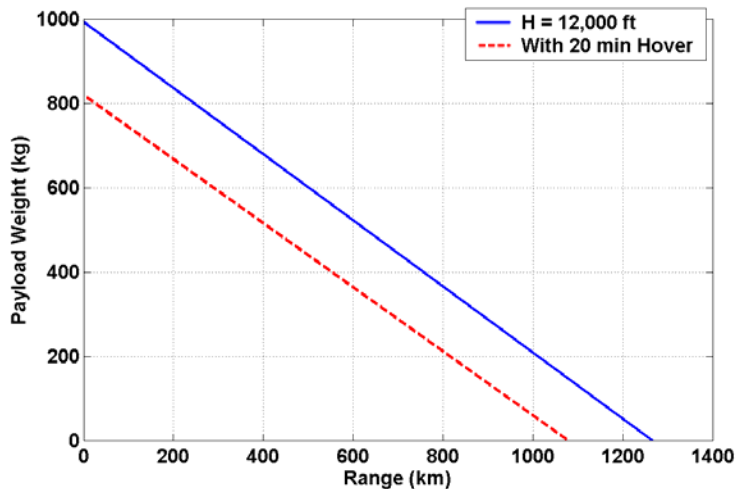
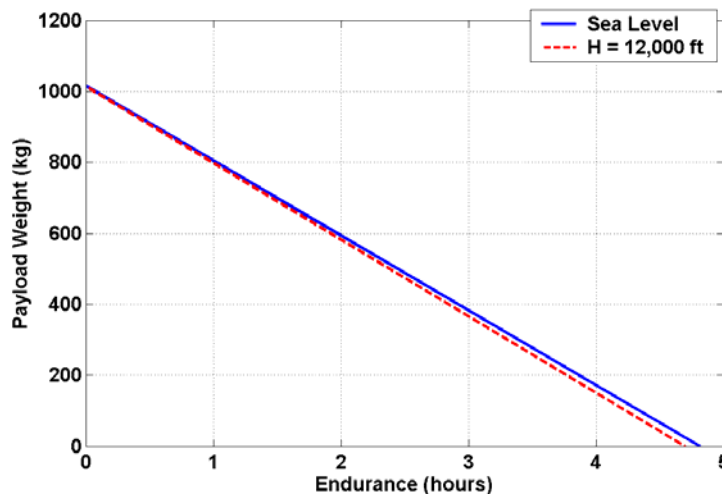


Figure 14.8 - Payload-Range at Altitude Incorporating Hover Time (20 min Reserve)

(215 nm). The RFP mission requirement is to take off with two paramedics and medical equipment (330 kg) and then return with this weight plus two patients (520 kg). During the outbound leg, over 200 kg of fuel will be burned, lowering the gross weight of the aircraft to more than make up for the additional weight of the patients. Taking into account the difference in



payload for the inbound and outbound legs and the fuel burned on the inbound leg, an average payload of 330 kg could be assumed as a conservative estimate. From Figure 14.8, it can be seen that for this average payload, the Condor has a range of over 640 km (345 nm), exceeding the range requirements of the RFP by over 20%. The payload-endurance capability of the Condor is shown in Figure 14.9.



**Figure 14.9 - Payload-Endurance at Sea-level and at Altitude (20 min Reserve)**

It can be seen in Figure 14.9 that the endurance at sea-level and at altitude are similar, with slightly better capability at sea-level. Both of these cases were calculated using their respective cruise speed for maximum endurance (minimum power). The endurance is particularly important for a search and rescue mission, which the Condor is specifically designed to perform. The higher the endurance, the longer the helicopter is capable of searching for the victims, while still having the capability to rescue them and return safely to base. It is clear that the Condor has excellent payload-endurance performance.

It has been shown that the Condor greatly exceeds the major performance requirements given by the RFP. The Condor exceeds the AEO HOGE ceiling by over 45%, the maximum cruise speed by over 15% and range with design payload by over 20%. The required OEI HOGE ceiling is achieved at continuous power with a 25% increase at emergency power (2 min). The Condor's superior high altitude performance is perfectly suited to the mountain rescue role.



## **Section 15 - Conclusions**

The Condor is a dedicated mountain search and rescue helicopter designed for high altitude performance, operational safety, and rescue mission capability. It features a high-powered twin engine system, an efficient rotor for hovering at extreme altitudes, state-of-the-art search and rescue equipment, and subsystems designed for reliability, safety, and cost effectiveness. The Condor's superior performance and SAR capabilities make it the ideal search and rescue helicopter for mountain extractions.

The Condor features a state-of-the-art twin-engine power plant designed for continuous OEI HOGE capability at 3,658 m (12,000 ft). The excess installed power is utilized in other flight modes to attain performance capabilities in excess of the requirements of the RFP. The performance capabilities of the Condor are:

- (i) Continuous HOGE at altitudes up to 6,700 m (22,000 ft) with 4 crew members and 2 patients
- (ii) OEI continuous HOGE at altitude up to 3,658 m (12,000 ft)
- (iii) Cruise speeds of up to 170 knots from sea-level to 3,658 m (12,000 ft)
- (iv) OEI Cruise speed of up to 140 knots from sea-level to 3,658 m (12,000 ft)
- (v) Range of over 640 km with designed payload and 20 minute hovering rescue operation
- (vi) Endurance of over 3 hours with designed payload
- (vii) Maximum vertical rate of climb of 13 m/sec at 3,658 m (12,000 ft)

In addition to superior performance, the Condor has many features designed specifically for mountain rescue mission capability. An integral fan-in-fin anti-torque system is used for ground and flight operational safety. The fan-in-fin system is designed with a high stall margin for control authority during hover at high altitudes in cross winds of over 40 knots. With a bearingless hub and an aerodynamically clean fuselage, the Condor has low parasitic drag for high speed cruise capabilities critical in rescue missions. A retractable landing gear with attachable skis provides the Condor with snow landing capabilities, and, unlike a fixed skid landing gear, does not interfere with hoisting operations. State-of-the-art search equipment and high endurance capabilities provide unsurpassed victim location performance. Utilizing internal volume, the Condor's cabin is laid out to allow paramedics easy access to the patients and required medical equipment so that proper care can be applied in-flight. These features along with unsurpassed high altitude capabilities make the Condor the perfect solution for mountain rescue tasks.

GROUP WEIGHT STATEMENT

AIRCRAFT

(INCLUDING ROTORCRAFT)

ESTIMATED - CALCULATED - ACTUAL

(CROSS OUT THOSE NOT APPLICABLE)

CONTRACT NO.

AIRCRAFT, GOVERNMENT NO.

AIRCRAFT, CONTRACTOR NO.

MANUFACTURED BY

ENGINE QUANTITY

ENGINE MANUFACTURED BY

ENGINE MODEL

ENGINE TYPE

MAIN

2.00

LHTEC

CTS-800

AUX

PROPELLER QUANTITY

PROPELLER MANUFACTURED BY

PROPELLER MODEL

PAGES REMOVED

PAGE NO.

MIL-STD-1374- PART I

GROUP WEIGHT STATEMENT  
WEIGHT EMPTY

PAGE 2  
MODEL Condor  
REPORT

NAME UMD  
DATE 30 MAY 2004

1	WING GROUP			WINGLETS	GLOVE / LEX	WING	
2	TOTAL						
3	BASIC STRUCTURE						
4	CENTER SECTION						
5	INTERMEDIATE PANEL						
6	OUTER PANEL						
7	SECONDARY STRUCTURE	( FOLD WT _____ LBS. )					
8	AILERONS / ELEVONS	( BAL WTS _____ LBS. )					
9	SPOILERS						
10	FLAPS - TRAILING EDGE						
11	- LEADING EDGE						
12	SLATS						
13							
14							
15	ROTOR GROUP						
16	BLADE ASSEMBLY			125.65			
17	HUB & HINGE	( FOLD WT _____ LBS. )		88.90			
18							
19	EMPENNAGE GROUP	CANARD	HORIZ. STAB.	VERTICAL FIN	VENTRAL FIN	TAIL ROTOR	
20	TOTAL						
21	BASIC STRUCTURE		15				
22	SECONDARY STRUCTURE						
23	CONTROL SURFACES						
24	( INCL. BALANCE WEIGHTS )	( )	( )	( )			
25	BLADES					10.10	
26	HUB & HINGE					11.50	
27	ROTOR / FAN DUCT & ROTOR SUPTS						
28							
29							
30	FUSELAGE GROUP				FUS. / HULL	BOOMS	
31	TOTAL				278.20		
32	BASIC STRUCTURE						
33	SECONDARY STRUCTURE						
34	ENCLOSURES, FLOORING, ETC.						
35	DOORS, RAMPS, PANELS & MISC.						
36							
37							
38	ALIGHTING GEAR GROUP TYPE *	MAIN	NOSE / TAIL		ARR. GEAR	CAT. GEAR	
39	TOTAL	68.80	11.20				
40	RUNNING GEAR / FLOATS / SKIS						
41	STRUCTURE						
42	CONTROLS						
43							
44							
45	ENGINE SECTION OR NACELLE GROUP	AUXILIARY ENGINES		MAIN ENGINES			
46	LOCATION **						
47	TOTAL - EACH LOCATION						
48							
49							
50	AIR INDUCTION GROUP	AUXILIARY ENGINES		MAIN ENGINES			
51	LOCATION **						
52	TOTAL - EACH LOCATION						
53	INLETS						
54	DUCTS, ETC.						
55							
56							
57	TOTAL STRUCTURE						0

\* LANDING GEAR "TYPE": INSERT "TRICYCLE", "TAIL WHEEL", "BICYCLE", "QUADRICYCLE", OR SIMILAR DESCRIPTIVE NOMENCLATURE.

\*\* WING, FUSELAGE, ETC.

MIL-STD-1374 PART I

GROUP WEIGHT STATEMENT  
WEIGHT EMPTY

PAGE 3  
MODEL Condor  
REPORT

NAME UMD  
DATE 30 MAY 2004

58	PROPULSION GROUP		AUXILIARY		MAIN		
59	ENGINE				185.10	185.10	
60	ENGINE INSTALLATION				25.70		
61	ACCESSORY GEAR BOXES & DRIVE						
62	EXHAUST SYSTEM						
63	ENGINE COOLING				25.60		
64	WATER INJECTION						
65	ENGINE CONTROLS						
66	STARTING SYSTEM						
67	PROPELLER / FAN INSTALLATION						
68	LUBRICATING SYSTEM						
69	FUEL SYSTEM						
70	TANKS - PROTECTED				49.70		
71	- UNPROTECTED						
72	PLUMBING, ETC.						
73							
74	DRIVE SYSTEM						
75	GEAR BOXES, LUB SYS & RTR BRK		22.40		112.40		
76	TRANSMISSION DRIVE						
77	ROTOR SHAFT		21.10				
78	GAS DRIVE						
79							
80	FLIGHT CONTROLS GROUP						
81	COCKPIT CONTROLS						
82	AUTOMATIC FLIGHT CONTROL SYSTEM						
83	SYSTEM CONTROLS				40.80		
84	AUXILIARY POWER GROUP				17.30		
85	INSTRUMENTS GROUP						
86	HYDRAULIC GROUP				18.60		
87	FIRE PROTECTION GROUP				19.90		
88	PNEUMATIC GROUP						
89	ELECTRICAL GROUP						
90	AVIONICS GROUP				0.00		
91	EQUIPMENT				181.00		
92	INSTALLATION						
92	ARMAMENT GROUP		( INCL. PASSIVE PROTECTION		LBS.)		
93	FURNISHINGS & EQUIPMENT GROUP						
94	ACCOMMODATION FOR PERSONNEL						
95	MISCELLANEOUS EQUIPMENT				77.00		
96	FURNISHINGS						
97	EMERGENCY EQUIPMENT				143.50		
98	ENVIRONMENTAL CONTROL GROUP						
99	ANTI-ICING GROUP						
100	PHOTOGRAPHIC GROUP						
101	LOAD & HANDLING GROUP						
102	AIRCRAFT HANDLING						
103	LOAD HANDLING						
104							
105	TOTAL SYSTEMS AND EQUIP. ( LINES 80 - 104 )						
106	BALLAST GROUP						
107	MANUFACTURING VARIATION						
108	CONTINGENCY						
109							
110	TOTAL CONTRACTOR CONTROLLED						
111	TOTAL GOVERNMENT FURNISHED EQUIP.						
112	TOTAL CONTRACTOR - RESPONSIBLE						
113	TOTAL GOVERNMENT - RESPONSIBLE						
114	TOTAL WEIGHT EMPTY PG. 2-3						1734.55

**SAWE RP NO. 8A - PART I**

NAME UMD  
DATE 30 MAY 2004

**GROUP WEIGHT STATEMENT  
USEFUL LOAD AND GROSS WEIGHT**

PAGE 4  
MODEL Condor  
REPORT

115	LOAD CONDITION						
116							
117	WEIGHT EMPTY			1734.55			
118	CREW (QTY <u>4</u> )			381.80			
119	UNUSABLE FUEL (TYPE <u>    </u> ) (GALS <u>    </u> )			11.60			
120	OIL	TYPE	GALS				
121	TRAPPED			2.50			
122	ENGINE			12.90			
123							
124	AUX. FUEL TANKS	QTY	CAP. EA. (GALS)				
125	INTERNAL						
126	EXTERNAL						
127							
128	WATER INJECTION FLUID		(GALS <u>    </u> )				
129	BAGGAGE						
130	GUN INSTALLATIONS						
131	GUNS	LOC	FIX. OR FLEX.	QTY	CAL.		
132							
133							
134	SUPPORTS *						
135	WEAPONS PROVISIONS **						
136							
137							
138							
139							
140	CHAFF (QTY <u>        </u> )						
141	FLARES (QTY <u>        </u> )						
142							
143							
144	SURVIVAL KITS			22.70			
145	LIFE RAFTS						
146	OXYGEN			17.40			
147							
148							
149							
150	OPERATING WEIGHT						
151	PASS. / TROOPS (QTY <u>2</u> ) (WT. EA. <u>210</u> )			95.45			
152							
153	CARGO						
154							
155	AMMUNITION		QTY	CAL.			
156							
157							
158	WEAPONS **						
159							
161							
162							
163							
164	ZERO FUEL WEIGHT						
165	USABLE FUEL	TYPE	LOC	GALS			
166	INTERNAL			650.00			
167							
168	EXTERNAL						
169							
170	TOTAL USEFUL LOAD			1290.00			
171	GROSS WEIGHT			3024.35			

\* IF REMOVABLE AND SPECIFIED AS USEFUL LOAD.

\*\* LIST STORES, MISSILES, SONOBUOYS, ETC. AND PYLONS, RACKS, LAUNCHERS, CHUTES, ETC. THAT ARE NOT PART OF WEIGHT EMPTY. LIST NOMENCLATURE, LOCATION, AND QUANTITY FOR ALL ITEMS SHOWN INCLUDING INSTALLATION.

## References

- [Alex86] Alex, F. W., and McCoubrey, G. A., "Design and Structural Evaluation of the SH-2F Composite Main Rotor Blade," *Journal of the American Helicopter Society*, April 1986, pp. 345-359.
- [AMCP74] *Engineering Design Handbook - Helicopter Engineering Part One: Preliminary Design*, Headquarters, U.S. Army Material Command, Alexandria, VA, 1974.
- [Bao04] Bao, J., Nagaraj, V.T., Chopra, I., and Bernhard, A.P.F., "Wind Tunnel Testing of Low Vibration Mach Scale Rotor with Composite Tailored Blades", To be presented at 60th Annual Forum of the American Helicopter Society International, Baltimore, MD, June 7-10, 2004.
- [Bao03] Bao, J., Nagaraj, V.T., Chopra, I., and Bernhard, A.P.F., "Design and Hover Test of Low Vibration Mach Scale Rotor with Twisted Composite Tailored Blades", Presented at the 44th AIAA/ASME/ASCE/AHS Structures, Structural Dynamics, and Material Conference, Norfolk, VA, 7-10 April, 2003.
- [Buet01] Bueter, A., Ehlert, U.C., Sachau, D., and Breitbach, E., "Adaptive Rotor Blade Concepts: Direct Twist and Camber Variation", *Active Control Technology for Enhanced Performance Operational Capabilities of Military Aircraft, Land Vehicles*, June 2001, pp. 11
- [Card04] Cardiac Science, [www.cardiacscience.com](http://www.cardiacscience.com), 2004.
- [Celi04] Celi, R., Helicopter Stability and Control, Class Notes, 2004.
- [Chen95a] Chen, Y.J., Heath, G.F., Gilbert, R., and Sheth, V., "Advanced Rotorcraft Transmission Development - A Technology Reconversion Program", Presented at the 51st American Helicopter Society Forum, Fort Worth, TX, May 1995.
- [Chen95b] Chen, Y.J., and Bossler, R.B., "Design, Analysis, and Testing Methods for a Split-Torque Face-Gear Transmission", Presented at the 31st Joint Propulsion Conference, San Diego, CA, Jul. 1995.
- [Chop02] Chopra, I., "Review of the State-of-Art of Smart Structures and Integrated Systems", *AIAA Journal*, Vol. 40, No. 11, November 2002.
- [Chop00] Chopra, I., "Status of Application of Smart Structures technology to Rotorcraft Systems", *Journal of American Helicopter Society*, October 2001, pp. 228-252.
- [Curr88] Currey, N. S., *Aircraft Landing Gear Design: Principles and Practices*, AIAA Education Series, Washington, D.C., 1988.

- [Dado82] Dadone, L., Cowan, J., and McHugh, F.J., "Variable Camber Rotor Study", Technical Report NASA-CR-166382, 1982.
- [Deck94] Decker, H.J., Handschuh, R.F., and Zakrajsek, J.J., "An enhancement to the NA4 gear vibration diagnostic parameter". Technical Report NASA TM-106553, ARL-TR-389, NASA and the U.S. Army Research Laboratory, July 1994.
- [Dudl84] Dudley, D, *Handbook of Practical Gear Design*, McGraw-Hill Cook Company, New York, 1984.
- [Dyes91] Dyess, S., "Drive System Weight Optimization". Technical Report 2004, Society of Allied Weight Engineers, May 1991.
- [Elli04] Ellison, J., "Design and Testing of a Bi-directional Magnetostrictive-Hydraulic Hybrid Actuator". Proceedings of the 11<sup>th</sup> SPIE Conference on Smart Structures and Integrated Systems, San Diego, CA, March 2004.
- [Fill02] Filler, R.R., Heath, G.F., Slaughter, S.C., and Lewicki, D.G., "Torque Splitting By a Concentric Face Gear Transmission", Proceedings of the 58th American Helicopter Society International Forum, Montreal, Quebec, Canada, Jun. 2002.
- [Flir01] "FLIR Systems Star SAFIRE II",  
<http://www.flir.com/imaging/Airborne/Products/StarSAFIREII.aspx>, May 2004.
- [Gang94] Ganguli, R., and Chopra, I., "Aeroelastic Optimization of a Helicopter Rotor to Reduce Vibration and Dynamic Stresses", Presented at 35th AIAA Structural Dynamics, and Materials Conference, Hilton Head, SC, April 18-20, 1994.
- [Gast04] GasTops, [www.gastops.com](http://www.gastops.com), 2004.
- [Good04] Goodrich Inc., [www.hoistandwinch.com](http://www.hoistandwinch.com), 2004.
- [Ham83] Ham, N.D., "Helicopter Individual Blade Control and Its Applications", American Helicopter Society 39th Annual Forum Proceedings, St. Louis MO, May 9-11 1983.
- [Hand96] Handschuh, R.F., Lewicki, D.G., Heath, G.F., and Bossler, R.B., "Experimental Evaluation of Face Gears for Aerospace Drive System Applications", Proceedings of the 7th International Power Transmission and Gearing Conference, San Diego, CA, Oct. 1996, pp. 581-588.
- [Hand94] Handschuh, R.F., Lewicki, D.G., and Bossler, R.B., "Experimental Testing of Prototype Face Gears for Helicopter Transmissions", *Journal of Aerospace Engineering*, Vol. 208, No. G2, Oct. 1994, pp. 129-135.
- [Hand92] Handschuh, R.F., Lewicki, D.G., and Bossler, R.B., "Experimental Testing of Prototype Face Gears for Helicopter Transmissions", Presented at the Gearbox Configurations of the 90's Conference, Solihull, United Kingdom, Oct. 1992.

- [Heat02]** Heath, G.F., Filler, R.R., and Tan, J., "Development of Face Gear Technology for Industrial and Aerospace Power Transmission", NASA Contractor Report CR-2002-211320, Army Research Laboratory Contractor Report ARL-CR-0485, The Boeing Company, Cooperative Agreement NCC3-356, May 2002.
- [Heat93]** Heath, G.F., and Bossler, R.B., "Advanced Rotorcraft Transmission (ART) Program - Final Report", NASA Contractor Report CR-191057, Army Research Laboratory Contractor Report ARL-CR-14, McDonnell Douglas Helicopter Company, Contract No. NAS3-25454, Jan. 1993.
- [Hone04a]** "Honeywell FMZ-2000 Flight Management System",  
<http://www.myflite.com/brochures/CD820brochure20000926.pdf>, May 2004
- [Hone04b]** "Helicopter EGPWS", <http://www.egpws.com/helo/helo.htm>, May 2004
- [Hone04c]** - "Honeywell Weather Avoidance System",  
<http://www.myflite.com/DBAccess?operation=systems&category=Weather+Avoidance+Systems>, May 2004.
- [Hone04d]** "Honeywell TCAS Systems",  
<http://www.myflite.com/DBAccess?operation=systems&category=TCAS+Systems>, May 2004.
- [Hous98]** Houston, S.S., "Identification of Autogyro Longitudinal Stability and Control Characteristics", *Journal of Guidance, Control, and Dynamics*, Vol. 21 - May-June 1998, pp. 391-399
- [Irvi00]** Irving, P.E., Place, S., Strutt, J.E., Allsopp, K.E. "Life prediction, maintenance and failure probabilities in rotorcraft gear boxes equipped with health and usage monitoring systems." Cranfield University, Cranfield, Beds MK 43 0AL, UK.
- [Kay02]** Kay, B., "RWSTD Structures Technology Improvements and Validation", 58th Annual Proceedings of the American Helicopter Society, Montreal, Canada, 2002.
- [Keys91]** Keys, C., Sheffler, M., Weiner, S. and Heminway, R., "LH Wind Tunnel Testing: Key to Advanced Aerodynamic Design", Proceedings of the 47th Annual American Helicopter Society Forum, May 1991, pp. 77-87.
- [Kubo01]** Kubo, Y., Kuraya, N., Ikarashi, R., Amano, T., Ikeuchi, K., and Tobari, S., "The Development of FBW Flight Control System and Flight Management System for ATIC BK117 Experimental Helicopter", Proceedings of the 57th Annual Forum of the American Helicopter Society International, Washington, DC, May 9-11, 2001.
- [Kuche53]** Kuchemann, D. and Weber, J., *Aerodynamics of Propulsion*, McGraw-Hill Book Company. Inc, pp 125-139.

- [Lard99] Larder, Brian D., "Helicopter HUM/FDR: Benefits and Developments". Presented at American Helicopter Society 55th Annual Forum, Montreal, Quebec, May 25-27 1999.
- [Leis00] Leishman, J.G., *Principles of Helicopter Aerodynamics*, Cambridge University Press, Cambridge, 2000.
- [Lewi00] Lewicki, D.G., Handschuh, R.F., Heath, G.F., and Sheth, V., "Evaluation of Carburized and Ground Face Gears", *Journal of the American Helicopter Society*, Vol. 45, No. 2, Apr. 2000, pp. 118-124.
- [Lewi99] Lewicki, D.G., Handschuh, R.F., Heath, G.F., and Sheth, V., "Evaluation of Carburized and Ground Face Gears", Proceedings of the 55th American Helicopter Society International Forum, Montreal, Quebec, Canada, May 1999, pp. 723-731.
- [Lewi96] Lewicki, D.G., "Face Gear Technology for Aerospace Power Transmission Progresses", Research and Technology Article, NASA Glenn, 1996.
- [Life04] Lifesaving Systems Corporation, [www.lifesavingsystems.com](http://www.lifesavingsystems.com), 2004.
- [Litv00] Litvin, F.L., Egelja, A., Tan, J., Chen, Y.J., and Heath, G.F., "Handbook on Face Gear Drives With a Spur Involute Pinion", NASA Contractor Report CR-2000-209909, Army Research Laboratory Contractor Report ARL-CR-447, The Boeing Company, Cooperative Agreement NCC3-356, Mar. 2000.
- [Litv94] Litvin, F.L., Wang, J.C., Bossler, R.B., Chen, Y.J., Heath, G.F., and Lewicki, D.G., "Application of Face-Gear Drives in Helicopter Transmission", *ASME Journal of Mechanical Design*, Vol. 116, No. 3, Sep. 1994, pp. 672-676.
- [Litv92a] Litvin, F.L., Wang, J.C., Bossler, R.B., Chen, Y.J., Heath, G.F., and Lewicki, D.G., "Application of Face-Gear Drives in Helicopter Transmission", Proceedings of the 1992 International Power Transmission Conference, Phoenix, AZ, Sep. 1992.
- [Litv92b] Litvin, F.L., Wang, J.C., Bossler, R.B., Chen, Y.J., Heath, G.F., and Lewicki, D.G., "Face-Gear Drives: Design Analysis and Testing for Helicopter Transmission Applications", Presented at the 1992 AGMA Fall Technical Meeting, Baltimore, MD, Oct. 1992.
- [Lord04] "Lord Corporation - Lead Lag Dampers", <http://www.lord.com>, 25th May 2004.
- [Moui86] Mouille, R. and d'Ambra, F., "The 'Fan-in-fin': A shrouded Tail Rotor Concept for Helicopters", Proceedings of the 42nd Annual American Helicopter Society Forum, 1986, pp. 597-606.
- [Niwa98] Niwa, Y., "The Development of the New Observation Helicopter(XOH-1)", Proceedings of the 54th Annual American Helicopter Society Forum, May 20-22, 1998.

- [Noon91] Noonan, Kevin W, "Aerodynamic Characteristics of a Rotorcraft Airfoil Designed for the Tip Region of a Main Rotor Blade", NASA TM-4264, 1991.
- [Noon90] Noonan, Kevin W, "Aerodynamic Characteristics of Two Rotorcraft Airfoils Designed for Application to the Inboard Region of a Main Rotor Blade", NASA TP-3009, 1990.
- [Nort04a] "Northrop Grumman Navigation System Division - Product Detail",  
<http://nsd.es.northropgrumman.com/Automated/products/LN-100G.html>, May 2004.
- [Nort04b] "Northrop Grumman Smart MFDs",  
[http://nsd.es.northropgrumman.com/Automated/categories/Display\\_Systems.html](http://nsd.es.northropgrumman.com/Automated/categories/Display_Systems.html), May 2004.
- [Ormi01] Ormiston, R.A., "Aeroelastic Considerations for Rotorcraft Primary Control eith on Blade Elevons", Proceedings of the 59th Annual Forum of the American Helicopter Society International, Pheonix, AZ, May 2003.
- [Padf96] Padfield, G. D., *Helicopter Flight Dynamics: The Theory and Application of Flying Qualities and Simulation Modeling*, 1st ed., AIAA Educational Series, 1996.
- [Prou89] Prouty, R. W., *Military Helicopter Design Technology*, Jane's Information Group Limited, 1989.
- [Prou86] Prouty, R. W., *Helicopter Performance, Stability, and Control*, PWS Engineering, Boston, 1986.
- [Roge04] Roget, B., and Chopra, I., "Wind Tunnel Testing of an Individual Blade Controller for a Dissimilar Rotor," To be presented at 60th Annual Forum of the American Helicopter Society International, Baltimore, MD, June 7-10, 2004.
- [Roge02] Roget, B., and Chopra, I., "Robust Individual Blade Control Algorithm for a Dissimilar Rotor," *Journal of Guidance, Control and Dynamics*, Vol. 25, No. 4, July-Aug. 2002.
- [Samu99] Samuel, P.D., "Helicopter Transmission Diagnostics using Constrained Adaptive Lifting", PhD Dissertation, University of Maryland, College Park, MD, February 1999.
- [Satt01] Sattler, D., and Reid, L., "Automatic Flight Control for Helicopter Enhanced/ Synthetic Vision," *AIAA Journal*, 2001.
- [Schm76] Schmidt, A., "A Method for Estimating the Weight of Aircraft Transmissions". Technical Report 1120, Society of Allied Weight Engineers, May 1976.
- [Shen03] Shen, J., Chopra, I., and Johnson, W., "Performance of Swashplateless Ultralight Helicopter Rotor with Trailing-Edge Flaps for Primary Flight Control", Proceedings of the 59th Annual Forum of the American Helicopter Society International, Pheonix, AZ, May 2003.

- [Shen03a] Shen, J., "Comprehensive Aeroelastic Analysis of Trailing Edge Flap Helicopter Rotors", PhD Dissertation, University of Maryland, College Park, MD, 2003.
- [Shin84] Shinn, R., "Impact of Emerging Technology on the Weight of Future Rotorcraft", 40th Annual Proceedings of the American Helicopter Society, Arlington, Virginia, 1984.
- [Siro01] Sirohi, J. and Chopra, I., "Design and Development of a High Pumping Frequency Piezoelectric-Hydraulic Hybrid Actuator," *Journal of Intelligent Material Systems and Structures*, Vol. 14, No. 3, pp. 135-147, March 2003.
- [Sked04] Skedco, Inc., [www.skedco.com](http://www.skedco.com), April 2004.
- [Spec01] "Spectrolab Illumination Systems",  
[http://www.spectrolab.com/DataSheets/SX5/ILS\\_SX-5.pdf](http://www.spectrolab.com/DataSheets/SX5/ILS_SX-5.pdf), May 2004.
- [Stew77] Stewart., R.M., "Some useful analysis techniques for gearbox diagnostics". Technical Report MHM/R/10/77, Machine Health Monitoring Group, Institute of Sound and Vibration Research, University of Southampton, July 1977.
- [Strau04] Straub, Friedrich K., Kennedy, Dennis K., Domzalski, David B., Hassan, Ahmad A., Ngo H., Ananad, V., and Birchette, T., "Smart Material-actuated Rotor Technology - SMART", *Journal of Intelligent Materials and Structures*, Vol. 15, April 2004 .
- [Strau95] Straub, F.K., "A Feasibility Study of Using Smart Materials for Rotorcraft", *Smart Materials and Structures*, Vol 5, 1995, pp. 1-10.
- [Tan03] Tan, J., "Face Gearing With A Conical Involute Pinion Part 2. The Face Gear - Meshing With The Pinion, Tooth Geometry And Generation", Proceedings of DETC'03 ASME 2003 Design Engineering Technical Conferences and Computers and Information in Engineering Conference, Chicago, IL, Sep. 2003.
- [Tish04] Tishchenko, M.N. and Nagaraj, V. T., ENAE 634 Helicopter Design Lecture Notes, University of Maryland, College Park, 2004.
- [Unsw84] Unsworth, D. and Sutton, J., "An Assessment of the Impact of Technology on VTOL Weight Prediction", 40th Annual Proceedings of the American Helicopter Society, Arlington, Virginia, 1984.
- [Urne96] Urnes Sr., J. M., Cushing, J., Bond, B., Nunes, S., "On-Board Fault Diagnostics for Fly-By-Light Flight Control Systems Using Neural Network Flight Processors", Proceedings of SPIE – The International Society for Optical Engineering, Fly-by-Light III, vol. 2840, August 1996.
- [Vuil86] Vuillet, A. and Morelli, F., "New Aerodynamic Design of the Fan-in-fin for Improved Performance", Proceedings of the 12th European Rotorcraft Forum, September 22-25, 1986.

- [Wei03]** Wei, Fu-Shang (John), “Design of an Integrated Servo-flap Main Rotor”, Proceedings of the 59th Annual Forum of the American Helicopter Society International, Phoenix, AZ, May 2003.
- [Yoo04]** Yoo, J., “A Magnetorheological Hydraulic Actuator Driven By A Piezopump”. *Journal of the American Society of Mechanical Engineers*, Aerospace Division (Publication) AD, v 68, 2003, p. 389-397.
- [Zakr93]** Zakrajsek, J.J., Townsend, D.P., and Decker, H.J. “An analysis of gear fault detection methods as applied to pitting fatigue failure data”. Technical Report NASA TM-105950, AVSCOM TR-92-C-035, NASA and the U.S. Army Aviation Systems Command, January 1993.
- [Zoll04]** Zoll Medical Corporation, [www.zoll.com](http://www.zoll.com), 2004.